UNIVERSITY OF OKLAHOMA

GRADUATE COLLEGE

NORTHWEST AUSTRALIAN TROPICAL CYCLONES: VARIABILITY AND SEASONAL PREDICTION

A DISSERTATION

SUBMITTED TO THE GRADUATE FACULTY

in partial fulfillment of the requirements for the

Degree of

DOCTOR OF PHILOSOPHY

By

KEVIN HAROLD GOEBBERT

Norman, Oklahoma

2009

NORTHWEST AUSTRALIAN TROPICAL CYCLONES:
VARIABILITY AND SEASONAL PREDICTION

A DISSERTATION APPROVED FOR THE
SCHOOL OF METEOROLOGY

By

Dr. Lance M. Leslie

Dr. Susan Postawko

Dr. Michael Richman

Dr. Randa L. Shehab

Dr. David J. Stensrud

Acknowledgements

It is impossible to say enough words of thanks to all of the people that have supported me along the way to finishing this dissertation and really all of my schooling since beginning in preschool so many years ago. The completion of this dissertation would not have been possible with the support of my advisor, Lance Leslie, whom I have learned much from during the past six years. Additionally, the support of Woodside Petroleum Ltd., especially Stan Stroud, for providing the primary TC dataset used in this dissertation as well as some financial support and discussion of the topic was exceptionally helpful in the completion of this project. Additionally, personal communications with Bruce Buckley have enlightened this work with his complete knowledge of the Australian region TC basins. I would also like to thank my committee, Drs. David Stensrud, Susan Postawko, Michael Richman, and Randa Shehab, as their input have made this a better body of work. Additionally, the office staff (Celia, Nancy, Marcia, and Judy) have helped and supported me throughout my graduate career. Without them the School of Meteorology would not be the home away from home that it is, and will always remain, as long as they are there.

My interest in science and particularly meteorology has been fostered by many teachers and professors over the years. I would especially like to thank my high school science teachers Fred Rassmussen and Leslie Silver; two teachers who told me I could do anything, and then challenged me to do even more than I thought I could accomplish. Thank you for instilling in me the wonders of science and pushing me to always strive for more.

My education then took me to Valparaiso University where Drs. Bart Wolf, Teresa Bals-Elsholz, and Craig Clark inspired me to learn everything about the weather, from severe storms and tornadoes to dynamics and the boundary layer. Their guidance and knowledge have prepared me well for a career in meteorology. Thank you to Dr. Michael Barrett of NASA for encouraging me and developing my research skills as

an undergraduate. A special thanks to Dr. John Knox of the University of Georgia for being a wonderful teacher, mentor, and friend. John helped me to believe in me, thanks for inspiring not only me, but all the students you have taught over the years.

Through all of life's trials we move up and down with the rolling sea. Many times it may feel like we are standing in one place, neither stepping forward for falling backward – suspended in time. When we finally take that step to finish, it is then that we reflect on the journey traveled and marvel at where we've gone. To say that this has been hard would be an understatement. To say it was fun would be sugar-coating the experience beyond satisfaction. However, it would not have been the same without my fellows to accompany me through the trip. For two such people, there are not enough words to express the gratitude with which their friendship has made each day, month, and year bearable to get through. Somer and Chad, without those late Friday night dinners, long lunches, and general venting sessions, this whole experience would have been substantially more difficult. Know that you are the best and I couldn't have done this without you both.

Not many people study tropical meteorology at OU, however, I was fortunate to know Dr. Bradford Barrett during his time as a graduate student. While we only shared an office for a short time, Brad has helped me become a better scientist through his willingness to read through very early drafts of the prospectus and dissertation and just general chats about the research he and I were doing. Without his help, there is no way that this work would be as good as it is. His mentorship, and more importantly, his friendship will be treasured forever.

I don't think many graduate students can make it through without all of the fun times at the office (or wherever else we may go to get away from the office) and I would be remiss if I did not acknowledge all of them for their help and getting through it all. To Patrick who graciously read through an early draft of this manuscript and is always there to lend a helping hand, I could not have done all of this without your support. To

Sean and Ryan M., this past year would not have been the same without our weekly "meeting of the minds", I'll miss them. To Mark, while not a graduate student, has been a great mentor over the past six years, but more importantly I will always cherish the "morning after" analyses of political events, all of your help throughout my graduate career helped to get through it all. To Bryan, Jeremy, Ryan S., Charlotte, Nate, James, Tiffani, Kenny, Nick B., Craig, Chris, Kim, Angelyn, Mike, Jen, Matt, and Alex S., you have all provided the entertainment, encouragement, and love that everyone needs to get through a degree like this – Thank you.

Each Sunday provided me a special opportunity to sing praise and love with a wonderful choir at University Lutheran Church. Without their love and support it would have made this process a lot tougher than it already was. I will miss you all dearly and wish the peace of Christ for each and everyone of you. I would like to thank Alex F. for the early morning raquetball games and endless conversation, I always enjoyed a deep conversation, especially when they last until 4am! Your friendship has brightened my time in Oklahoma.

My family will always mean more to me than I can ever express in words or deeds, without them I would not be who I am today. To Mom, Dad, Krissy, Grandma, Aunt Marilyn, Uncle Gary, Aunt Pam, Uncle Alan, Aunt Donna, David, Emily, Jonathan, Jane, Steve G., Heather, Laney, Brooke, Ellie, Lori, Fawn, Emma, Steve, Kim, and Declan: your love and compassion have lifted me up throughout everything. Thanks for your support and encouragement. You have all inspired me to do great things.

Finally, after finishing this dissertation I found this quote from Voltaire, which I can attest to.

"The more I read, the more I meditate; and the more I acquire, the more I am enabled to affirm that I know nothing." – Voltaire

Contents

List Of Tables

List Of Figures

Abstract

Global teleconnections, involving geopotential height, air temperature, and sea surface temperature, are found for the interannual variability of tropical cyclone (TC) activity in Northwest-Australian (NWAUS) basin of the Southeast Indian Ocean ($105 - 135°$E). The NWAUS basin averages 5.5 TCs per year, 42 TC days, and 3 TC landfalls. Additionally, a wavelet analysis yields wavelet power maximum in the $4 - 6$ year and the decadal time periods for both yearly TC frequency and TC days. To identify significant correlates, the global atmospheric and oceanic parameters mentioned above were correlated with the TC frequency and TC days from the Woodside Petroleum Ltd. TC data set. Large correlations were obtained between the NWAUS TC frequency and the following variables: Apr–Jun 700-hPa geopotential heights over North America ($r \sim -0.64$), May–Jul 850-hPa geopotential heights over the south Indian Ocean ($r \sim 0.60$), May–Jul 850-hPa air temperature ($r \sim -0.63$), Jun–Aug 925-hPa geopotential heights over the south Atlantic Ocean (r ~ -0.65), and Jun–Aug 925-hPa geopotential heights over the Eastern Pacific Ocean ($r \sim -0.59$). The collinearity among the five correlates are generally $\mid r \mid < 0.4$. Additionally, large correlations were obtained between the NWAUS TC days and the following variables: Jan–Mar 100-hPa v-component of the wind over the Southern Pacific Ocean ($r \sim 0.52$), Apr-Jun 850-hPa geopotential heights over North America ($r \sim -0.58$), and Jul–Sep 1000-hPa geopotential heights over the South Altanic Ocean ($r \sim -0.7$). These variables can be utilized as seasonal predictors for the upcoming TC season in terms of frequency and days with a lead-time of at least three months for TC frequency and two months for TC days. This set of seasonal predictors includes, intra-basin, inter-basin, and cross-hemispheric regions, unlike previous Australian TC activity studies, which stress the primacy of ENSO. Here it is noted that the traditional Niño 3.4 and Niño 4 regions were not highly correlated with the NWAUS TC activity ($\mid r \mid < 0.5$). No local predictors based on SST, geopotential height, or

air temperature resulted from the correlation analysis. The predictors are used in a multiple linear regression model for forecasting the coming seasons number of TCs and TC days. Finally, both prediction schemes are then compared to forecasts made using persistence, climatology, and random forecasts to determine if they perform better than these reference forecasts.

Chapter 1

Introduction

For millennia, tropical cyclones (TCs) have been affecting the lives of people. Before the advent of modern meteorological sensing instrumentation, TCs often hit with little or no advance warning. Without comprehensive data coverage it was difficult to ascertain the different types of meteorological phenomena, let alone predict them. One notable early U.S. hurricane impact was the Galveston 1900 storm, that decimated the Galveston, TX area. The people of Galveston received minimal advance warning. Prior to landfall, Galveston meteorologist Isaac Cline was warned by Cuban meteorologists about a possible TC moving toward Galveston (Larson 2000), but Cline did not hold the warnings in high regard and did not warn the residents until it was too late. As a result, many people lost their lives and the town was nearly completely destroyed.

Even today, with advanced remote sensing technology, potential impacts of TCs are often misestimated. During the 2005 Atlantic hurricane season the remnants of Hurricane Stan crossed over the Central American countries of Belize, Honduras, and Guatemala. The Guatemalan government told its citizens that there was nothing to worry about from the storm (Flayer 2007; personal communication). Unfortunately, the remnants of Hurricane Stan produced large amounts of rainfall on the highlands of Guatemala which caused massive mudslides that destroyed parts of the village of Panabaj near Santiago/Atitlan. In addition to the homes and lives lost as a result of the mudslides, the economy of the region was almost destroyed when nearly the entire coffee bean crop failed. The mudslides were up to 12 m (40 ft) deep in areas

near Panabaj, resulting in more than 1000 deaths in this area. Knowing that TCs affect all parts of society, it is important to understand and predict TCs to better serve society.

Predicting the number of tropical cyclones that will affect a region is one aspect of forecasting TCs. Early seasonal prediction schemes were developed for the Australian region (Nicholls 1979, 1985) and the Atlantic region (Gray 1984a,b) using El-Niño–Southern Oscillation (ENSO) standard parameters as primary predictors of future TC activity. These schemes have had varying degrees of success. In general, schemes have improved with increasing understanding of the large scale forcings affecting different ocean basins. Since these early works, much focus has been on understanding the role of global atmospheric parameters in modulating interannual TC activity (e.g., Nicholls 1992; Chan 1985; Solow and Nicholls 1990; Gray et al. 1992; Evans and Allan 1992; Gray et al. 1993; Nicholls et al. 1998; Chan and Liu 2004; Klotzbach and Gray 2004; Ramsay et al. 2008) in all of the global TC basins.

The Southern Hemispheric TC basins have not been studied as extensively as the North Atlantic and Western North Pacific TC basins. The Australian TC basin ($90 - 170^\circ$ E; Fig. 1.1) typically has been investigated as a single TC basin (e.g., Nicholls 1979, 1984, 1985, 1992; Evans and Allan 1992; Nicholls et al. 1998; Hall et al. 2001; Ramsay et al. 2008). However, a few studies have focused on one of the two distinct primary subbasins of the Australian TC basin, the Southwest Pacific (SWPAC) Ocean basin ($135 - 170^\circ$ E; e.g., Revell and Goulter 1986; Hastings 1990; Basher and Zheng 1995), and the Southeast Indian (SEIND) Ocean basin ($90 - 135^\circ$ E; e.g., Broadbridge and Hanstrum 1998).

The Northwest Australian (NWAUS) TC basin, itself a subbasin of the SEIND Ocean (Fig. 1.1), is a major economic center for Australia, yielding a large portion of its raw materials (e.g., oil, natural gas, iron ore) whose production is greatly disrupted by yearly TC activity. The NWAUS TC basin is the most active portion

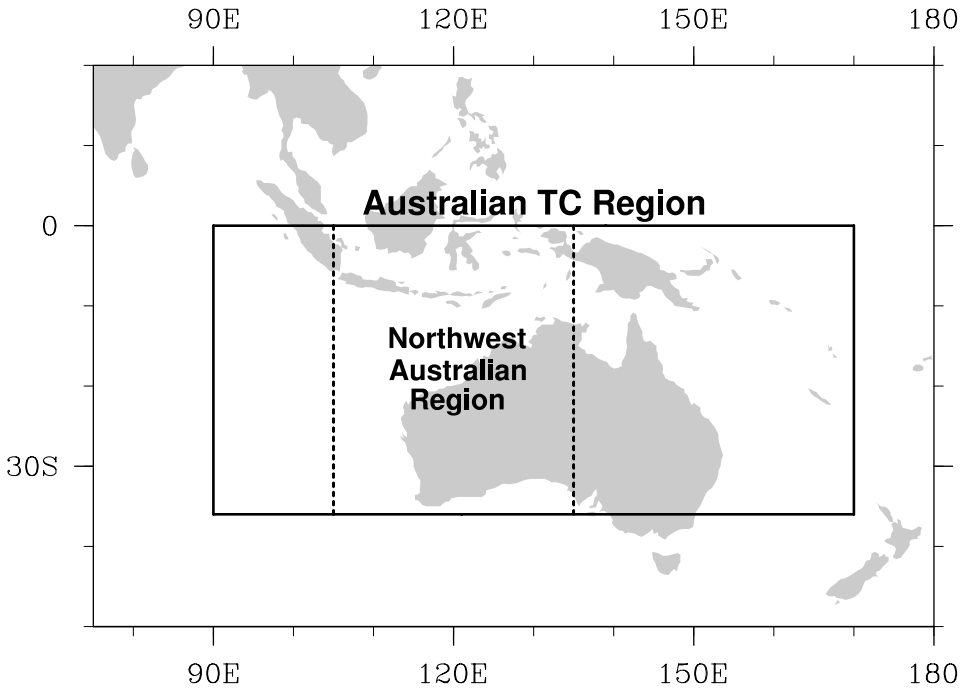

Figure 1.1 A map of the Australian TC region ($90 - 170°$ E; $0 - 35°$ S), with the Northwest Australian Region ($105 - 135°$ E) identified between the dashed lines.

of the Australian region (Fig. 1.2). While there is much TC activity throughout the Australian region, the bounds of the NWAUS basin readily can be identified through the local minima in TC occurrence around the 105° and 135° longitudes, which denote the ends of the NWAUS region. Thus the ability to accurately predict seasonal variability of TC frequency is needed to limit the impact that a TC season will have on the vital industries in the NWAUS region. In addition to the impacted industries, TCs in the NWAUS TC basin, are a substantial source of Northwest Australian rainfall.

Previous work in the Australian region generally has not focused on the NWAUS TC subbasin but on the entire Australian TC basin. Additionally, the seasonal prediction schemes for the Australian region in the literature have not used global predictors for seasonal TC prediction. This work extends similar work done for the Atlantic (e.g., Gray 1984a,b; Gray et al. 1992, 1993; Klotzbach and Gray 2003) and Northwest Pacific (NWPAC) TC regions (e.g., Chan 1985; Chan et al. 1998) to the NWAUS subbasin of the SEIND Ocean.

In this study, I seek global predictors of TC activity in a subbasin of the SEIND Ocean and use these newly found predictors in a seasonal forecast scheme. New global predictors are determined by investigating the interannual variability of TC frequency and TC days in the NWAUS region and identifying which known global modes or atmospheric parameters explain the largest part of the TC metric variance. These global teleconnections are not be limited to the Southern Hemisphere, but are intra-basin, inter-basin, and cross-hemispheric. The identified global teleconnections are used to develop a seasonal prediction scheme for yearly TC counts. The prediction scheme developed outperforms the forecasts using persistence or climatology as the predictor.

The prediction scheme is developed using seasonal TC data from the 1970/71 to 2004/05. All predictors input into the model go through a stepwise regression, using

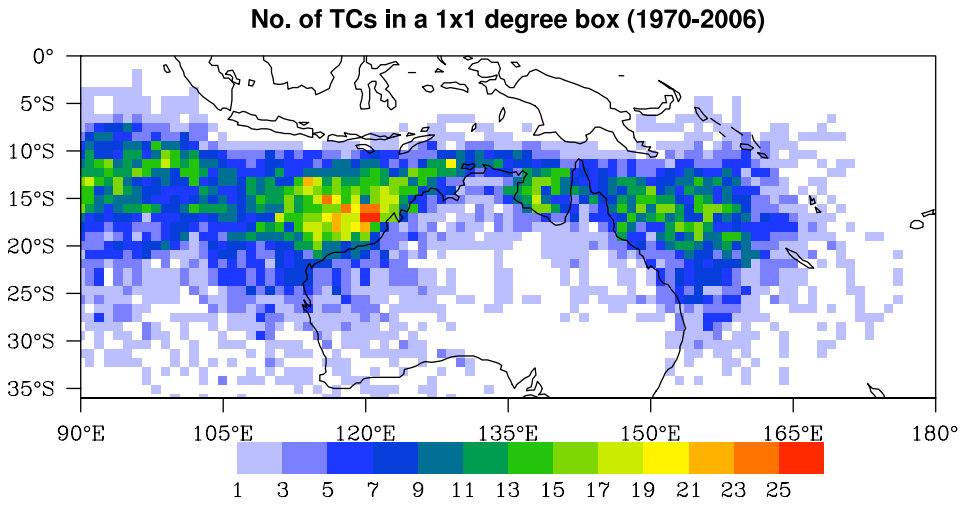

Figure 1.2 The number of TCs that crossed into each 1° latitude by 1° longitude box within the entire Australian region during the period 1970/71 to 2005/06. This map was compiled from the Australian Bureau of Meteorology best-track dataset.

the Akaike Information Criterion (AIC) statistic to select the minimum number of predictors needed to minimize the prediction error. The "leave-one-out" and leave-five-out, predict three cross validation method are used to determine the independent forecast ability of the seasonal prediction scheme. This allows for an estimation of the skill of the prediction scheme over climatological and persistence forecasts, which are commonly used to assess forecast skill. Finally, the four most recent TC seasons, which have not been used in the development dataset, will be presented as case studies using the developed forecast scheme. The predictors are all available before the beginning of the NWAUS TC season so that a forecast can be made prior to the beginning of the oncoming season.

Nearly all of the studies conducted on the Australian TC basin have focused primarily on the role of ENSO. However, there has been an increasing interest in the role of global teleconnections in modulating TC activity world-wide. Many studies of the Atlantic and NWPAC TC basins have identified key parameters in addition to ENSO variables that are important to describing the interannual variability of TC frequency (e.g., Gray 1984a,b; Gray et al. 1992, 1993; Chan 1985; Chan et al. 1998; Klotzbach and Gray 2003). Some of the parameters identified in previous work for the Atlantic and NWPAC TC basins are the, Quasi-biennial Oscillation (QBO), Caribbean sea-level pressure, and November 500-hPa geopotential height.

A literature review is presented in Chapter 2, highlighting key issues of variability in TC metrics for the Australian region including seasonal TC prediction methods developed by Nicholls (1979, 1985, 1992) and Klotzbach and Gray (2003, 2004) prior to this work. Additionally, a brief review of global teleconnections is presented as well as TC prediction methods from other basins. The data and prediction selector methodology used in this study are discussed in Chapter 3. The results of the search for TC predictors are presented in Chapter 4. The seasonal prediction scheme is

developed and cross-validated in Chapter 5. Finally, some conclusions and future work are discussed in Chapter 6.

Chapter 2

Literature Review and Historical Background

There are many different names for the same atmospheric phenomenon known as a tropical cyclone (TC). For example, in the North Atlantic basin, named storm systems are called tropical storms and hurricanes, where hurricanes are further delineated by a five category rating system depending on wind speed. However, in the Northwest Pacific basin tropical cyclones are referred to as tropical storms, severe tropical storms, and typhoons. In the Australian region the terms used are five categories of tropical cyclones and severe tropical cyclones (Cats. $3-5$).

Before regular weather observations began, people living along coastal regions and sailors at sea were the only people who experienced tropical cyclones. These storms would often hit without warning and cause major damage to homes and ships. Even in $1944-45$, with improved, but still limited meteorological knowledge, there was still conflicting meteorological information that caused the U.S. Third fleet stationed in the Pacific Ocean to be caught in two typhoons (Emanuel 2005).

Regular observations of TCs have been taken in the North Atlantic region since the mid-1940s using airplane reconnaissance, which left many regions still uncovered, including the Pacific Ocean and the U.S. Third fleet. Globally, TCs have only been observed extensively since the deployment of satellites, which has provided an ongoing source of regular observations. Currently, the main method of observing TCs is through the use of various kinds of satellites, and where intensity usually is estimated through an interpretation scheme developed by Dvorak (1975, 1984). The Dvorak

technique uses cloud pattern recognition to estimate the strength of the storm while out at sea, away from any in situ observations.

There are a number of TC basins globally, including the North Atlantic, Eastern Pacific, Northwest Pacific, North Indian, Southwest Indian, and Australian basins. No observations of TCs have occurred in the South Atlantic Ocean[1]. Global TC tracks are illustrated in Figure 2.1 and through inference illustrate the locations of the TC basins. These different ocean basins around the world have different initiating mechanisms for development, but Gray (1984a,b) hypothesized that within each basin the processes involved in TC development and intensification were similar. The set of necessary, but not sufficient conditions for TC development defined by Gray (1968), are as follows:

a. frictionally forced low-level moisture convergence;

b. upper-level divergence leading to deep cumulus convection;

c. upper-level divergence exceeds low-level convergence;

d. horizontal low-level wind shear, but minimal vertical wind shear;

e. sea surface temperatures exceeding 26.5°C;

f. low-level disturbance develops poleward of 5° latitude for Coriolis turning;

g. an established low-level vorticity disturbance.

The initiating mechanisms vary by TC basin; in the Atlantic basin the main initiating mechanism are African Easterly Waves, whereas in the Australian region a more common initiator is the monsoon trough.

[1]In January 2003 satellites observed a storm that appeared to have characteristics of a TC. The fact as to whether this was a TC is still debated within the meteorological community.

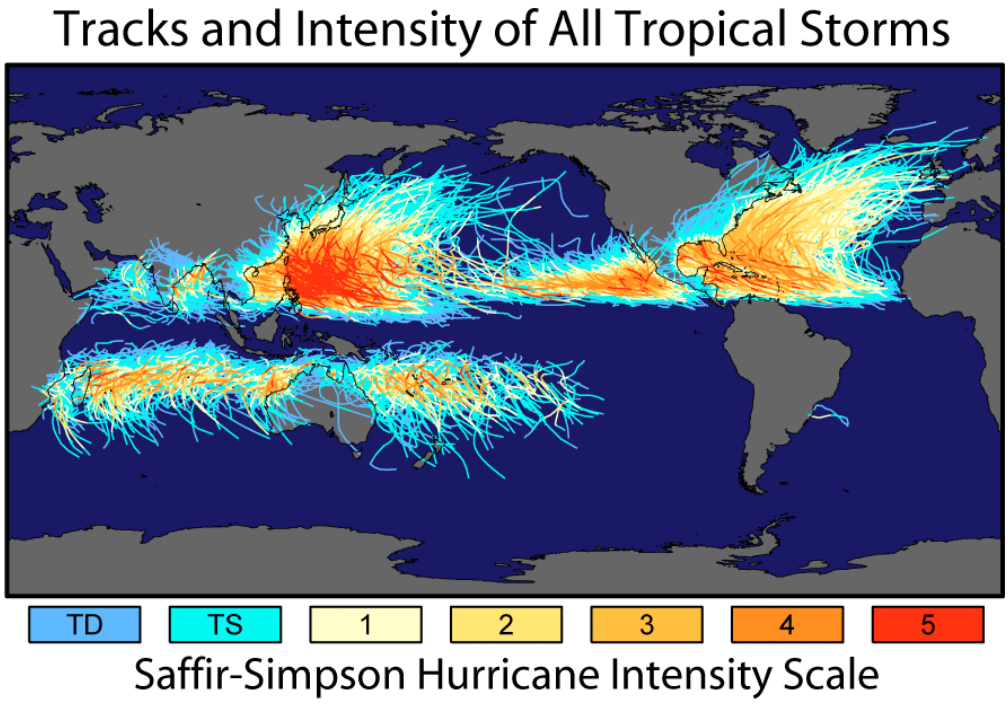

Figure 2.1 Nearly 150 years of storm tracks. Courtesy of the Earth Observatory Daily Image Archive (http://earthobservatory.nasa.gov/IOTD/view.php?id=7079)

The American Meteorological Society defines a TC as a disturbance originating over tropical oceans (AMS 2000), whereas Gray (1968) more precisely defines a tropical storm as a "warm-core cyclonically rotating wind system in which maximum sustained winds are 17 m s^{-1} (35 kt; 40 mph) or greater." In the Australian region the Australian Bureau of Meteorology categorizes TCs by maximum wind gusts into five categories of severity: category 1 maximum wind gust below 125 km h^{-1}; category 2, maximum gust $125 - 164$ km h^{-1}; category 3, maximum gust $165 - 224$ km h^{-1}; category 4, maximum gust $225 - 279$ km h^{-1}; category 5, maximum gust above 279 km h^{-1}.

Observations of TCs have improved with the aid of satellites, which have advanced the meteorological understanding of what is and is not a TC. Even with the advances in satellite technology, including advanced wind observing satellites, there is debate about individual storms and how they should be classified. With this said, the mean number of global TCs has been estimated to be 90 TCs per year[2] (Frank and Young 2007), with a standard deviation of 10 (Lander and Guard 1998), for TCs with sustained wind speeds greater than 17 m s^{-1} (34 kts).

There are three main stages in the life cycle of a TC: genesis, maturation, and dissipation stages. During the genesis stage, convection is typically quite disorganized, with little or no rotation occurring in the storm. A cyclonically rotating circulation with a nearly axisymmetric low-pressure center signifies the mature stage. Finally, during the dissipation stage the vortex weakens and elongates asymmetrically from the center.

[2]While the average is 90, the yearly number of TCs does indeed vary. The myth that the number of TCs that occur annual across the globe is constant is not true ((Frank and Young 2007)). A common thought was that when there is an active season in one basin, it is compensated by less activity in the other basins. Frank and Young (2007) have recently proven this myth false using global TC counts from the $1985 - 2003$ seasons.

A mature TC (hurricane strength or stronger) typically has a well-defined eye and often is approximated as axisymmetirc (Ooyama 1982; Moller and Montgomery 1999). The eye region is usually nearly cloud free, with stronger storms more likely to have a clear eye (Palmén and Newton 1969). The convective region surrounding the eye is called the eye wall and is the location of the strongest winds within the entire storm (Willoughby et al. 1982). Within this region we find the radius of maximum winds (RMW). The cyclonic flow around a TC from the center of the eye to the RMW can be approximated by solid-body rotation, with winds decreasing radially outward from the RMW until reaching equilibrium with the environmental flow. This relationship of winds and radial distance within a TC can be approximated mathematically as a modified-Rankine vortex where

$$Vr^{-1} = \text{constant}, \tag{2.1}$$

outside the RMW, and

$$Vr = \text{constant}, \tag{2.2}$$

within the RMW (Depperman 1947). However, the air flow within the RMW does not exactly conform to solid-body rotation due to frictional effects and was later modified by Gray and Shea (1973) to be

$$Vr^{x} = \text{constant}, \tag{2.3}$$

where x was determined empirically from wind observations to lie between 0.4 and 0.6. Outside the eye wall region, convection forms in outer rain bands that spiral into the storm (Maynard 1945; Wexler 1947) and these rain bands can be approximated as breaking Rossby waves (Montgomery 1997; Moller and Montgomery 1999).

Using a parametric fit of the gradient wind balance, Holland (1980) developed an empirical relationship for the RMW (R_w) and the maximum wind (V_m)

$$R_w = A^{1/B}, \tag{2.4}$$

and

$$V_m = (B/\rho e)^{1/2}(p_n - p_c)^{1/2}, \tag{2.5}$$

where A and B are climatological scaling parameters based on maximum wind, ρ is the air density (assumed to be 1.15 kg m^{-3}), e is the natural logarithm base, p_n is the ambient surface pressure (assumed to be the pressure of the first anticyclonic curved isobar), and p_c is the central pressure of the TC vortex. The relation for the RMW is useful in that it does not depend on the ambient or central pressure, only the scaling parameters A and B. The scaling parameters must be determined for each TC and the resulting radial values of pressure and wind are sensitive to the choice of A and B. However, Holland (1980) was able to fit the observed data by choosing $A = 23$ and $B = 1.5$. Subsequent attempts to calculate the RMW and maximum wind have also yielded additional empirical relationships for the TC vortex (e.g., Large and Pond 1982; Emanuel 1986, 1995; Andreas and Emanuel 2001; Emanuel 2003a; Makin 2005).

A TC can be defined mathematically in cylindrical coordinates (r, λ, z),with a set of equations whose origin is at the center of a stationary TC. This set of equations describes the flow and energtics surrounding a mature TC. Beginning with the radial, u, and tangential, v, components of the wind

$$\frac{\partial u}{\partial t} + u\frac{\partial u}{\partial r} + \frac{v}{r}\frac{\partial u}{\partial \lambda} + w\frac{\partial u}{\partial z} - fv - \frac{v^2}{r} = -\frac{1}{\rho}\frac{\partial p}{\partial r} + \frac{1}{\rho}\frac{\partial \tau_{zr}}{\partial z} + F_{Hr}, \tag{2.6}$$

$$\frac{\partial v}{\partial t} + u\frac{\partial v}{\partial r} + \frac{v}{r}\frac{\partial v}{\partial \lambda} + w\frac{\partial v}{\partial z} + fu + \frac{uv}{r} = -\frac{1}{\rho r}\frac{\partial p}{\partial \lambda} + \frac{1}{\rho}\frac{\partial \tau_{z\lambda}}{\partial z} + F_{H\lambda}, \tag{2.7}$$

where u is dr/dt and v is $d\lambda/dt$, w is the vertical velocity component, f is the Coriolis parameter, ρ is the air density, $\tau_{z\lambda}$ and τ_{zr} are the tangential and radial stresses due to small-scale vertical momentum mixing, and $F_{H\lambda}$ and F_{Hr} are the tangential and radial components of horizontal mixing. The vertical component (w) of the equation of motion can be expressed as

$$\frac{dw}{dt} = -\frac{1}{\rho}\frac{\partial p}{\partial z} - g + F_z, \tag{2.8}$$

where F_z is a summary term representing forces associated with precipitation particle drag and turbulent mixing. Generally, the terms dw/dt and F_z are several orders of magnitude smaller than the vertical pressure gradient force, which allows (2.8) to be approximated as the hydrostatic balance

$$\frac{\partial p}{\partial z} = -\rho g, \tag{2.9}$$

while noting that vertical motions in TCs are produced by imbalances in the right hand terms in (2.8). To complete the equations of motion, the full continuity equation is written as

$$\frac{\partial \rho}{\partial t} + \frac{\partial \rho r u}{r \partial r} + \frac{\partial \rho v}{r \partial \lambda} + \frac{\partial \rho w}{\partial z} = 0, \tag{2.10}$$

where the changes of air density are related to horizontal and vertical advection. The first law of thermodynamics, expressed in terms of temperature (T), is written as

$$\frac{\partial T}{\partial t} = -u\frac{\partial T}{\partial r} - \frac{v}{r}\frac{\partial T}{\partial \lambda} - w\frac{\partial T}{\partial z} - \frac{\omega}{\rho c_p} + \frac{Q}{c_p} - \frac{1}{\rho c_p}\frac{\partial H_s}{\partial z} + F_{HT}, \tag{2.11}$$

where $\omega = dp/dt$, Q is the diabatic heating rate, H_s is the vertical heat flux due to turbulent eddies, and F_{HT} represents horizontal mixing due to turbulence. Additionally, the continuity equation for water vapor is written as

$$\frac{\partial q}{\partial t} = -u\frac{\partial q}{\partial r} - \frac{v}{r}\frac{\partial q}{\partial \lambda} - w\frac{\partial q}{\partial z} - C - \frac{1}{\rho}\frac{\partial H_q}{\partial z} + F_{Hq}, \tag{2.12}$$

where q is the specific humidity, C is the condensation (evaporation rate), H_q the vertical flux of water vapor, and F_{Hq} the effect of horizontal mixing of water vapor. These equations, along with the equation of state

$$p = \rho R T, \tag{2.13}$$

where R is the universal gas constant, complete the system of equations that describe the dynamics and moist thermodynamic process of a mature TC (Anthes 1982). Additionally, there are two conserved quantities that are useful to describe the physics

of TCs, absolute angular momentum (M) and entropy (s). Angular momentum is conserved for axisymmetric displacements around a TC and is defined as

$$M = rV + \frac{1}{2}fr^2, \tag{2.14}$$

where r is the radius from the center of the storm, V is the tangential velocity, and f is the Coriolis parameter. Entropy is conserved following reversible adiabatic displacements of air and is approximated as

$$s \approx C_p \ln(T) - R_d \ln(p) + \frac{L_v q}{T} - qR_v \ln(H), \tag{2.15}$$

where C_p is the specific heat at constant pressure, T is the absolute temperature, R_d is the universal gas constant for dry air, p is pressure, L_v is latent heat of vaporization, q is the concentration of water vapor, R_v is the universal gas constant for water vapor, and H is the relative humidity (Emanuel 2003b).

The main source of energy for TCs is the heat transfer from the ocean (Riehl 1950; Kleinschmidt 1951). The mature TC with steady, axisymmetric flow has been approximated as an ideal Carnot engine (Emanuel 1986). As air flows into the center of the TC it experiences a pressure drop, and entropy increases owing to heat transfer from the ocean and dissipation of kinetic energy in the atmospheric boundary layer (Bister and Emanuel 1998). Angular momentum also decreases at this time due to frictional torque with the sea surface. This frictional torque is the most important sink of kinetic energy within the TC (Emanuel 2003b), needed to maintain the Carnot-like cycle. Strong upward vertical velocity in the eyewall forces air upwards where it ascends to lower pressure with constant entropy and constant angular momentum. This portion of the energy cycle is nearly adiabatic and free of frictional torque. Air begins to descend as it moves from the center of the storm to the distant environment. During this leg, the air loses the entropy gained from the inflow leg through longwave radiation emitted to space and gains angular momentum through

mixing with the environment. This segment is nearly isothermal. Finally, the cycle is closed by an angular momentum conserving segment where air descends adiabatically on the periphery of the TC (Bister and Emanuel 1998) back to the surface. The energy production in a TC is highly dependent on the saturated specific humidity, which increases exponentially with temperature. Unlike energy production, the energy dissipation within the storm is not dependent on temperature (Lighthill 1998).

2.1 TC data quality in Australian region

The Australian region has observations of TCs dating back to the beginning of the 19^{th} century, and reliable observations increased through the middle part of the 20^{th} century, with the onset of the satellite era around 1970 (Holland 1981). However, some observations, especially of TC intensity, remain questionable during the early satellite era. Some factors in changing observations of tropical cyclones in the Australian region include (Holland 1981; Nicholls et al. 1998; Buckley et al. 2003):

- changes in definition;
- changing analysis techniques;
- improvements in satellite technology;
- increased radar coverage of coastal regions;
- increased in situ observations (surface and upperair).

These factors identify the key problems that must be accounted for within any Australian region TC dataset. Most of these effects are not mutually exclusive; often better understanding of TCs lead to changes in analysis techniques and possible changes in what may be defined as a TC. For example, there have been changes in analysis techniques, which are linked to changes in the definition of what constitutes

a TC, as knowledge about TCs grew during and after World War II (Holland 1981). Nicholls et al. (1998) noted a marked change in the reported number of weak cyclones in the mid-1980s, which they hypothesized was attributable to a change in the understanding of TCs and thus the naming of TCs. Additionally, a dramatic change also occurred in the relationship between the Southern Oscillation Index (SOI) and Australian region TCs in the mid-1980's as noted by Nicholls (1992) and is potentially artificial due to the abrupt nature of the change. One notable example of persistent artifacts in Australian region TC datasets can be found in the 1962/63 TC season. During that season, a record number of 19 TCs were reported in the Bureau of Meteorology (BoM) official TC dataset. At one point, three TCs were reported within 150 km of each other (Solow and Nicholls 1990) simultaneously, which is unlikely to have been the case as TCs typically have sizes much larger that 150 km across.

The regular use of satellites in the Australian region did not begin until 1966 with geostationary satellites beginning routine observations in 1978 (Holland 1981). Even today there is limited in situ observations of TCs in the Australian region, especially storms that never make landfall, as there is no regular aircraft reconnaissance to TCs in the region. Obviously, the Australian region is not alone in these problems as many of these issues are valid in other TC basins.

To account for possible shortcomings in the NWAUS region TC dataset, a reanalysis of the TCs occurring within the region was undertaken by Harper et al. (2008). The study attempted to clarify the historical accuracy of reported TCs by comparing the Bureau of Meteorology (BoM) official TC dataset with an explicitly reviewed dataset commissioned by Woodside Petroleum Ltd. (WPL). When studying TCs in any basin, a primary concern is whether the historical datasets are reliable and accurate. The WPL study investigated the reliability and accuracy of the BoM historical dataset, especially with regards to intensity estimates, as they are the most critical to an accurate risk assessment for the region. In addition to the intensity

estimates, the reanalysis effort afforded the opportunity to assemble information on radii of gale force winds and eye diameter. These additional parameters can be utilized in various empirical techniques to accurately estimate the intensity of each TC. After the WPL reanalysis was reviewed by ex-BoM meteorologists, it was concluded that "the WPL Reviewed dataset, albeit far from perfect, is likely to be of an overall superior quality and consistency relative to any other long-term dataset available for this region" (Harper et al. 2008). Initially this study will consider only yearly TC counts and number of TC storm days. However, in the future, a seasonal prediction on the yearly TC count of intense (< 970 hPa central pressure) TCs and intense TC storm days will be conducted. Therefore, using one common dataset to develop a set of seasonal prediction models is preferred, especially in light of the quote from the Harper paper that their dataset is considered to be the most reliable.

2.2 Characteristics of Australian TCs

2.2.1 Development of TCs in the Australian Region

Research has identified major differences between tropical disturbances that developed and did not develop into TCs in the Northwest Pacific and North Atlantic regions by McBride and Zehr (1981). Development is preferred in areas of high low-level vorticity, where divergence exceeds 100 hPa or more per day over a 4° radius area, with nearly zero vertical wind shear near circulation center, and when large positive (negative) zonal shear is to the north (south) of a developing system. For the NWAUS region Foster and Lyons (1988) found that the most important discriminator between developing and non-developing TCs is the location of the upper-level ridge. Developing TCs possessed greater anticyclonic vorticity at 200 hPa. While TCs need similar conditions to develop in each TC basin world-wide, the initiating mechanisms can vary widely between basins.

In the Australian region the initiation mechanisms are different from the common mechanism of tropical easterly waves in the North Atlantic basin . McBride and Keenan (1982) identified the main Australian region initiation mechanism as the Southern Hemisphere monsoon trough. The monsoon trough is an area of maximum cyclonic vorticity, and depending on where it is located across the Australian region different parts of the region are more susceptible to TC formation (Dare and Davidson 2004). Dare and Davidson (2004) found that two regions of preferred tropical cyclogenesis in the Australian region were associated with regions of maximum cyclonic vorticity. Another location of preferred cyclogenesis was associated with a local minimum in cyclonic vorticity for which Dare and Davidson (2004) hypothesized there are other factors, such as weak vertical wind shear, that are important in the formation of TCs in that region.

Dare and Davidson (2004) identified three characteristics of the surrounding environment unique to the Australian region: 1) the Southern Hemisphere monsoon, 2) close interaction with mid-latitude westerlies, and 3) the major continental landmass in the tropical development area. These factors are hypothesized to influence the behavior of TCs in the Australian region, compared to other TC basins where TC motion is considered less erratic.

2.2.2 Australian TC Yearly Storm Counts

The average number of TCs in the Australian region is 12.5 per year, with half of the cyclones occurring in the western region (Dare and Davidson 2004), which is called NWAUS region in this study. The mean first day of occurrence of a TC in the entire Australian basin is 19 December and there is a 64% chance that the first cyclone will be in the NWAUS region (Dare and Davidson 2004). The average life-span of a TC for the entire Australian region is 7.5 days with an average of 75.4 TC days per season. For a full listing of the climatological mean characteristics of the Australian

region and the three identified TC regions refer to Dare and Davidson (2004, see their Table 3).

The trend in TCs for the entire Australian region was investigated by Nicholls et al. (1998), who found that the frequency of all TCs was decreasing. When the time series was split into weak (> 990 hPa), moderate (between 970 and 990 hPa), and intense TCs (< 970 hPa), both the weak and moderate storms decreased while the frequency of intense TCs increased marginally. Similarly, Ramsay et al. (2008) obtained similar results with approximately ten more years of data for the weak and moderate TCs. Intense TCs (defined as < 965 hPa central pressure) had no discernable trend in frequency.

Kuleshov et al. (2008) observed a statistically significant increasing trend in the number of intense (< 945 hPa) TCs in the entire Southern Hemisphere, especially in the southern Indian Ocean and southern Pacific Ocean. It should be noted that the time series of data used by Kuleshov et al. only covered the time period from 1980 to 2005 and likely did not account for a longer, multi-decadal, variability in the frequency of TCs in the Australian region. For all TCs, Kuleshov et al. (2008) did not observe any statistically significant trend in the frequency of TCs or in the number of TC days in the Southern Hemisphere.

These papers highlight the concerns regarding how many years to use for a development dataset. Depending on how many years (and exactly what years) are used in a study of the variability of TC storm counts, different trends appear. Additionally, there are a number of different cut-off points that have been used in the literature for classifying the intensity of TCs. It is therefore important to keep these issues in mind when developing a seasonal prediction scheme as they could have an impact on the final forecast skill of any given scheme. In later sections the frequency of storm counts will be presented, which indicate similar results to that of Nicholls et al. (1998) and Ramsay et al. (2008), except for only the NWAUS region, which in not too surprising

considering that the NWAUS region constitutes approximately half of the Australian region TCs.

2.2.3 ENSO and Australian Region TCs

Ballenzweig (1957) hypothesized that the variability of TC frequency is related to the variability of global circulation patterns. A study of the relationship between the large-scale circulation and the frequency of TCs resulted in noted differences between active and inactive years for TC counts (Ballenzweig 1959). This has lead to much research into various global circulation patterns and its effect on TC frequency and TC days variability. In many regions the circulation pattern of primary focus for many years has been the El Niño–Southern Oscillation (ENSO).

The regular occurrence of ENSO events identified by Bjerknes (1969), and its impact on the Pacific and global circulations, lead him to believe that ENSO events could be used for long-range forecasting. In addition, the Walker Circulation is associated with the equatorial Pacific sea-surface temperature variations. Due to its known effects on equatorial (and more broadly tropical) circulations it is not surprising that ENSO became a leading candidate to help understand the variation of TCs in many of the global TC basins.

The Australian region is directly impacted by changes in the phase of ENSO, as shifts in the normal Walker Circulation to an El Niño phase results in higher surface pressure over eastern Australia. This relationship was used in the development of the Southern Oscillation Index (SOI), which computes the difference in standardized anomalies between Tahiti and Darwin, Australia. In the first seasonal prediction scheme, Nicholls (1979) used Darwin winter sea-level pressure to predict the number of Australian region TCs as they were highly correlated to the Darwin winter pressure during the period $1959-1970$, especially for the early part of the TC season (October–December). This result was further supported by strong, stable relationships found

prior to the beginning of the TC season by Nicholls (1984). Nicholls (1985) predicted both seasonal TC frequency and seasonal TC days using Darwin pressure as an SOI surrogate parameter. Additionally, for the southwest Pacific Ocean, Revell and Goulter (1986) found weak, but statistically significant, relationships between the origin points of TCs and the SOI. (TC prediction is discussed further in section 2.4.)

The strength of the ENSO phase was found to be important with respect to the overall effect on TC frequency in the Australian region (Dong 1988). During strong and very strong El Niño phases of the ENSO cycle, there is a large reduction in the number of TCs compared to neutral or La Niña ENSO phases. In the NWAUS region, Dong (1988) separates the area into two regions. The eastern region ($105 - 125°$E) TC frequency is not substantially different between the different phases of ENSO, whereas in the western NWAUS region ($125 - 145°$E) there is a notable decrease in TCs during an El Niño. Overall, this should lead to a slightly lower number of TCs occurring in the NWAUS region during an El Niño event, especially during strong El Niño's. This is likely the result of a shift in the Walker circulation, where the upward branch is situated over the central Pacific Ocean during El Niño seasons. The relationship between ENSO and TC frequency is even stronger in the southwest Pacific Ocean, where a more direct connection can be attributed to changes in the Walker circulation.

Other research that focuses on the Australian region has investigated how ENSO affects the seasonal variation of TCs. During an El Niño event the Australian monsoon is displaced equatorward relative to the normal and La Niña phases. This displacement, coupled with weak vertical wind shear, and warmer SSTs, leads to more TCs forming in the northern Australian region (Evans and Allan 1992). In general, the NWAUS and southwest Pacific regions, experience fewer TCs during an El Niño phase (Evans and Allan 1992). However, at the same time, there is an increased preference

for storms to track along the coast of northwest Australia leading to an enhanced risk for coastal and near-coastal entities (Evans and Allan 1992).

For the southwest Pacific region, Basher and Zheng (1995) studied several subregions and the association with the phase of ENSO. The authors found that local seasonal atmospheric conditions were sufficient to describe seasonal variability of TC occurrence in the western subregion. The primary effect of higher local SSTs before the beginning of the season leads to an extension of the active TC season. The eastern subregion, however, is principally controlled by the phase of ENSO and not local parameters. During an El Niño event the South Pacific Convergence Zone (SPCZ) is shifted east-northeastward across the eastern subregion (Trenberth 1976; Rasmusson and Carpenter 1982), which moves the main initiating mechanism farther away from the development area.

In the SEIND Ocean, specifically the NWAUS region, Broadbridge and Hanstrum (1998) investigated the relationship between SOI and SOI trend, prior to the TC season, and TC frequency. The authors found that when SOI values were large and strongly positive there was an increase in TC frequency and, when coupled with strong positive SOI trends, there were more coastal impacts. Furthermore, when there were both strong positive values of SOI and strong positive trends in SOI, a substantial increase in early season TCs was found. Correlations between SOI and mid-season TCs were not significant. Additionally, Broadbridge and Hanstrum (1998) found that coastal impacts of severe TCs did not vary with the phase of the SOI; a location was equally likely to have a severe TC hit in an El Niño or La Niña dominated season. This work confirmed similar work done for the entire Australian basin, and Broadbridge and Hanstrum (1998) hypothesized that this work could be used to predict the frequency of TCs in the NWAUS region.

Recently, the interannual variability of TC frequency in the Australian region has been investigated to ascertain the role of the large-scale environment. The role of

SSTs over the central and eastern tropical Pacific is found to be the main contributing factor in the interannual variability of TC frequency (Ramsay et al. 2008). The highest correlation between the frequency of TCs in the Australian region and central Pacific SSTs was present prior to the onset of the active Australian region TC activity. Ramsay et al. (2008) also observed that during a positive ENSO phase there was decreased cyclonic vorticity over the Australian region, in conjunction with increased vertical wind shear and subsidence. The combination of decreased cyclonic vorticity, increased vertical wind shear, and increased subsidence lead to atmospheric conditions over Australia detrimental to the development of the long-lasting organized convection necessary for TC development. Similarly, Kuleshov et al. (2008) presented statistical results on the connection between TC frequency in the Southern Hemisphere and ENSO that support the Ramsay et al. (2008) results.

2.3 Cross-Hemispheric Global Teleconnections

During the 1950s, pioneering work done by Radok and Grant (1957) and Ballenzweig (1959) led to a better understanding of the role of large-scale variations in the global circulation in long-range forecasting. Radok and Grant (1957) specifically looked at the upper-air record over Australia and New Zealand to identify Southern Hemispheric patterns prevalent during different seasons, and began using those patterns for long-range forecasting. They also noted a possible connection between the Northern Hemispheric flow and the resulting Southern Hemispheric flow during November 1950, which may be important to understanding the variability of the atmospheric pattern of the Southern Hemisphere. Ballenzweig (1959) investigated the role of large-scale circulation teleconnections to TC formation in the Atlantic (discussed in the previous section).

Webster and Holton (1982) developed a theoretical dynamical framework of cross-hemispheric (cross-equatorial) teleconnection patterns. The authors used a barotropic model with a free surface (namely the shallow water equations) to study the effect a longitudinally asymmetric base state would have on global patterns through different forcings. The model was initially run using zonally-symmetric basic state conditions, which confirmed the development of a critical line that mid-latitude forcings could not penetrate. This result confirms the work of Charney (1969) and Bennett and Young (1971), who claimed that mid-latitude forcings could not penetrate into the equatorial regions.

However, when the model was conditioned with a longitudinally asymmetric base state, the weak westerly and strong westerly cases were found to have a response in the equatorial and high-latitude regions of the other hemisphere (Webster and Holton 1982). Thus the large-scale disturbances in the mid-latitudes propagated past the critical line that would be predicted using a zonally-symmetric base state. Webster and Holton claimed this was possible only if there existed a westerly wind duct within a longitudinal zone. Additionally, it was found that the amplitude of the response in the other hemisphere or the equatorial region was proportional to the magnitude of the westerlies in the equatorial duct. The authors argue that these results suggest mid-latitude disturbances can be reflected at a tropical critical line or propagate into the other hemisphere depending on the zonal wind distribution in the tropics (Webster and Holton 1982), thus allowing for cross-hemispheric teleconnections.

Love (1985) showed that events occurring in the mid-latitudes in one hemisphere could lead to the development of TCs in the other hemisphere. Love specifically investigated TCs developing in the Pacific and Indian Oceans. His analysis also indicated that a transition from a pattern not conducive to one that is conducive to TC formation is related to an intensification of the winter hemisphere's Hadley circulation. In general, the mid-latitude disturbances preceded TC development by

three days and were located along the same longitude. The teleconnections therefore ranged from the subtropical ridge in one hemisphere to the subtropical ridge in the other hemisphere. While this work is not directly applicable to seasonal predictions of the number of TCs, it is likely that similar interactions can be occurring on the longer time scales.

Elsner and Kocher (2000) investigated the role the North American Oscillation (NAO) in global TC activity. They found that an index of the global TC activity was moderately correlated with NAO, but not with indices associated with ENSO. The authors speculate that the dynamical mechanism is related to changes in the global-atmosphere ocean circulations and the fact that the NAO displays these pattern changes across a wide range of atmospheric scales. Finally, Elsner and Kocher (2000) suggested that other extratropical forcings should be investigated for their ability to describe the interannual variability of TC frequency globally.

Much work has been done on the role of global teleconnections modulating various atmospheric parameters, such as SSTs, from the Northern Hemisphere to the Southern Hemisphere and vice versa. However, there are few studies relating cross-hemispheric patterns to TC development in the opposite hemisphere. Recently, Klotzbach and Gray (2003) have included Southern Hemispheric predictors for their North Atlantic TC forecasts, which will be discussed in more detail in the section 2.5.

2.4 Australian Region Prediction Schemes

From earlier suggestions by Ballenzweig (1959) that large-scale circulation anomalies can be used to predict the characteristics of seasonal TC frequency variability, Nicholls (1979) proposed a possible prediction scheme for the number of TCs per season in the Australian region. He found that anomalies in the pressure field over Australia remained entrenched for a while, which meant that surface sea-level pressure from

earlier months could be used to predict later months TC activity. Specifically, Nicholls found a correlation of +0.63 between the winter and following summer pressures at Darwin. Nicholls subsequently calculated that the winter pressure at Darwin (part of the SOI) had a high negative correlation with TC frequency in the Australian region and therefore could be used to predict the number of TCs in the following season. For the years 1959 to 1974 Nicholls calculated a correlation of −0.68 between the June, July, August pressure anomalies at Darwin and the TC frequency for the entire Australian basin.

The method proposed by Nicholls (1979) was used by Nicholls (1985) to predict the number of TC days for the entire Australian region. Nicholls confirmed the strong correlation of his previous work between TC numbers and winter pressure at Darwin. Nicholls (1985) used TC data from 1909/10 to 1982/83 season, correlating the entire dataset as well as subsets to confirm the statistical relationship between Australian TCs and surface pressure. Over this 74-yr period, the number of TCs and TC days increased substantially. Nicholls attributes this trend in TC characteristics to the improvements of observing systems (e.g., satellites) in detecting and properly identifying TCs. Therefore, Nicholls assumes there would be no trend in the TC data when adjusted for improvements in reporting. A cubic spline was used to de-trend the time series of TC numbers and TC days due to errors in reporting. They were then correlated to the number of TCs and TC days. The method proposed by Nicholls (1979) was tested by making a prediction of TC days. This was done because of the high correlation of the number of TC days with Darwin July–September pressure (−0.54).

Nicholls (1985) used a simple linear regression between TC days and Darwin July–September mean sea level pressure to arrive at the following prediction equation:

$$\text{Cyclone Days} = 224.5 - [11.6 \times (\text{pressure} - 1000\text{mb})] \tag{2.16}$$

This prediction method was tested using the leave-one-out cross-validation technique on the TC data from $1959/60 - 1982/83$. The mean absolute error (MAE) for the 25 forecasts was 9.4 days, compared to the persistence forecast MAE of 19.5 days, and climatological forecast MAE of 12.7 days. This forecast equation, while simple, presents an improvement over both persistence and climatological forecasts.

Another approach to predict TCs in the Australian region was developed by Solow and Nicholls (1990) who use a Poisson statistical model to account for possible missing observations from early in the TC record. A Poisson model is typically used for seasonal prediction schemes under two different conditions: the TC data record has a non-linear trend that may or may not be artificial, or when the counts are particularly small, as in the case of predicting the number of intense TCs in a given year. A regression using a Poisson distribution

$$\Pr\{I = \mathrm{n}|\mu\} = \frac{\mu^n e^{-\mu}}{n!}, \tag{2.17}$$

where I is the probability of occurrence, $n = 0, 1, 2, 3$, etc., and μ is the Poisson parameter (Elsner and Schmertmann 1993), can be dependent on one or more variables as a non-linear function

$$\mu_i = \exp[b_0 + \sum_{k=1}^{n} b_k x_k], \tag{2.18}$$

or taking the natural log,

$$\ln(\mu_i) = b_0 + \sum_{k=1}^{n} b_k x_k, \tag{2.19}$$

where (2.19) explicitly requires that the predicted Poisson mean is not negative. Therefore the distribution of I varies with the independent variables $x_i = x_1$, x_2, $\ldots$, x_k (Wilks 2005). The unknown parameters, b_k, are estimated by maximizing the Poisson log-likelihood procedure, which must be solved numerically. Thus, the expected value of the modeled parameter can be written as

$$E(\mathrm{I}|\, x) = \exp[b_0 + \sum_{i=1}^{k} b_k x_k], \tag{2.20}$$

and from (2.20), the expected value can never be less than zero (Wilks 2005). A Poisson scheme developed by Solow and Nicholls (1990) was done to accurately represent the TC data record in order to not preclude any real trends in the data while still removing the trend due to changes in observations of TCs. The resulting fitted model was

$$\mathrm{m}_t^* = \exp(2.30 + 0.021X_t), \tag{2.21}$$

where m_t^* is the expected number of TCs for the predicted season and X_t is the September SOI index preceding the beginning of the TC season and is normalized to a mean of zero with standard deviation of 10. This model was cross-validated using the TC record from $1965/66 - 1988/89$ and yielded a mean square error 6.5. When cross-validating the entire period $1909/10 - 1988/89$, the cross-validated mean square error was 11.7, likely higher due to a larger number of anomalous years associated with poor observation techniques during the early part of the TC record.

Nicholls (1992) further tested the use of SOI as a predictor of yearly TC counts by using the first differences of SOI. The first difference method takes the difference of the previous year SOI from the current year SOI. Using the first differences of monthly SOI values, Nicholls (1992) predicts the change in TCs from the previous year. Then to make the final prediction, the previous year's TC count is added to the predicted change in the number of TCs. Nicholls found that using first differences of September–November SOI to predict the following TC season was more successful than using just the observed SOI values for TC predictions.

The prediction relationship was developed from the $1959/60 - 1978/79$ seasons and then tested on the 1979/80 to 1990/91 TC seasons. The prediction scheme root mean square errors: (1) using observed September–November SOI was 3.26; (2) using first differences of September–November SOI was 2.79; (3) using climatological forecasts was 3.71; and (4) using persistence forecasts was 4.77. Both the current year SOI and first difference SOI prediction schemes yielded superior results over the climatological

and persistence forecasts, with the first difference having a noticeable advantage over the observed SOI prediction scheme. Nicholls (1992) preferred the technique of first differences to minimize the impact of the non-stationary relationship between SOI and TC numbers in the Australian region. The author proposed a number of reasons for the non-stationary relationship including: increased spatial coverage of the tropical regions with the onset of the satellite era, changes in satellite image interpretation, and results of spurious trends in either SOI or TC numbers. With these changes in mind, the first differences provided more consistent correlations for all subsets of the TC data.

Prediction of the number of TCs for different intensities was investigated by Nicholls et al. (1998). They obtained similar results to Nicholls (1979, 1985, 1992) that confirmed the relationship between all Australian region TCs and the SOI. The relationship with SOI was then tested on different TC intensities (All TCs, >= 990 hPa, < 990 hPa and greater than 970 hPa, <= 970 hPa) for the period $1969/70 - 1995/96$. Each TC intensity block was correlated with three-month and monthly SOI averages prior to the beginning of the active Australian TC season. The correlation between SOI and all TCs was 0.65, whereas removing the weakest cyclone (> 990 hPa central pressure), the correlation value increased to 0.69. This stronger correlation was postulated to be a result of changes in identifying weak TCs, through an improved understanding of TCs. By not considering the weakest TCs, Nicholls et al. (1998) claimed that a more accurate prediction can be made for TCs with central pressures <= 990 hPa using the following equation

$$\mathrm{TC}_{<=990} = 8.5 + 0.167\mathrm{SOI}_{August}, \tag{2.22}$$

where SOI_{August} is the average August value of SOI. The decrease in observed TCs and observed August SOI values corresponds well for TCs with central pressures <= 990 hPa. The authors did not provide any statistical measure on the accuracy

of the prediction equation, but they did present graphics to illustrate the predictive ability (see Nicholls et al. 1998, Figs. 6 and 7). To predict the number of strongest TCs (central pressures < 970 hPa), Nicholls et al. (1998) derived an equation using the first difference method of Nicholls (1985), which yielded the following prediction equation

$$\delta \mathrm{TC}_{intense} = 0.126 + 0.138 \delta \mathrm{SOI}_{August}, \tag{2.23}$$

where $\delta \mathrm{TC}_{intense}$ is the change from the previous year to current year TC numbers, and $\delta \mathrm{SOI}_{August}$ is the change from the previous year to current year August SOI values. The predicted change in intense TCs ($\delta \mathrm{TC}_{intense}$) can then be added to the previous year's total number of intense TCs to get the final prediction value for the upcoming TC season. In this case, the number of intense TCs slightly (although not statistically significantly) increased, while August SOI values decreased. The authors concluded that this result indicated that SOI was not a good predictor of the number of intense TCs in the Australian region.

The predictive power of the first difference method were presented by Nicholls (1999) using a linear regression with a zero intercept and October SOI as the predictor variable. The equation

$$\delta \mathrm{TC} = 0.22 \delta \mathrm{SOI}_{October}, \tag{2.24}$$

provided skillful forecasts with root mean square error of hindcasts on independent data of 2.8, compared to the persistence forecast RMS error of 4.8. Additionally, two seasonal case studies were presented for the 1997/98 and 1998/99 seasons, which predicted 15 and 12 storms respectively and were generally good predictions with 12 TCs occurring during each season.

Predictors outside of the traditional ENSO parameter SOI have received substantially less attention in seasonal prediction schemes for the Australian region. McDonnell and Holbrook (2004a) developed a number of Poisson regression models to

predict seasonal TC activity using SOI as well as new, physically meaningful predictors. They presented Poisson regression models that predicted the number of TCs in a 2° latitude by 5° longitude grid each month using predictors from ranging SOI and equivalent potential temperature gradients to relative vorticity of varying lead times. The new predictors studied were those relating to the parameters discussed by Gray (1968). The values of the predictors were associated with their respective latitude/longitude coordinates when possible, so most of the predictors investigated were local.

Elsner and Schmertmann (1993) presented the possibility of using the Poisson regression for prediction of TCs, specifically for intense TCs, due to the fact that they were rare occurrences and the regression would always yield a positive number (see discussion above for a description of the Poisson model). The work of McDonnell and Holbrook (2004a) also utilized the Poisson regression for the same reasons. Their implementation of the regression was slightly different, as they wanted to predict the total number of TCs that occur in a grid box for a particular month of the TC season, before the season begins. McDonnell and Holbrook (2004a) used varying lead times for the predictor variables, as well as the time trends of the data. This wide variety of predictors yielded many different prediction schemes, and through utilizing the cross-validation technique, they found that the vertical saturated equivalent potential temperature gradient was the most successful predictor for Australian region TCs. For all the models, predictions improved up to a 26% over a climatological forecast, and three schemes (saturated equivalent potential temperature, thermal Gray parameters, and all-Gray parameters) yielded significant results at the 98% confidence interval.

A later study by McDonnell and Holbrook (2004b) found the best Poisson regression model used September SOI with spatial and temporal variations of vertical saturated equivalent potential temperature gradient as predictors. This scheme yielded

results 34% better than climatology and a correlation coefficient with observed seasonal TCs of +0.60. McDonnell and Holbrook (2004b) claim that this model provides better results than the first difference method using SOI alone and that their method works best for the Southwest Pacific subregion of the Australian basin.

2.5 TC Prediction Methods in Other Basins

Many different techniques have been used to predict TCs in different basins across the globe. Regression models have ranged from simple linear regressions, to simple multiple linear regression models to Poisson regression models. The following is a summary of various techniques used for prediction of seasonal TCs worldwide. A complete review of places and their techniques for seasonal tropical cyclone forecasts can be found in Camargo et al. (2007).

A significant advancement in seasonal tropical cyclone forecasting has come from William Gray and his research group at Colorado State University. The next section will outline the papers that have resulted from their work and highlight the techniques used to make forecasts at different times of year. The last section will focus on the contributions of others to the study of seasonal prediction of tropical cyclones.

2.5.1 Seasonal Prediction by Gray

For the Atlantic region, Gray (1984a,b) developed the first seasonal TC forecast scheme. In his initial work, the primary predictor was the average number of TCs, corrected by various factors such as the Quasi-biennial Oscillation (QBO), ENSO, and Caribbean sea-level pressure anomaly (SLPA). Through this scheme, minimum hurricane occurrence values were also used: no less than three hurricanes could be predicted when El Niño conditions dominated, and no less than four hurricanes could be predicted in a non-El Niño pattern. Similar forecast systems were developed for

the total number of TCs (hurricanes plus tropical storms) and hurricane days in the Atlantic region. Gray (1984b) also states that other global, as well as regional predictors for forecasting seasonal TCs should be investigated.

In later work, Gray (1990) identified a relationship between wet and dry multi-decadal trends in West African rainfall and the number of intense Atlantic hurricanes. Gray contends that we need to improve the monitoring and forecasting West African weather on multiple time scales to better understand any causal relationship with intense Atlantic hurricanes.

Gray et al. (1992) investigated extended range predictors using a least-absolute deviation (LAD) model to predict multiple seasonal TC metrics $6 - 11$ months in advance. The predicted value from a LAD method can be written as

$$\hat{y} = \hat{\beta}_0 + \sum_{j=1}^{r} \hat{\beta}_j x_j, \tag{2.25}$$

where $\hat{y}$ is the predicted TC metric, (0, 1, ... , r) are the values of β_0, β_1, ... , β_r that minimize the sum of absolute differences given by

$$\sum_{i=1}^{n} [|y_i - \beta_0 - \sum_{j=1}^{r} \beta_j x_{ij}|], \tag{2.26}$$

where n is the number of years used in the prediction scheme development and y_i is the observed value of the TC metric being predicted. The two extended range predictors were the extrapolated phase of the QBO and the extrapolated western Sahel rainfall. Seven different models are presented and cross-validated: 1) number of named storms (NS), 2) number of named storm days (NSD), 3) number of hurricanes (H), 4) number of hurricane days (NHD), 5) number of intense hurricanes (IH), 6) number of intense hurricane days (IHD), and 7) hurricane destruction potential (HDP). Unlike Gray's previous studies, this one used the cross-validation technique to determine the ability of the forecast scheme to make accurate predictions (scoring metrics will be discussed in detail in Chapter 5). The highest measure of agreement between the hindcast and

observations was for the number of named storm days model ($\rho = 0.514$), which is given by,

$$\text{NSD} = 64.072 + 1.031(1.0U_{50} + 0.252U_{30} - 0.64|U_{50} - U_{30}| + 7.149(1.0R_S + 2.39R_G) \tag{2.27}$$

where U_{50} and U_{30} are the extrapolated (November to September) upperair zonal wind at 50 and 30 hPa in ms^{-1}, respectively, R_S is the August–September western Sahel rainfall index, and R_G is the August-November Gulf of Guinea rainfall index. Each rainfall index is based on a regional average of normalized precipitation (for description of the western Sahel rainfall index calculation see Landsea and Gray 1992). The model that explained the largest variance of any TC metric was the predictive equation for the number of intense hurricanes ($r^2 = 0.581$; see their Table 9), given by

$$\text{IH} = 3.571 + 0.042(1.0U_{50} + 0.103U_{30} - 1.415|U_{50} - U_{30}| + 0.717(1.0R_S + 2.455R_G), \tag{2.28}$$

The results of all the prediction schemes yield many different skillful long-range predictions of seasonal TC activity in the Atlantic[3]. The authors stated that the strong association of seasonal TC activity and the climate system were not expected.

Two more papers by Gray et al. (1993, 1994) refined the least absolute deviation method for predicting the assortment of seven TC metrics as well as introducing a measure of net tropical cyclone (NTC) activity, where NTC is defined as

$$\text{NTC} = (\%\text{NS} + \%\text{H} + \%\text{IH} + \%\text{NSD} + \%\text{HD} + \%\text{IHD})/6, \tag{2.29}$$

where the percentage of each variable is a given seasons percentage from the long term mean of that measure's activity. The NTC activity is a combination of six of the seven separate previously defined TC metrics. In all, Gray et al. have developed

[3]Please see their Tables 8 and 10 for a full list of the final model parameters for all 7 prediction schemes.

prediction schemes for seasonal forecasts in the Atlantic basin, which are produced by 1 December, 1 June, and 1 August for the upcoming/ongoing TC season.

Klotzbach and Gray (2003) expanded their search for predictors of TC activity in the North Atlantic by using the NCEP–NCAR reanalysis data. They were looking to predict the September TC activity for the North Atlantic basin, using a total of nine different TC metrics: named storms, named storm days, hurricanes, hurricane days, intense hurricanes, intense hurricane days, tropical-only hurricanes, tropical-only named storms, and net tropical cyclone activity. From an initial set of 126 possible predictors, 25 were used in model development, but only 9 predictors had any appreciable partial correlations with September TC activity while correlating at least 0.3 with the predictand itself. Klotzbach and Gray then choose up to the best five predictors for the various TC metrics using an all-subset technique. The predictors used in the statistical forecast models spanned the globe, including zones in both the Northern and Southern hemispheres, and consisted of geopotential heights, various levels of the U and V components of the wind, and SLP. The seasonal forecasts were found to be statistically significant for all predictions of the 9 different metrics calculated on 1 August and 1 September, except for the 1 August prediction of the number of named storms.

With the success of forecasting September TC activity using global reanalysis data, Klotzbach and Gray (2004) updated the previous work of Gray et al. (1992). Using a similar all subset technique from Klotzbach and Gray (2003), an ordinary multiple linear regression scheme[4] was used to predict most metrics of TC activity $6 - 11$ months in advance. For intense hurricanes a Poisson model similar to that developed by Elsner and Schmertmann (1993) was used. Predictors for these models were generally in either the equatorial region or the Northern Hemisphere and produced hindcast skill explaining nearly 50% of the variance in the net tropical cyclone

[4]Mathematical development of multiple linear regression is done in Chapter 5

activity. Using similar global reanalysis datasets and multiple linear regression techniques, Blake and Gray (2004) and Klotzbach (2007) updated the August prediction of TC activity as they continually seek better more accurate predictors.

2.5.2 Seasonal Prediction by Others

Predicting the number of intense hurricanes or tropical cyclones is a difficult task, especially with ordinary linear or multiple linear regressions, because the possibility of predicting a negative number of events is possible. Due to the small number of storms that reach a high intensity in a given season, it is difficult to make accurate, positive predictions using simple methods that work well for other TC metrics. In order to deal with this problem, Elsner and Schmertmann (1993) used a Poisson regression model instead of a multiple linear regression model to predict the number of intense hurricanes occurring in the Atlantic basin (see the previous discussion of the Poisson model in earlier sections). They noted that a Poisson model is better suited to predicting rare events because the model will never predict a non-negative number. For counts, such as the number of intense hurricanes, this is ideal since in a given season there can never be a negative number of TC occurrences.

Elsner and Schmertmann (1993) compared the results from their Poisson model and a simple linear model to determine which would be better suited for the task of predicting the number of intense hurricanes. They found that the Poisson model made better predictions in years where there were either very few or many intense hurricanes, while a linear model performed slightly better during average years. Due to these results, the Poisson model method has been used in other basins to predict similar rare events (McDonnell and Holbrook 2004a,b; Klotzbach and Gray 2004).

In a study by Lehmiller et al. (1997), linear discriminant analysis was used to forecast whether a subbasin of the Atlantic region (Caribbean, Gulf of Mexico, Southeast U.S., and Northeast U.S.) would be active or inactive in the coming hurricane season.

The set of predictors used in this study consisted of the predictors used in previous Atlantic basin studies from Gray et al. (1992, 1993). However, these predictors were insufficient to predict hurricanes in the east coast subbasins. Therefore, additional predictors were investigated, including SLP along the east coast of the U.S., $700-200$ hPa vertical wind shear, and least squares estimated east coast SLP gradient. The updated models perform better than climatology for each of the subbasins and allows for a better sense of where an active hurricane season may occur in the Atlantic region.

In the Northwest Pacific basin, Chan et al. (1998, 2001) developed a season prediction scheme using the Projection Pursuit Regression technique. The predictors used are parameters related to ENSO, the large-scale circulation, with additional climatological and persistence predictors. The ENSO and large-scale circulation predictors are similar to those used in the Atlantic and Australian regions already discussed in this study. The Projection Pursuit Regression technique is an extension of the basic linear model and the authors used a multiple-response regression to use multiple predictor variables. This scheme was the first developed for the Northwest Pacific region and yielded measure of agreement of 0.562 for the predicted tropical cyclone activity.

The Northwest Pacific forecast scheme was updated by Chan et al. (2001) due to the inaccurate forecasts during the $1997-1998$ changing ENSO patterns. As a result, new predictors were identified for the region to better account for ENSO. The final results suggested that two schemes would be appropriate for the region, one issued in April, which is a combination of old and new scheme predictors, and an update in June to incorporate more recent data related to ENSO.

There have been other models used, such as the space-time model to predict hurricane probabilities in grid cells by Jagger and Elsner (2002). Elsner and Jagger (2004, 2006) used Bayesian modeling to predict hurricane and landfalling hurricane counts. This statistical method provides the ability to use a longer data set that can

correct differing levels of uncertainty in the data, especially with rare event scenarios. Finally, Chan (2008) recently presented a method for predicting whether the rest of the season will be above or below normal using categorizations of the early season TCs and comparing to historical seasons. This method is meant to be a mid-season update to seasonal predictions as it takes into account the numbers of storms that have already occurred during the early part of a given TC season.

Chapter 3

Data and Predictor Selection Methodology

In recent years, there has been much discussion on the reliability of TC observations. In the Australian region, Holland (1981) and Buckley et al. (2003) discussed uncertainties in the quality of observations in the Australian Bureau of Meteorology (BoM) TC best track dataset. Some of these uncertainties are a result of a lack of routine satellite observations prior to 1970. Therefore, only TCs occurring in the 1970/71 TC season, or later, are used in this study. This section describes the TC dataset and the analytic methods used in this study. Additionally, the parameters considered in this study will be defined.

3.1 Tropical cyclone data

The Australian TC season spans across years and for the purpose of this paper the first year will be used to identify the season (i.e., The 1970/71 season will be identified as the 1970 TC season) and all TCs that crossed into the NWAUS TC basin are included in this analysis. Recently, a reanalysis of TCs was undertaken for the NWAUS region ($105 - 135°$E) by Harper et al. (2008) to improve intensity estimates and make a historically consistent TC dataset for the region. This reanalysis produced substantial changes to the reported TC intensities from the BoM dataset. By comparison, only a few differences in the reported TC frequency were made. The Harper reanalysis was conducted with Woodside Petroleum Ltd. (WPL) and will be referred to as the WEL

TC dataset. A more complete discussion of the WEL TC dataset, which is used in this study, is found in Chapter 2.

3.2 SST data

The global SST data used in this study were obtained from the National Oceanic and Atmospheric Administration (NOAA) extended reconstructed SST (ERSST) dataset (Smith and Reynolds 2004) for the period January 1970–December 2005. This dataset was constructed from the most recent International Comprehensive Ocean-Atmosphere Data Set (ICOADS) and, through improved statistical methods, is able to produce a stable reconstruction, even when data is sparse. The data is available for monthly SST values on a 2° longitude by 2° latitude grid from January 1854 to present.

3.3 Global modes

Many global teleconnections previously have been identified and are routinely monitored by the NOAA/Climate Prediction Center (CPC). These modes, especially ENSO, have commonly been used to predict seasonal TC activity in global TC basins. Most of the global modes were obtained from the CPC (http://www.cdc.noaa.gov/-ClimateIndices/List/) including: Niño 3.4 SST box (5°N–5°S, 170 − 120°W), Niño 4 SST box (5°N–5°S, 160°E–150°W), Southern Oscillation Index (SOI), Northern Oscillation Index (NOI; Schwing et al. 2002), North Atlantic Oscillation (NAO; Walker and Bliss 1932), Pacific-North American pattern (PNA; Wallace and Gutzler 1981), Pacific Decadal Oscillation (PDO; Walker and Bliss 1932; Zhang et al. 1997; Mantua et al. 1997), Artic Oscillation (AO; Thompson and Wallace 1998; Higgins et al. 2000),

and Quasi-biennial Oscillation (QBO). The Indian Ocean Dipole (IOD) was calculated from the NOAA ERSST dataset (described previously) and was based on the dipole discussed by Saji et al. (1999). Because only seasonal, but not intra-seasonal parameters are being investigated in this study, the Madden-Julian Oscillation is not currently considered.

3.4 Atmospheric data

Monthly values of geopotential height, air temperature, sea level pressure, and the u- and v-components of the wind were obtained from the National Center for Environmental Prediction–National Center for Atmospheric Research (NCEP–NCAR) reanalysis dataset (Kalnay et al. 1996), which has a horizontal grid spacing of 2.5°. Except for the mean sea-level pressure, data were obtained for 17 vertical levels: 1000, 925, 850, 700, 600, 500, 400, 300, 250, 200, 120, 100, 70, 50, 30, 20, and 10 hPa. All of the variables used in this study were classified as class A variables, which indicates that the reanalysis variables are strongly influenced by observational data and are considered the most reliable (Kalnay et al. 1996).

3.5 Correlation analysis

The time series of the global modes (discussed previously) were correlated with the NWAUS TC frequency time series using the Pearson product-moment correlation. The Pearson correlation can be written as,

$$r_{xy} = \frac{\frac{1}{n}\sum_{i=1}^{n}\left[\left(x_i-\overline{x}\right)\left(y_i-\overline{y}\right)\right]}{\left[\frac{1}{n-1}\sum_{i=1}^{n}\left(x_i-\overline{x}\right)^2\right]^{1/2}\left[\frac{1}{n-1}\sum_{i=1}^{n}\left(y_i-\overline{y}\right)^2\right]^{1/2}} \tag{3.1}$$

where normal mathematical conventions apply to the notation (Wilks 2005). Each known global mode was grouped in three-month bins starting with the January–March

bin preceding the onset of the TC season, through the June–August bin following the TC season for the period $1970 - 2005$. Correlation analyses also were performed between the frequency of TCs in the NWAUS TC basin and the monthly anomaly values of SST, geopotential height, air temperature, mean sea level pressure, and the u- and v-components of the wind in three-month bins beginning with January–March (preceding the TC season) through September–November (the beginning of the TC season) over the entire observational domain. Anomalies are based on the long-term mean from $1970 - 2005$.

To determine the significance of a correlation between a TC metric and a global teleconnection variable the student t-test is used, which is defined as

$$t = \frac{r}{\sqrt{\frac{1-r^2}{N-2}}}, \tag{3.2}$$

where r represents the Pearson correlation coefficient between the TC metric and the variable it is correlated against, and N is the number of predicted years. The value obtained for t, can then be compared with the t-distribution to determine the significance of each trend. For 34 degrees of freedom $(N - 2)$ the two-sided t value is 1.6909 for the 90% confidence interval (Wilks 2005). Neither the all-TC trend $(t = 1.026)$ nor the intense-TC trend $(t = 0.058)$ is significant. Additionally, the TC time series has a serial correlation of $\sim +0.32$, which is taken into account for testing the significance of correlations values in Chapter 4.

3.6 Composite analysis

Composite analyses were calculated for the geopotential height and SLP anomaly fields by averaging the 10 most active and inactive years. The long-term means calculated for the NCEP-NCAR reanalysis dataset are based on $1968 - 1996$ values of each individual field. The most active years were: 1974, 1984, 1999, 1981, 1972,

1973, 1983, 1985, 1980, 1993, 1995 and 1998 (Table 3.1). The least active years were: 1987, 1991, 1992, 1978, 1994, 2001, 1976, 1977, 1982, and 1988 (Table 3.2). For each set of years, the individual seasons were combined, divided by the total number of years, and then subtracted from the long-term mean to produce composite maps.

Table 3.1 Most active years for NWAUS region

Year	No. of TCs
1974	11
1984	10
1999	9
1981	9
1972	8
1973	8
1983	8
1985	8
1980	7
1993	7
1995	7
1998	7

Table 3.2 Least active years for NWAUS region

Year	No. of TCs
1987	1
1991	2
1992	2
1978	2
1994	3
2001	3
1976	3
1977	4
1982	4
1988	4

Chapter 4

NWAUS Variability

4.1 NWAUS TC Variability

There are a number of different TC metrics that can be used in describing the year to year variation of Tropical Cyclones (TCs) in any given ocean basin. There are numerous ways to describe the yearly activity within an ocean basin; here, thirteen TC metrics have been chosen for the Northwest Australian (NWAUS) region. They are:

(1) Number of TCs;

(2) Number of Intense TCs;

(3) Number of TC days;

(4) Number of Intense TC days;

(5) Number of Landfalling TCs;

(6) Number of Intense Landfalling TCs;

(7) Accumulated Cyclone Energy (ACE);

(8) Power Dissipation Index (PDI);

(9) Mean Storm Duration;

(10) Intense Mean Storm Duration;

(11) Season Start Day;

(12) Season End Date; and

(13) Season Length.

An intense TC is considered to be a TC with a minimum central pressure of 970 hPa or lower and an intense TC day has at least one intense TC occurring on that day (Tables 4.1 and 4.2). Each of these metrics have been calculated using the Woodside Petroleum Ltd. (WPL) TC dataset, which was discussed in detail in Chapter 2.

Recently, there has been a substantial amount of work examining trends of TC metrics within ocean basins around the world. Kossin et al. (2007) conducted a reanalysis of yearly hurricane variability using a new global reanalysis dataset from Knapp and Kossin (2007). Kossin et al. (2007) concluded that using the globally consistent dataset only trends in North Atlantic TCs are significant. However, the reanalysis only includes data from July 1983 to December 2005, which is not long enough to identify multi-decadal signals present in the TC time series. As described below, the Northwest Australian region does not exhibit any significant upward or downward linear trends in any of the TC metrics mentioned previously.

The NWAUS TC basin averaged 5.5 TCs per year during the 39-yr period from the 1970 to 2008 TC seasons with a standard deviation of 2.4 TCs (Fig. 4.1). In general, there is a small downward linear trend in the frequency of all TCs over this period, but the slope of the trend is not significantly different from zero. For intense TCs, with minimum central pressures below 970 hPa, there is no discernable linear tread over the same period (Fig. 4.1). The significance of the linear trends of all TC metrics is determined by a hypothesis test on the slopes of the trend lines. If the slope is not significantly different than zero, then the time series of the TC metric is considered to have no discernible linear trend through time.

Table 4.1 Summary of TC metrics for the NWAUS region.

Years	No. of TCs	No. of Intense TCs	TC Days	Intense TC Days	TC Landfall	Intense TC Landfall
1970	5	2	37.75	3	5	1
1971	6	3	40.75	9.75	1	0
1972	8	5	61.75	10.5	3	2
1973	8	4	73	6.5	4	2
1974	11	3	76	10.25	4	1
1975	6	3	48.75	12.5	2	2
1976	4	2	24.5	2.25	2	1
1977	4	3	35.5	12.5	1	1
1978	2	1	13	3.5	1	1
1979	6	5	51.5	16.25	3	3
1980	7	4	63	15	1	1
1981	9	2	68.25	4.75	6	0
1982	4	2	31.25	3.25	3	1
1983	8	4	45.25	7.5	3	2
1984	10	6	102.25	14.25	5	1
1985	8	2	50	4.5	1	0
1986	4	2	32.25	3.25	2	2
1987	1	1	6.25	2	0	0
1988	4	4	31	9.75	3	2
1989	5	3	43.25	6.25	1	0
1990	5	1	36.5	3.5	1	0
1991	2	2	15.25	6	1	0
1992	2	0	17.5	0	0	0
1993	7	4	55.25	9	1	0
1994	3	3	24	8.25	3	2
1995	7	5	59.25	11.25	4	3
1996	5	2	35.75	2.75	1	1
1997	5	3	40.25	5	3	1
1998	7	7	49	18.25	5	1
1999	9	6	75.75	13.25	4	2
2000	5	2	36.75	6	2	1
2001	3	1	16	2.5	1	1
2002	6	2	43	7.75	3	0
2003	5	4	38.5	13.75	3	3
2004	4	1	20.25	3.5	2	1
2005	7	4	44.75	8.25	5	1
2006	3	3	25.5	7.25	3	2
2007	5	3	35.25	8	1	0
2008	8	2	49.5	5.5	2	1
Mean	5.5	2.94	42.03	7.61	2.42	1.11
Std. Dev.	2.38	1.58	20.59	4.55	1.52	0.92

Table 4.2 Summary of TC metrics for the NWAUS region cont.

Years	ACE	PDI	Mean Storm Duration	Intense Mean Storm Duration	Start Day	End Day	Season Length
1970	4.97	4.14	7.55	1.5	331	88	122
1971	7.63	9.07	6.79	3.25	336	88	117
1972	11.29	11.76	7.72	2.1	373	120	112
1973	11.49	10.28	9.12	1.62	321	84	128
1974	15.31	17.47	6.91	3.42	301	145	209
1975	13.19	17.77	8.12	4.17	334	76	107
1976	4.34	4.1	6.12	1.12	371	123	117
1977	8.99	11.94	8.88	4.17	375	104	94
1978	0.45	0.26	6.5	3.5	407	73	31
1979	12.82	16.92	8.58	3.25	369	88	84
1980	14.94	18.39	9	3.75	346	77	96
1981	6.07	3.8	7.58	2.38	334	66	97
1982	4.98	4.83	7.81	1.62	367	119	117
1983	8.17	8.49	5.66	1.88	330	63	98
1984	13.67	12.7	10.22	2.38	337	114	142
1985	8.76	8.84	6.25	2.25	329	99	135
1986	3.88	3.77	8.06	1.62	380	107	92
1987	2.02	2.52	6.25	2	402	43	6
1988	6.49	7.57	7.75	2.44	346	114	133
1989	4.71	4	5.65	2.08	369	85	81
1990	5.47	5.82	7.3	3.5	342	110	133
1991	3.18	4.61	7.62	3	422	103	46
1992	0.94	0.57	8.75	0	389	103	79
1993	8.9	9.88	7.89	2.25	349	102	118
1994	5.28	7.08	8	2.75	346	98	117
1995	8.18	8.14	8.46	2.25	335	102	132
1996	3.66	2.74	7.15	1.38	343	137	159
1997	5.38	6.07	8.05	1.67	358	48	55
1998	16.15	24.1	7	2.61	334	98	129
1999	16.18	18.93	8.42	2.21	342	110	133
2000	6.05	7.4	7.35	3	335	115	145
2001	2.68	3.96	5.33	2.5	323	105	147
2002	5.57	5.56	7.17	3.88	386	98	77
2003	10.98	13.26	7.7	3.44	350	87	102
2004	3.7	5.03	50.6	3.5	364	73	74
2005	8.36	10.16	6.39	2.06	368	117	114
2006	4.91	5.98	8.5	2.42	429	89	25
2007	8.05	8.98	7.05	2.67	360	114	119
2008	9.21	10.33	7.07	2.75	323	119	161
Mean	7.59	8.67	7.55	2.54	356	97.44	106.44
Std. Dev.	4.36	5.67	1.14	0.91	29.14	22.55	41.09

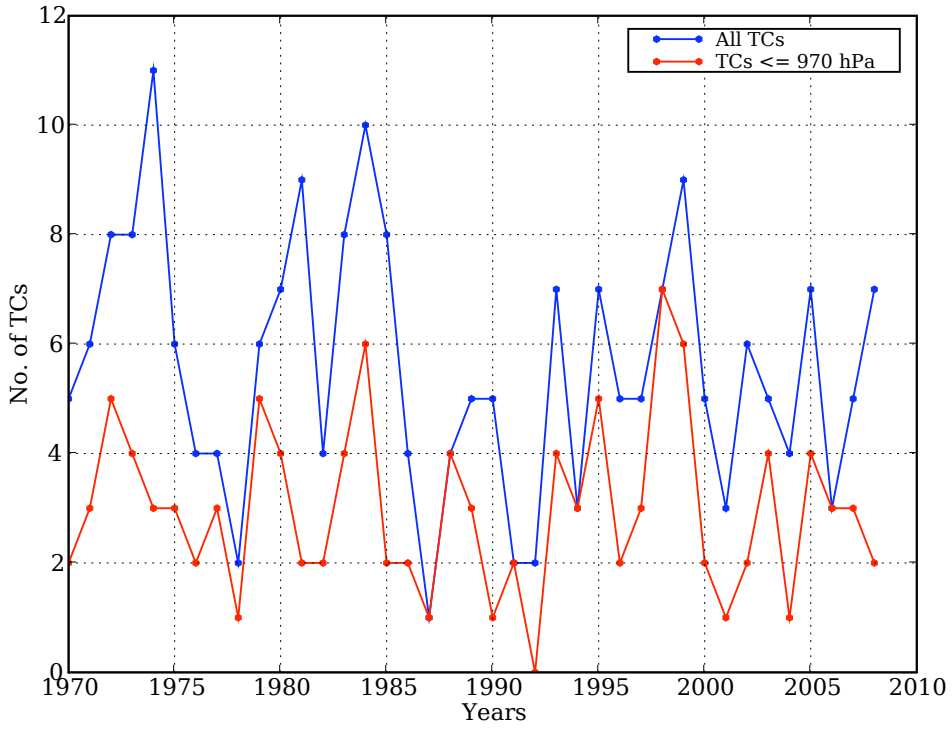

Figure 4.1 Time series of all the TCs (blue) in the Northwest Australian region ($105 - 135°$E) and the number of TCs with minimum central pressure less than 970 hPa (red) for the seasons from 1970 to 2009.

For the number of TC days and intense TC days similar trends are apparent (Fig. 4.2). Again neither trend is significant at the 90% confidence interval as the t values are 1.31 and 0.247 for TC days and intense TC days, respectively. The average number of TC days in the NWAUS region is 42 days with a standard deviation of 20.6 days.

Of great importance to population centers along the Northwest Australian coast are the number of TCs that make landfall. Part of the region is bounded by the Gulf of Carpentia, where any storm forming in the gulf is likely to make landfall and will invariably affect coastal regions. On average 3 TCs make landfall each year where ~ 1 of those landfall storms is an intense TC. Neither all landfalling TCs or intense landfalling TCs exhibit any linear trend (4.3).

The Accumulated Cyclone Energy (ACE) and Power Dissipation Index (PDI) are both calculated from the maximum sustained wind, which is determined using the current intensity estimates fitted to the Dvorak (1984) table utilizing the following parameter

$$V_{\max} = 5.37CI^{1.34}. \tag{4.1}$$

The ACE is defined as,

$$ACE = 10^{-4} \sum v_{\max}^2 \tag{4.2}$$

where v_{max} is the maximum sustained wind speed (Bell et al. 2000), and is accumulated over the season to give an estimate of the total length and strength of a given TC season. The PDI is defined as

$$PDI = \int_0^\tau v_{\max}^3 dt \approx \sum_{i=1}^{\tau} (v_{\max_i}^3 \cdot \Delta t), \tag{4.3}$$

where v_{max} is again the maximum sustained wind speed for a given time, t is time, and τ is the lifetime of a given storm, and the integral is calculated using the left endpoint approximation. The PDI is then summed over all TCs occurring during a given TC season to get the seasonal value. These indices are used to give a more

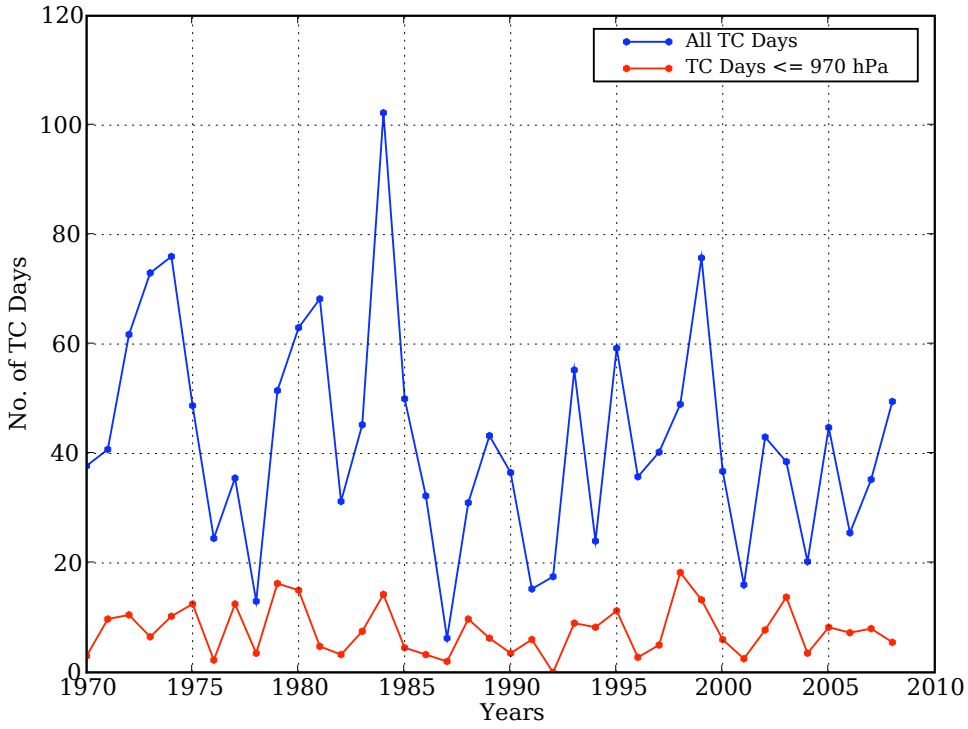

Figure 4.2 Time series of all TC days (blue) in the Northwest Australian region ($105 - 135°$E) and the number of TC days with minimum central pressure less than 970 hPa (red) for the seasons from 1970 to 2009.

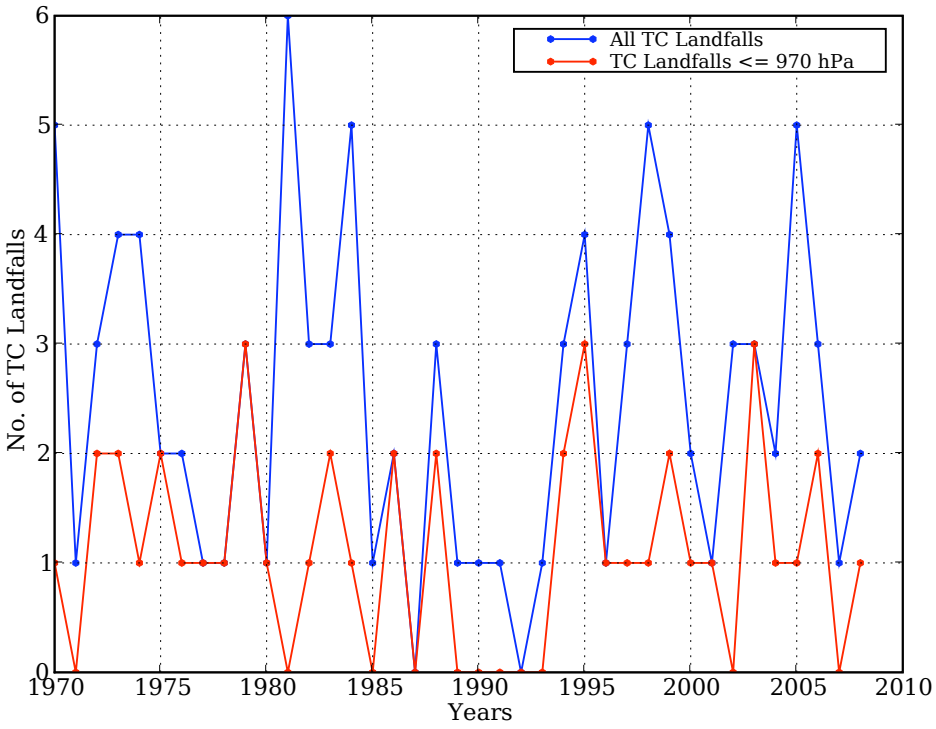

Figure 4.3 Time series of the number of TC landfalls (blue) in the Northwest Australian region ($105 - 135°$E) and the number of intense TC landfalls (red) for the seasons from 1970 to 2009.

accurate assessment of the total strength of the TC season. Simply looking at the number of TCs or TC days during a given season may not signify the true impact of the season. For example, if there were only three TCs in a season, but they were all intense and lasted for longer than average, the ACE and PDI values would be able to assess that in one statistic instead of two. The year to year fluctuations are evident in (Fig. 4.4), however, neither metric contains a trends significant at the 90% confidence interval. The t values are 1.011 and 0.492 for ACE and PDI respectively (Fig. 4.4).

The mean duration of storms is calculated from the number of TCs divided by the number of storms in a given year. The NWAUS region does not exhibit large year to year variations in mean storm duration (Fig. 4.5) with an average of 7.5 days and a standard deviation of 1.1 days. On average, storms in the NWAUS region are at intense strength for only 2.5 days per season with a standard deviation of ~ 1 day.

The NWAUS region TC season typically runs from November to April (Fig. 4.6), with the average date of the first storm forming on December 22nd and the last storm ending on April 7th. TCs can form outside the typical seasonal time frame, but in the 39 year record there have only been three TCs (one in October and two in May) that have formed outside of that time period (Fig. 4.6). Seasonal start dates are slightly more variable than season end dates, with standard deviations of 29 and 22.5 days, respectively. The number of TCs that form in a season is highly correlated (~ -0.67) with the season start date, but is not significantly correlated with season end date ($\sim +0.2$). Additionally, the range of yearly TC counts have varied from one TC in 1987 up to eleven in 1974 and the number of times each count has occurred is fairly well distributed for the period 1970 to 2008 (Fig. 4.7).

It is commonly believed that a NWAUS TC season in which the first storm forms before Christmas is considered to have an early start (Buckley 2009, personal communication). Inspecting the season start dates for the 39 year period in this study,

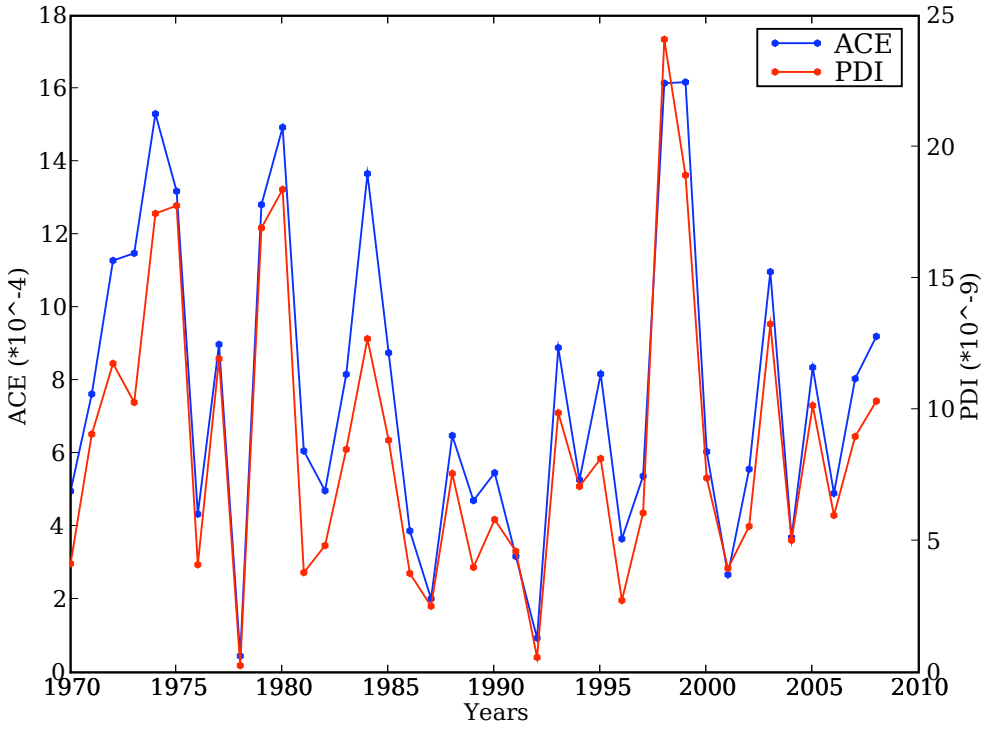

Figure 4.4 Time series of Accumulated Cyclone Energy (ACE; blue) with units of 10^4 m^2 s^2 in the Northwest Australian region ($105 - 135°E$) and the Power Dissipation Index (PDI; red) with units of 10^9 m^3 s^2 for the seasons from 1970 to 2009.

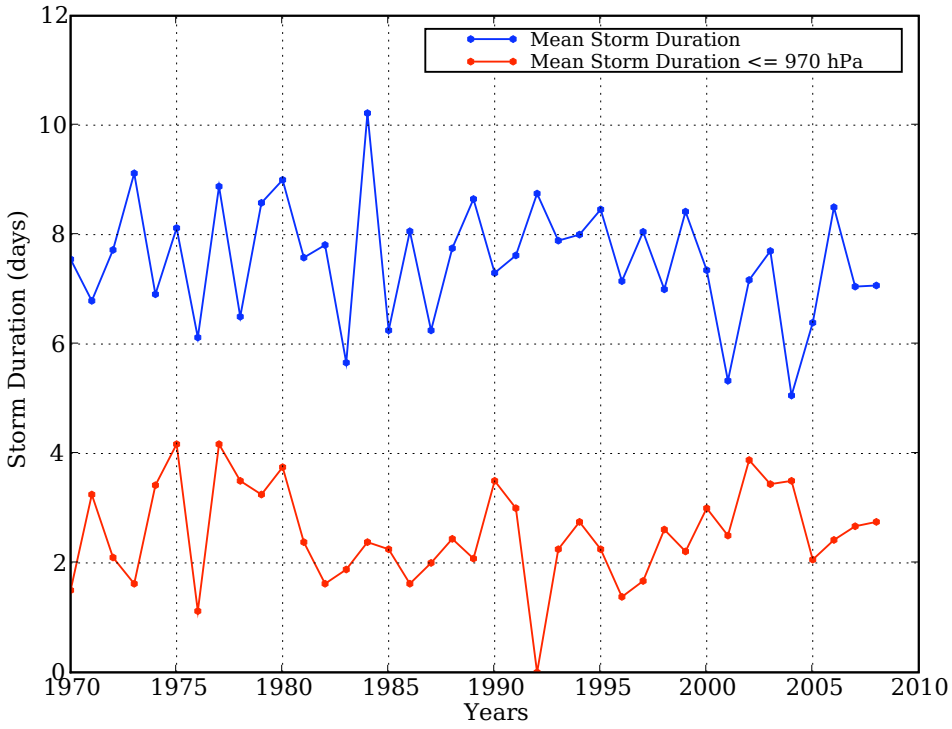

Figure 4.5 Time series of mean storm duration (blue) and mean intense storm duration (red) in the Northwest Australian region ($105 - 135°$E) for the 1970 to 2008 seasons.

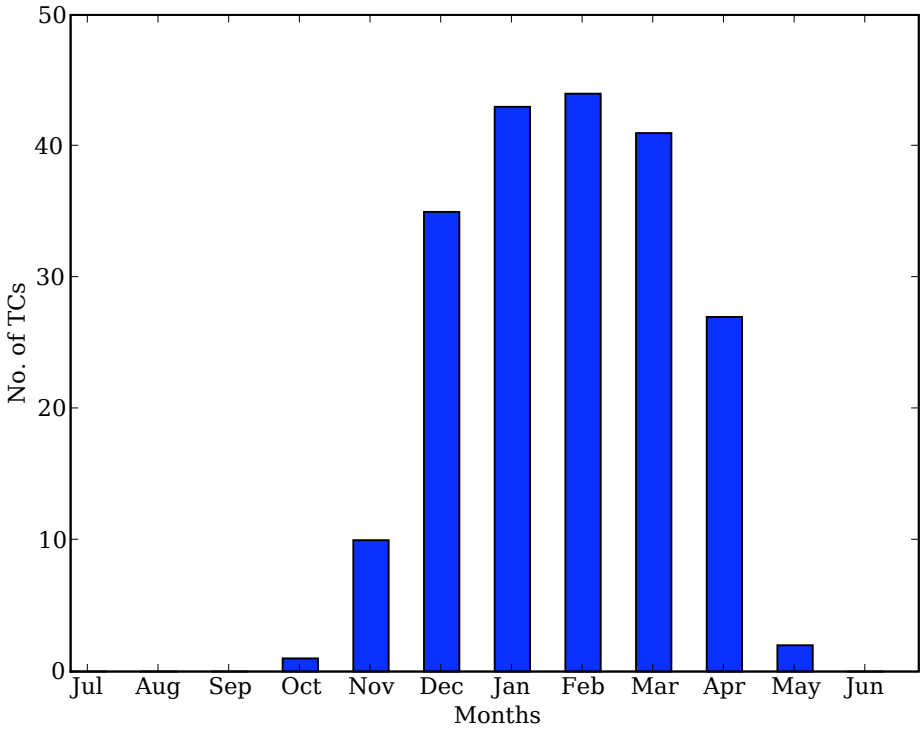

Figure 4.6 The number of TCs that began in each calendar month in the Northwest Australian region during the period 1970 to 2005.

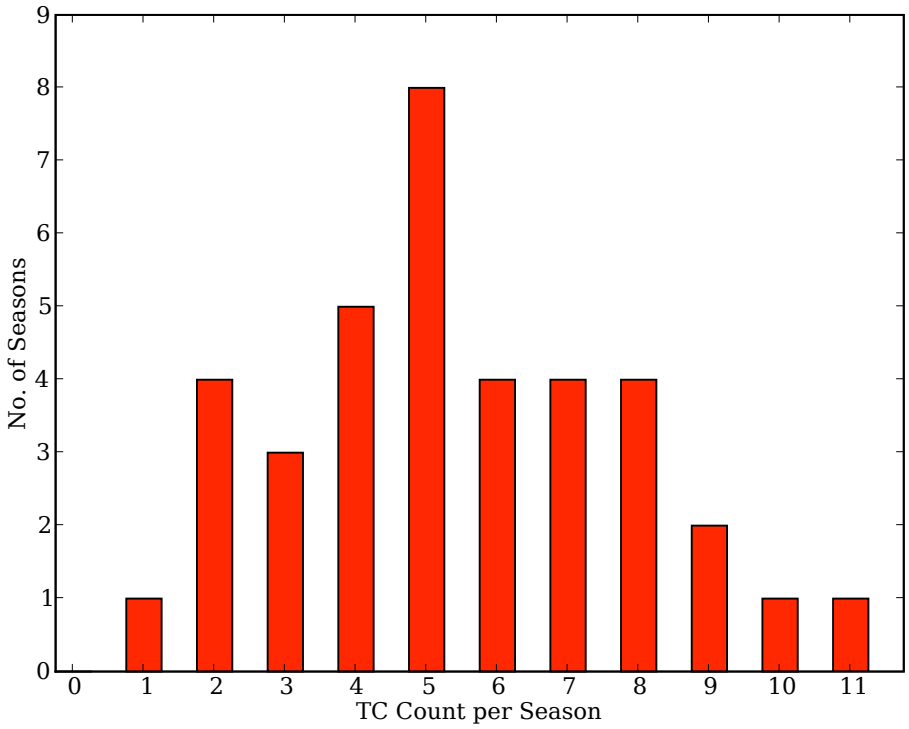

Figure 4.7 The number of TC seasons that had TC counts ranging from 1 to 11 for the Northwest Australian region during the period 1970 to 2005.

57.5% of the seasons began on or before December 25th. Clearly, with over half of the seasons beginning on or before Christmas, a storm forming in the NWAUS region during that time is not all that surprising.

A late starting NWAUS TC season is one in which the first storm does not form until February or later (Buckley 2009, personal communication). Only four seasons on record (1978, 1987, 1991, 2006) have started as late as 1 February, in fact they all started after 6 February. All of these seasons had well below average (three or less) number of TCs occurring in those seasons.

The middle 50% of the seasonal start date range from 335 to 370 (December 1st to January 5th), which is a total of 19 seasons, with ten seasons in the first and last quartiles. An early start (prior to 1 December) to the NWAUS region TC season increases the likelihood of an above-average number of TCs occurring during that season. Similarly, if a season does not have its first storm forms after 5 January, it is more likely to have a well below average number of TCs occurring during that season.

Computing season length from each start and end date yield an average season length of 106 days with a standard deviation of 41 days. An earlier starting season is more likely to have a longer season than one that starts late. Additionally, a late starting season is more likely to have a well below average season length compared to the middle 50% of seasons.

No statistically significant linear trends were found in any of the TC metrics discussed above; however, there could be other dominant modes of variation in the TC time series. To determine if there are other common frequencies within some of the TC metrics a wavelet analysis can be conducted. A Morlet wavelet analysis (Torrence and Campo 1998) is one of several different types of wavelet bases that can be used to perform the analysis. The Morlet wavelet function, ψ_0, can be defined as a function on a nondimensional "time" parameter, η,

$$\psi_0(\eta) = \pi^{-1/4} e^{i\omega_0 \eta} e^{-\eta^2/2} \tag{4.4}$$

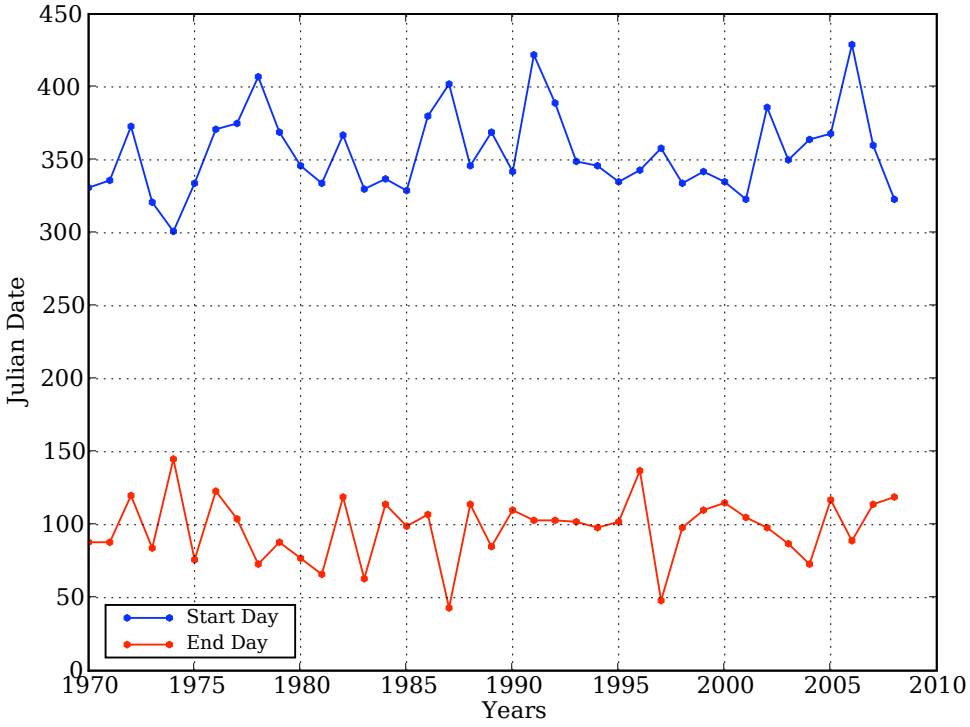

Figure 4.8 The Julian start date (blue) and end date (red) in the Northwest Australian region ($105 - 135°$E) for the seasons from 1970 to 2008.

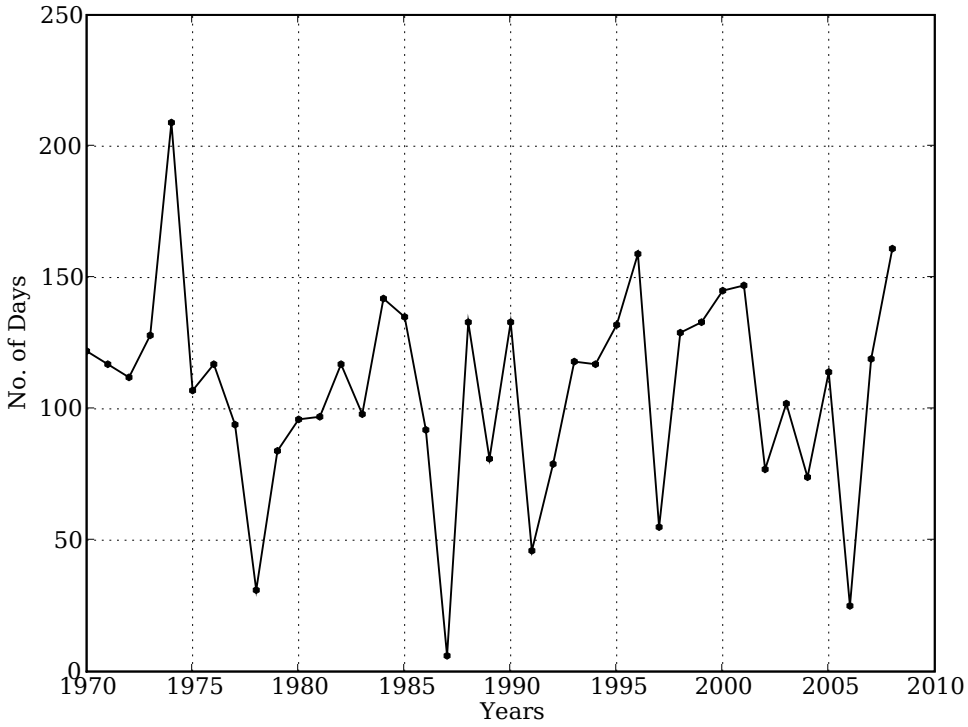

Figure 4.9 The Northwest Australian region (105−135°E) TC season length measured in days for the seasons from 1970 to 2009.

where ω_0 is the nondimensional frequency. To assess the wavelet function along in time, "scaled wavelets" can be defined as,

$$\psi\left[\frac{(n'-n)\delta t}{s}\right] = \left(\frac{\delta t}{s}\right)^{1/2} \psi_0\left[\frac{(n'-n)\delta t}{s}\right] \tag{4.5}$$

where s is the "dilation" parameter used to change the scale and n translates the function to slide in time. A normalization of the total energy to keep the scale wavelet constant is accomplished by the factor $s^{-1/2}$. The wavelet transform can then be calculated with the individual time series values, x_n, with time index n, and each value is separated by a constant time interval δt, by,

$$W_n(s) = \sum_{n'=0}^{N-1} x_{n'} \psi^*\left[\frac{(n'-n)\delta t}{s}\right] \tag{4.6}$$

where ψ^* is the complex conjugate of the wavelet function. The wavelet transform can then be evaluated for various values of the scale s as well as through time, n, between the start and end dates. The power spectra of the wavelet analyses are calculated by the absolute value squared of the wavelet transform (Torrence and Campo 1998).

A wavelet analysis of the time series of the number of TCs for the NWAUS region identifies two major peaks in the wavelet power spectra (Fig. 4.10a) at $4-6$ years. The peak in the wavelet power spectra around 12 years is largely influenced by numerical effects from a relatively short time series. A different wavelet function can be used to determine the viability of the decadal signal. The Mexican Hat wavelet function

$$\psi_0(\eta) = (\frac{2}{\sqrt{3}}\pi^{-1/4})(1-\eta^2)e^{-\eta^2/2}, \tag{4.7}$$

can be used as an alternative to the morlet wavelet to determine if there is a signal at the decadal time range of TC numbers (Fig. 4.10b).

Due to the relatively short reliable TC record for the NWAUS region, multidecadal variability cannot be ascertained from this wavelet analysis and therefore no multi-decadal trend can be reliably identified. With only a little over three decades in the

dataset, the decadal signal could be spurious; however, with the decadal signal appearing in both wavelet power spectrums (Morlet and Mexican Hat), we can be more confident that there is a signal. Similar results appear for a wavlet analysis of the number of TC days (Figs. 4.11).

4.2 MJO

In previous sections, the inter-annual variability of various TC metrics have been discussed. On intra-seasonal time scales the Madden-Julian Oscillation (MJO; Madden and Julian 1994) has been known to influence TC development in the Australian region (Hall et al. 2001). The $40 - 50$ day oscillation of wavenumber 1 generally consists of two phases that either enhance or inhibit convection in the Eastern Hemisphere, the "wet" and "dry" phases, respectively (Hendon and Liebmann 1994). Hall et al. (2001) created four categories for the MJO cycle and a fifth category of None for the Australian region were they found that during their category B, the western Australian region had enhanced cyclogenesis, where as during category D the western region had reduced activity. Cyclones that formed when during a time when no active or inactive MJO cycle could be determine (category None), cyclogenesis rates were at or just above average (Hall et al. 2001).

Recently, Wheeler and Hendon (2004) developed a new multivariate MJO index, which is used by the Australian Bureau of Meteorology for monitoring the current state of the MJO as well as using it in an intra-seasonal prediction scheme for probabilistic forecasting of TC formation. Their index identifies eight phases and a central weak MJO category. Wheeler and Hendon (2004) use Empirical Orthogonal Functions (EOFs) and minimal filtering to isolate the MJO signal, similar to Lo and Hendon (2000). Using this new MJO index to identify the influence of the MJO on NWAUS TCs similar results of Hall et al. (2001) were found. During phase 4 and 5 of the MJO

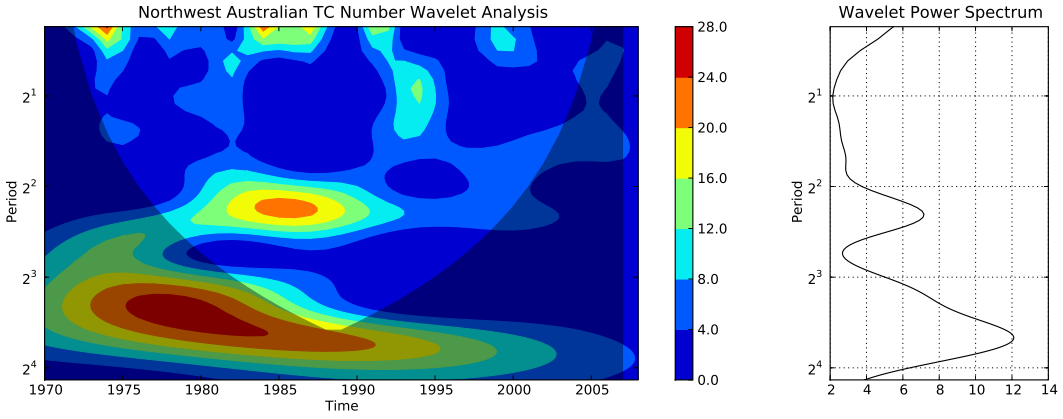

(a)

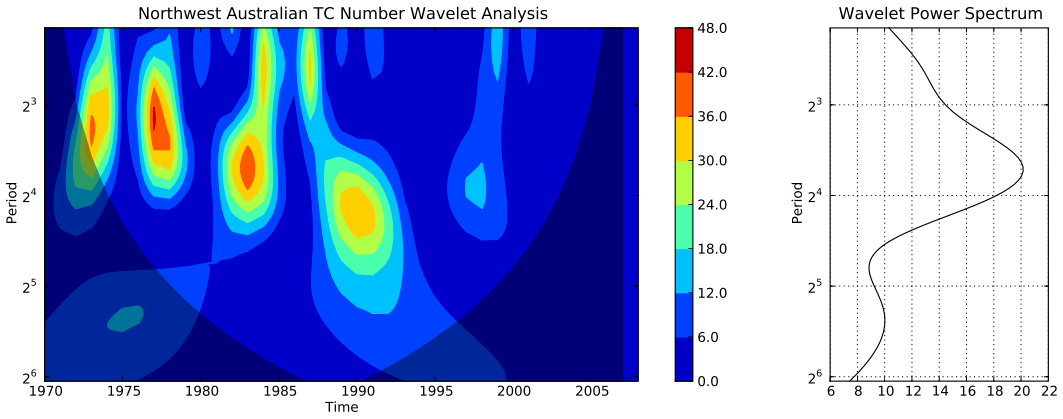

(b)

Figure 4.10 Wavelet power spectra of all TCs in the Northwest Australian region using the (a) Morlet mother wavelet and (b) Mexican hat mother wavelet. On the left had side is the wavelet scalogram of the time series (count^2) over the time period $1970 - 2008$ versus the Period (in years) and on the right side is the wavelet power spectrum (count^2) versus the period (in years). The shaded regions indicate the "cone of influence", where edge effects become important.

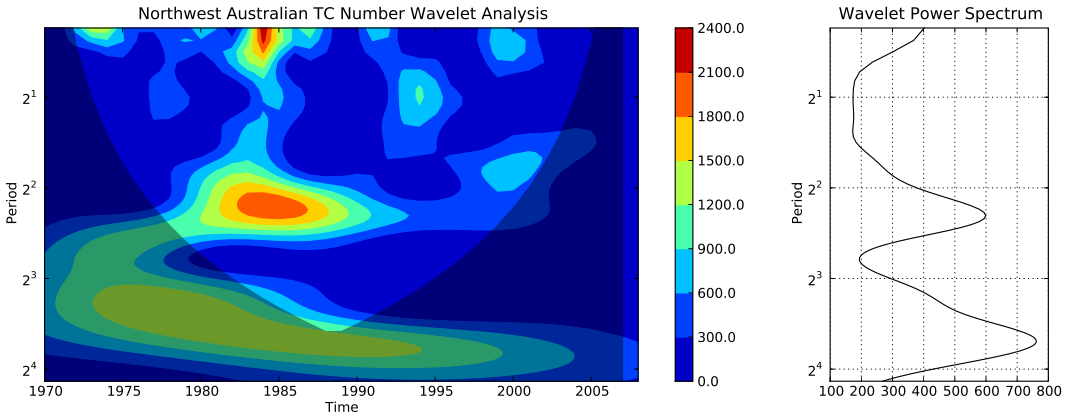

(a)

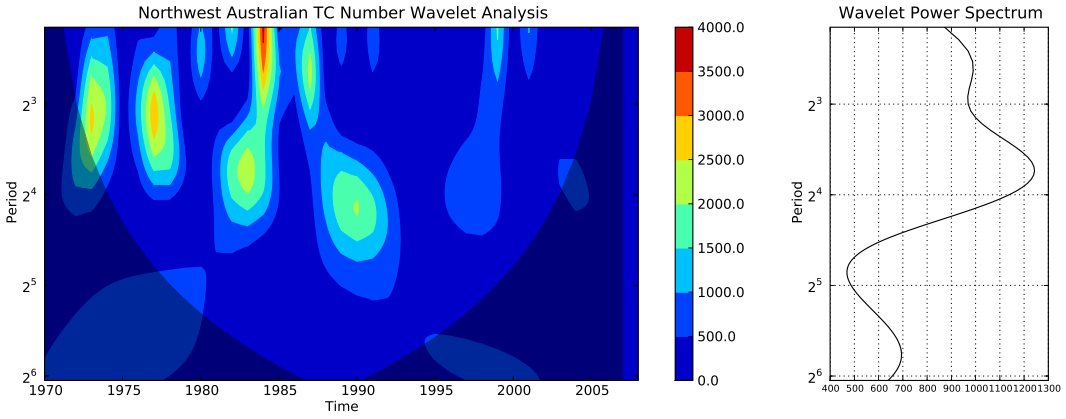

(b)

Figure 4.11 Same as in Fig. 4.10 except for TC days.

cycle, there was a statistically increased number of storms forming in the NWAUS region, significant at the 95% level. However, the number of TCs that formed during other phases was not statistically significant different from climatology.

The MJO has been used extensively for intra-seasonal prediction of TC formation, especially within the Australian region. However, can the MJO be used as a seasonal predictor? To answer this question the number of MJO passages from phase 3 to phase 4 were investigated for how well they relate to seasonal TC counts. There is almost no correlation between the two, and therefore it is not deemed to be a useful seasonal predictor.

4.3 ENSO Modes

There is considerable research on the relationship between Australian region TCs and various indicators of the mode of the El Niño–Southern Oscillation (ENSO) (e.g., Nicholls 1979, 1985, 1992; Revell and Goulter 1986; Solow and Nicholls 1990; Evans and Allan 1992; Nicholls et al. 1998; Broadbridge and Hanstrum 1998; Ramsay et al. 2008). Most studies that encompass the entire Australian region have found a significant relationship between TC activity and ENSO activity. This relationship is due mainly to the fact that a major part of the Australian region is directly impacted by changes in the Walker circulation, which is related to the convective activity in the western part of the Pacific Ocean basin. Additionally, in numerous prediction schemes for the Australian region ENSO is one of the main predictors. This section will investigate the different ENSO variables and determine whether they explain a large portion of the variance of TCs in the NWAUS region.

4.3.1 Niño SSTAs

There are numerous variables that can be used to identify the state of ENSO, including both atmospheric and oceanic variables. The variability of the Southern Oscillation first was noted by fisherman working off the coast of Peru, who noticed that during years when SSTs were warmer than normal there were fewer fish in the region. Therefore, one common way to identify the state of ENSO is to use one of a number of different SST regions. There are four areas of tropical Pacific SSTs that are commonly used, extreme Eastern Tropical Pacific SSTs termed Niño 1+2 ($0-10°$S, $90-80°$W), Eastern Tropical Pacific SSTs termed Niño 3 (5°N-5°S, $150-90°$W), Central Tropical Pacific SSTs termed Niño 4 (5°N-5°S, 160°E-150°W), and East-Central Tropical Pacific SSTs termed Niño 3.4, which is a combination of the Niño 3 and Niño 4 SSTs (5°N-5°S, $170-120°$W). Often the values for these SST boxes are reported as anomalies, defined as the difference between the current time period and some long term mean (typically 30 years). In this study the Niño 3.4 and Niño 4 boxes are used with anomalies from the 1971-2000 long term mean. When a large positive (negative) SSTA in either the Niño 3.4 or Niño 4 box occurs, it is associated with an El Niño (La Niña) events as SSTs in those regions increase above the long term mean, where temperature anomaly greater than 1°C (-1°C) in the Niño 3.4 region would indicate a likely El Niño (La Niña) conditions.

The frequency of TCs in the NWAUS basin was not highly correlated to Niño-SSTs prior to the beginning or during the TC season for the period 1970 to 2005 (Fig. 4.12). A two-sided t test (Wilks 2005) for significance needs to take into account the serial (lag-1) correlation of the TC time series (Bretherton et al. 1999). A correlation magnitude of 0.46 (0.57) or greater is significant at the 95% (99%) confidence interval under standard normality assumptions for the 36-yr TC dataset. The ENSO

parameter with the highest correlation was the Niño-4 SSTAs. Prior to the beginning of the TC season correlations peaked during June–August and July–September (-0.47). During the season the Niño-4 SSTAs reached a maximum correlation during March–May (-0.51). Another ENSO SST parameter, Niño 3.4, was initially less correlated to the TC frequency; however, correlations increased substantially during the season and the correlation peaked (-0.48) during February–April and March–May, the same time as the Niño 4 SSTAs. These correlations are substantially lower than those reported by Ramsay et al. (2008) for the entire Australian region and are barely significant at the 95% confidence interval. Ramsay et al. (2008) found statistically significant correlations for the Niño 3.4 SSTAs and Niño 4 SSTAs.

The correlations between Niño 3.4 and Niño 4 SSTAs with the number of TC days occurring during a season had similar values to the correlations for TC counts (Fig. 4.12). The largest correlations (~ -0.5) occur during the NWAUS TC season. Prior to the season beginning, Niño 4 SSTAs approach significance at the 95% level by the Jun–Aug three-month bin and maintains that level through the TC season. The Niño 3.4 SSTAs do not approach significance until after the TC season begins, during the Jan–Mar three-month bin. During the Feb–Apr time frame, Niño 3.4 and Niño 4 SSTAs have approximately the same correlation values (~ -0.5) for two three-monthly bins and diverge after the end of the TC season (Fig. 4.13).

4.3.2 SOI

Another parameter used to identify the ENSO mode is the Southern Oscillation Index (SOI). The SOI is a difference is sea level pressure between Tahiti and Darwin, Australia and is calculated as,

$$\text{SOI} = \frac{\left(\text{Tahiti SLP}_{\text{Stand}} - \text{Darwin SLP}_{\text{Stand}}\right)}{MSD} \tag{4.8}$$

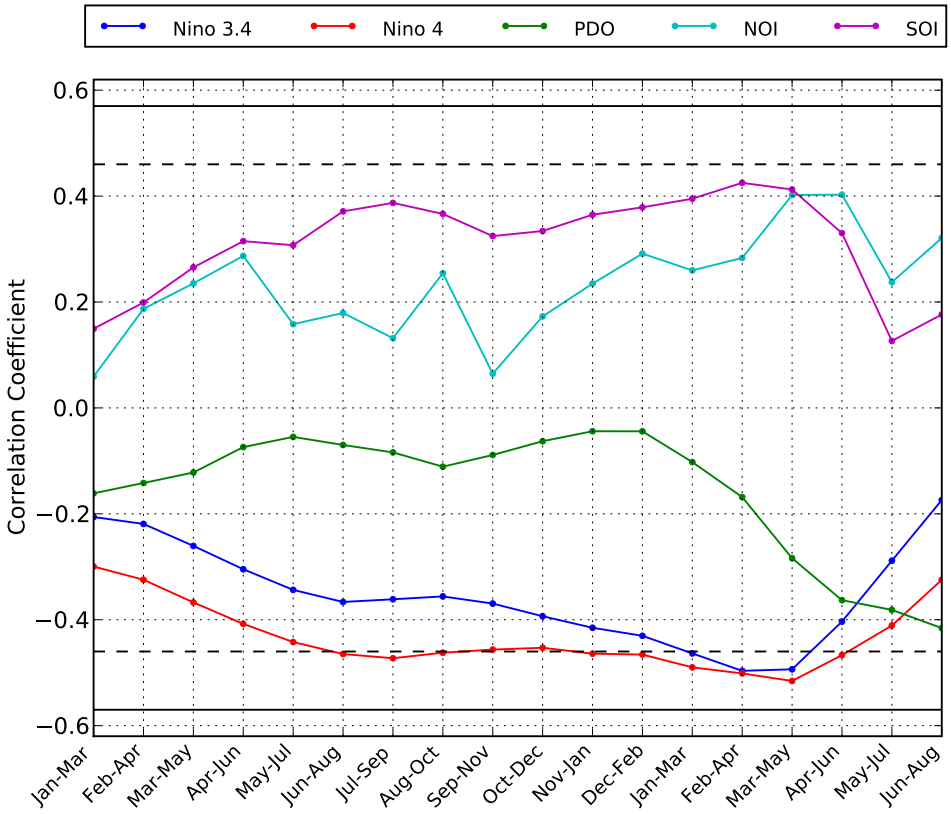

Figure 4.12 Correlations between five ENSO related parameters Niño 3.4, Niño 4, Sothern Oscillation Index (SOI), Pacific Decadal Oscillation (PDO), and Northern Oscillation Index (NOI) and the number of TCs, (defined in the text) beginning with the three-month bin Jan-Mar prior to the beginning of the NWAUS TC season through the Jun–Aug three-month bin following the end of the NWAUS TC season. The 95% and 99% confidence intervals are plotted in dashed black and solid black, respectively.

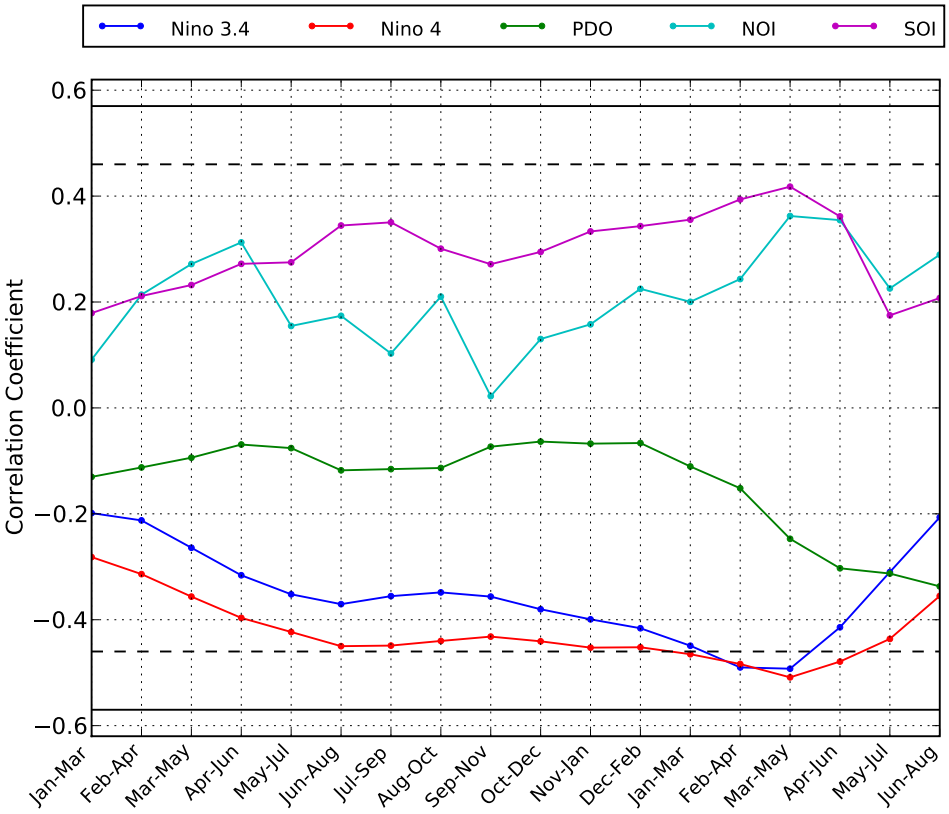

Figure 4.13 Correlations between five ENSO related parameters Niño 3.4, Niño 4, Sothern Oscillation Index (SOI), Pacific Decadal Oscillation (PDO), and Northern Oscillation Index (NOI) and the number of TC days, (defined in the text) beginning with the three-month bin Jan-Mar prior to the beginning of the NWAUS TC season through the Jun–Aug three-month bin following the end of the NWAUS TC season. The 95% and 99% confidence intervals are plotted in dashed black and solid black, respectively.

where Tahiti SLP_{Stand} and Darwin SLP_{Stand} are the standardized sea level pressure (SLP) anomalies for each city, which are calculated as,

$$\text{Tahiti SLP}_{\text{Stand}} = \left[\frac{(\text{Actual SLP} - \text{Mean SLP})_{Tahiti}}{\text{Tahiti SLP}_{\text{stdev}}}\right] \tag{4.9}$$

$$\text{Darwin SLP}_{\text{Stand}} = \left[\frac{(\text{Actual SLP} - \text{Mean SLP})_{Darwin}}{\text{Darwin SLP}_{stdev}}\right] \tag{4.10}$$

where Tahiti SLP_{stdev} and Darwin SLP_{stdev} are the standard deviations of SLP anomalies for each location and are defined as,

$$\text{Tahiti SLP}_{\text{stdev}} = \sqrt{\left[\frac{\sum (\text{Actual SLP} - \text{Mean SLP})^2_{Tahiti}}{N}\right]} \tag{4.11}$$

$$\text{Darwin SLP}_{\text{stdev}} = \sqrt{\left[\frac{\sum (\text{Actual SLP} - \text{Mean SLP})^2_{Darwin}}{N}\right]} \tag{4.12}$$

where N is the number of months, and the Monthly Standard Deviation (MSD) is written as,

$$MSD = \sqrt{\frac{\left(\text{Tahiti SLP}_{\text{Stand}} - \text{Darwin SLP}_{\text{Stand}}\right)^2}{N}} \tag{4.13}$$

where N is the number of summed months and the mean SLP for Tahiti and Darwin are calculated from the $1951 - 1980$ base period. An El Niño period occurs when the SOI values drops below -1.0. In a La Niña event, the opposite is true and a SOI value above $+1.0$ indicates the possible beginning of a La Niña period.

For the NWAUS region there is a substantially lower correlation with the NWAUS TC activity and SOI than has recently been reported for the entire Australian basin by Ramsay et al. (2008) (Fig. 4.12). The SOI correlation initially peaked during July–September (+0.38) before the season began and peaked a second time during the season in February–April (+0.39), which are not statistically significant at the 95% level. Ramsay et al. (2008) found correlations for SOI statistically significant at the 99% confidence interval for TCs occurring in the entire Australian region. The lower correlation values for the NWAUS region as compared to those correlations

found by Ramsay et al. may be attributable to the exclusion of Southwest Pacific TCs in the current study. Since the Southwest Pacific Ocean is directly connected to the changing conditions in the eastern and central Pacific Ocean, it is likely that that area would experience a larger influence from ENSO and subsequently have a diminished impact in the Southeast Indian Ocean.

Similar correlations are found between the SOI and TC days for a given TC season (Fig. 4.13). At no time prior to the beginning of the TC season are the correlations significant. Correlation values increase as the TC season approaches reaching maximum values at the end of the NWAUS TC season reaching values of +0.42 during Mar–May. As with TC numbers, SOI does not appear that it would serve as a suitable seasonal predictor for the number of TC Days.

4.3.3 NOI

The North Oscillation Index (NOI) is an analog climate index to the SOI, which was developed to more accurately assess the tropical-extratropical interactions that are resultant from El Niño and La Niña episodes. The NOI attempts to show the links between the tropical Pacific and extratropical Pacific for the Northern Hemisphere. Schwing et al. (2002) calculated the NOI as,

$$\text{NOI} = SLPA_{NPH} - SLPA_{DARWIN} \tag{4.14}$$

where SLPA_{NPH} is the sea level pressure anomaly of the North Pacific High (35°N, 130°W) and SLPA_{DARWIN} is the sea level pressure anomaly for Darwin, Australia (10°S, 130°E). The base period for the long term mean calculations for the NOI are from January 1948 to December 1997. An important feature of this index is the ability to determine not only changes in the Walker Circulation (as with the SOI), but also changes in the Hadley circulation, which impacts the meridional transport of momentum, energy, and mass between the tropics and extra-tropics (Schwing et al.

2002). The NOI might also highlight cross-equatorial teleconnections in the Pacific Ocean.

Correlations between the NOI and NWAUS TCs follow similar correlation trends to the SOI, with a pre-season peak in April–June (+0.30), then peaking after the season (+0.41) in March–May and April–June (Fig. 4.12). The NOI and SOI are correlated +0.72 across all three-month bins used in this study. The larger correlation after the season may indicate the tropical atmosphere having a greater impact on extratropics as opposed to the other way around.

The correlations between the number of TC days and the NOI yield similar correlations to that for TC numbers (Fig. 4.13). Correlations prior to the beginning of the TC season generally are less than +0.20, increasing during the season to a maximum of +0.35 during Mar–May three-month bin. The NOI, like the SOI, does not appear to be a candidate for inclusion as a predictor in a seasonal prediction scheme for TC frequency or TC days.

4.3.4 PDO

Initially discovered by Walker and Bliss (1932), the Pacific Decadal Oscillation (PDO) is an analogous oscillation to the North Atlantic Oscillation (NAO). The PDO is defined as a seesaw in north–south Pacific sea level pressure and is identified as the leading eigenvector in a principal component analysis of monthly SST anomalies poleward of 20°N between 110°E and 110°W (Mantua et al. 1997). This oscillation varies on interannual to decadal time scales and is widely used to describe decadal variations in the Northern Hemisphere and can modulate ENSO teleconnections. A positive PDO is indicated by a deeper Aleutian low and subsequently the mean extratropical storm track is pushed southward. When the positive phase of the PDO is in concert with an El Niño event, more moisture is available to the storms moving through the Pacific, thus altering precipitation patterns in the western Pacific Ocean. Conversely, during

the negative (cool phase) of the PDO, the Aleutian low is weaker and extratropical storms track farther to the north. When coupled with a La Nia phase, precipitation is enhanced in the Northwest U.S. and British Columbia, while in the Southwest U.S. precipitation is decreased (Gershunov and Barnett 1998; Goodrich 2007).

The interannual variability of the PDO does not correlate significantly with the NWAUS TC frequency before the beginning of the season, but does reach a peak in June–August after the TC season (−0.41; Fig. 4.12). Correlations between the PDO and the number of TC days are similar to those with the number of TCs, with the maximum occurring after the end of the TC season during the Jun-Aug three-month bin after the season has ended (Fig. 4.13). As with the NOI, the stronger correlations following the NWAUS TC season may be the influence of the tropical Pacific Ocean on Northern Hemispheric patterns during the late spring/early summer time frame. Additionally, the PDO has mainly been used for decadal oscillations and currently the period under consideration limits the ability to confirm any decadal or multidecadal trends with certainty. Thus, future studies may find a more substantial connection to the NWAUS TC frequency when multidecadal signals can be identified and researched.

There are a few time periods where the traditional ENSO parameters (Niño 3.4, Niño 4, and SOI) are statistically significant but, in general, the correlations are substantially less than those typically found for TC activity over the entire Australian region. The NOI and PDO, while important in describing interannual to decadal variations in the Pacific Ocean region, appear to have little modulation effect on NWAUS TCs. This greatly diminished role of traditional ENSO parameters for the NWAUS basin in contrast to recent results by Ramsay et al. (2008), which found highly statistically significant relationships between the TC frequency for the entire Australian basin and the traditional ENSO parameters. This studies results confirm

earlier findings by Broadbridge and Hanstrum (1998) that the correlation of SOI to TC numbers was substantially less in the NWAUS region, when compared to the correlations for the entire basin. These findings do not imply that ENSO does not play a role in the variability of TC frequency or TC days in the NWAUS region, just not a statistically significant role as has been found for Australian basin as a whole, or other TC basins around the world.

4.4 Other global modes

A primary difficulty with using these other global modes is that they are typically derived for the Northern Hemisphere. Despite that fact, it is important to consider these known global modes as they may indicate a Northern Hemispheric pattern, modulating the equatorial convergence patterns, which can have a large impact on the formation of TCs in the Australian region. In addition to the traditional global modes of the North Atlantic Oscillation (NAO), the Arctic Oscillation (AO), the Pacific-North American (PNA) pattern, and the Quasi-biennial Oscillation (QBO), an Indian Ocean mode termed the Indian Ocean Dipole (IOD) also is investigated due to its co-location with the NWAUS TC basin.

4.4.1 North American Oscillation and Arctic Oscillation

Two primarily Northern Hemispheric patterns are the NAO and the AO, which have been linked to the variability of temperature and precipitation over North America and Europe. The NAO has been defined several different ways, but has always referred to a north-south dipole on sea level pressure in the North Atlantic Ocean (e.g., Walker and Bliss 1932; Wallace and Gutzler 1981; Hurrell 1995; Ambaum et al. 2001). The NAO also appeared in the analysis by Barnston and Livezey (1987) as one of the ten

leading rotated principal components of Northern Hemispheric 500-hPa geopotential heights.

A common way to calculate the NAO is through the standardized (by standard deviation) SLP differences between Lisbon, Portugal and Stykkisholmur, Iceland (Hurrell 1995), which is in accord with the gradient in SLP observed in map analyses between the Azores high and the Icelandic low (Wallace and Gutzler 1981). Positive NAO values indicate a stronger Icelandic low, which produces colder temperatures over Greenland and warmer weather in the Eastern U.S. and Western Europe. The negative phase results in opposite responses from the Icelandic low, with colder temperatures across the Eastern U.S. and Western Europe.

The NAO has previously been linked to global TC activity by Elsner and Kocher (2000), who found that their global TC activity variable has a statistically significant link to the NAO over a 32 year period from $(1966 - 1997)$. Frank and Young (2007) found similar results to global TC activity, especially when a positive NAO phase coupled with a positive ENSO (El Niño) phase. During that coupled phase, TC activity in all basins studied by Frank and Young (2007) see an increase except for the North Atlantic, which has long been known to have decreased TC activity during positive ENSO phases. This trend is seen in other TC metrics as well, including storm days and the number of TCs to reach hurricane strength.

Closely related to the NAO is the Arctic Oscillation (AO) and thus their correlation exceeds +0.8 during one three-month bin. Overall, the correlation between the NAO and the AO exceeds +0.5 during most three-month bins throughout the year. The AO is identified as the leading mode of a principal component analysis of Northern Hemispheric sea level pressure and explains 25% of the variance (Ambaum et al. 2001). The AO index is calculated by projecting the 1000 hPa height anomalies poleward of 20°N on the loading pattern of the AO. The 1000 hPa height anomalies are calculated from the $1979 - 2000$ mean Positive (negative) values of the AO index

lead to higher (lower) sea level pressures in low latitudes, which results in a stronger (weaker) mid- and high-latitude winds. Over the U.S. there is also a marked difference in surface temperature, with positive (negative) values of the AO lead to warmer (cooler) surface temperatures.

The correlation of NWAUS TC frequency with NAO peaks in March–May (−0.36), but drops to zero correlation after June–August (Fig. 4.14). The AO correlation peaks in March–May (−0.34) and September–November (−0.43), which almost is significant at the 95% confidence interval. However, during the TC season the correlation values drop to near zero (Fig.4.14). Correlations between NWAUS TC days and the NAO index also peaks in Mar–May (−0.34), but the correlation quickly lowers to near zero as the TC season approaches, closely resembling the correlation pattern between the NAO and TC frequency (Fig. 4.15). The correlation between the AO and TC days are similar to those between the AO and TC frequency. The correlation peaks in Mar–May (−0.34) and Sep–Nov (−0.40). After the second peak, the correlation is close to zero (Fig. 4.15).

4.4.2 Pacific-North American Pattern

The Pacific/North American (PNA) pattern is a low-frequency teleconnection pattern in the North Pacific Ocean, which has similarities to the NAO. The calculation of the PNA pattern uses the method of rotated principal component analysis as discussed in Barnston and Livezey (1987). Each month the principal components are calculated for the 500-hPa geopotential heights and are then rotated using the Varimax rotation to obtain the rotated principal components. These rotated modes are then identified as different northern hemispheric patterns and then a least squares solution is found to the system of equations to calculate the final index values.

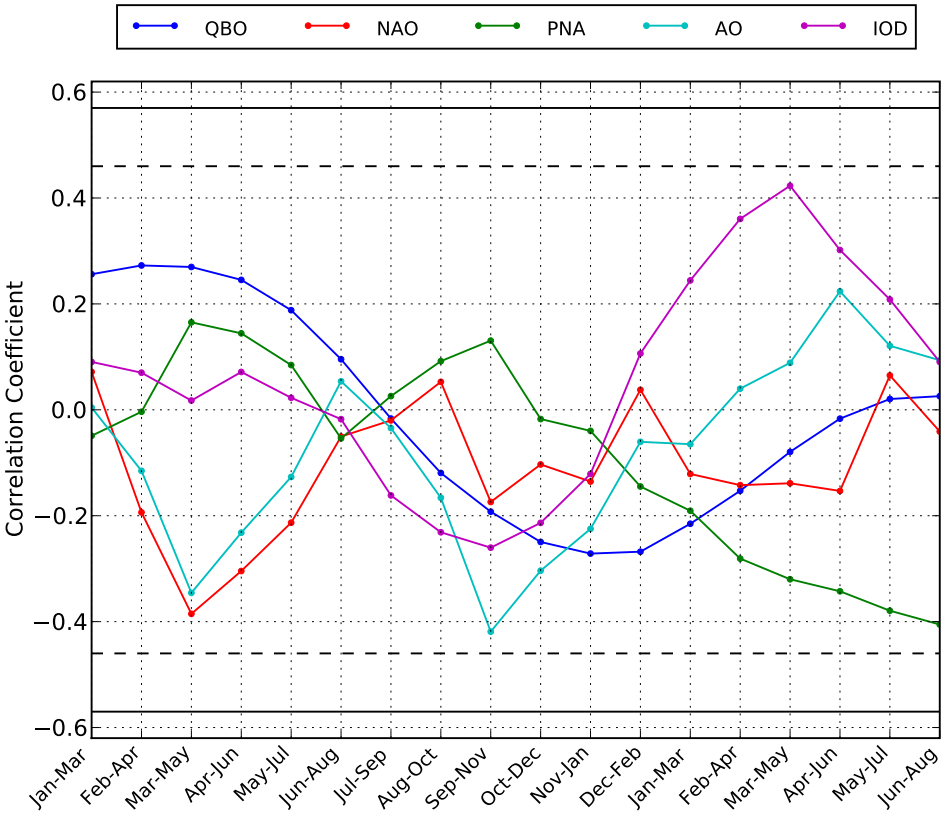

Figure 4.14 Same as in Figure 4.12 except for correlations between NWAUS TC activity and the Quasi-biennial Oscillation (QBO), North Atlantic Oscillation (NAO), PacificNorth American (PNA) pattern, Arctic Oscillation (AO), and the Indian Ocean Dipole (IOD).

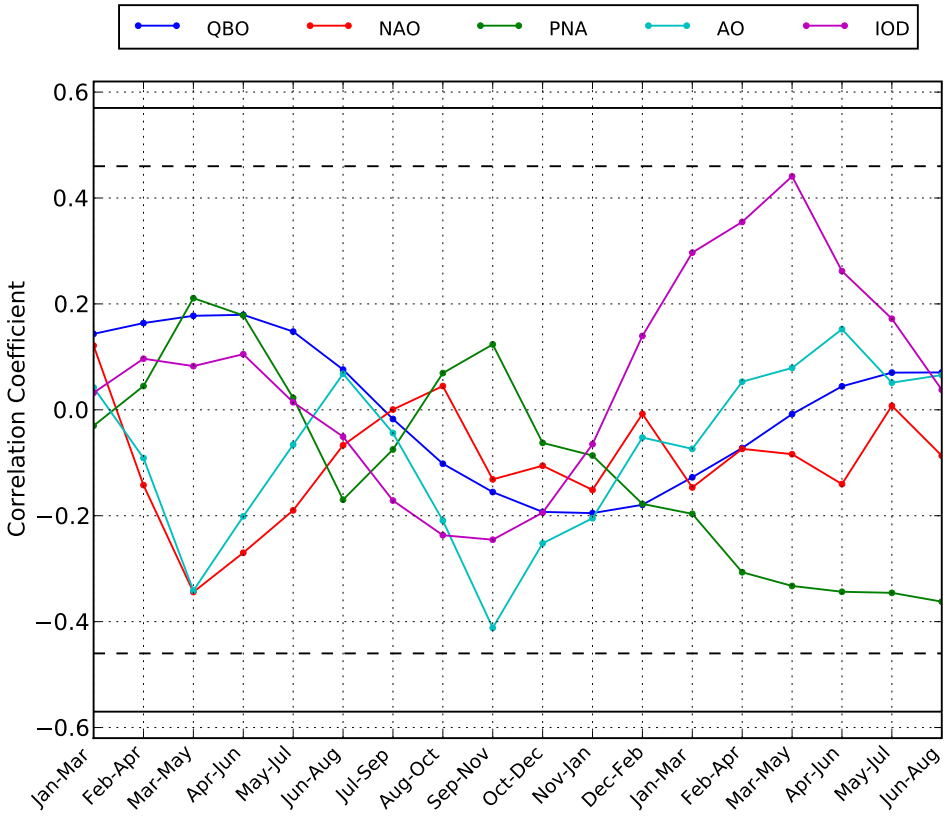

Figure 4.15 Same as in Figure 4.13 except for correlations between NWAUS TC activity and the Quasi-biennial Oscillation (QBO), North Atlantic Oscillation (NAO), PacificNorth American (PNA) pattern, Arctic Oscillation (AO), and the Indian Ocean Dipole (IOD).

A main feature of the positive phase of the PNA is below-average heights near Hawaii and above-average heights south of the Aleutian Islands, which is a north-south dipole similar to the NAO. The East Asian jet stream is shifted eastward during the positive PNA phase and the jet exit region nears the western U.S. coast. During the negative phase, the East Asian jet moves westward, creating a blocking pattern over the central Pacific, resulting in a split flow regime across the Pacific (Wallace and Gutzler 1981). Despite the fact that the PNA was defined to account for changes in Northern Hemispheric weather patterns, the PNA can lead to a shift in that pattern, which in turn can alter the location of the Southern Hemispheric Convergence Zone (or other global circulations). The PNA correlation with the number of TCs is less than $\mid 0.3 \mid$ until after the TC season, when correlations increase to the highest levels (-0.39) in the June–August (Fig. 4.14). Similarly, the correlation between the PNA and the number of TC days is near zero prior to the beginning of the NWAUS TC season (Fig. 4.15).

4.4.3 Quasi-biennial Oscillation

The Quasi-biennial Oscillation (QBO) is a monthly zonal average of the 30-hPa stratospheric wind at the equator. The QBO parameter is calculated from the global reanalysis data (Kalnay et al. 1996) and can be accessed from the Climate Prediction Center website. The QBO represents a change in sign of the zonally averaged wind at the equator from east to west. The QBO was originally introduced by Gray (1984a,b) as a predictor for TCs in the North Atlantic TC basin. Gray reported that in years when the QBO was in a westerly phase there were $50-100\%$ more TCs in the Atlantic region than during an easterly phase. This difference in TC activity has a couple of explanations one being a reduction in vertical wind shear during the westerly phase of the QBO (Gray et al. 1992). However, the physical link between TC activity and the QBO is still uncertain (Baldwin et al. 2001).

For the NWAUS region, the correlation between the QBO and TC frequency peaks in March–May (+0.30) and December–February (−0.25). The correlation between the QBO and TC days is never greater than magnitude 0.2 at any point before, during, or after the NWAUS TC season (Fig. 4.15). Even though the NWAUS region is situated in the deep tropics, the QBO does not appear to explain much of the variability in TC frequency or TC days (Fig. 4.14).

4.4.4 Indian Ocean Dipole

Finally, in the southern Indian Ocean, a dipole in the SSTs has been identified by Saji et al. (1999) as a leading mode of variability in the Indian Ocean. The Indian Ocean Dipole (IOD) is the second mode from the Empirical Orthogonal Function (EOF) analysis of Indian Ocean SSTs, with the first being an ENSO signal. Saji et al. (1999) calculated an index from SSTAs in the Indian Ocean and found that it correlated strongly ($> +0.7$) with the time series associated with the second mode of the EOF. The IOD is the difference in SST anomalies between the tropical western Indian Ocean (50−70°E, 10°S−10°N) and the tropical southeastern Indian Ocean (90−110°E, 10°S–Equator). This local mode peaks in September–November (−0.29) right before the TC season begins and peaks again after the season in March–May (+0.43). Similar correlation relationships appear for the IOD and TC days with the strongest correlation occurring after the season during Mar–May (+0.45; Fig. 4.15). Despite the fact that the IOD is independent of the phase of ENSO (Saji et al. 1999), the IOD does not explain a significant amount of variability in TC frequency or TC days in the NWAUS TC basin before the season begins (Figs. 4.14 and 4.15).

Overall the global modes do not adequately represent the variability of TC frequency or TC days in the NWAUS basin. This likely is due to many of these global

modes having been identified solely for Northern Hemispheric patterns. Due to the lack of landmass area in the Southern Hemisphere and fewer studies of teleconnections in that hemisphere, there are not as many identified global modes. Despite that, previous literature on global teleconnections indicates that patterns in the opposite hemisphere can have an impact on TC development in the opposite hemisphere (Love 1985). Thus it is important to understand the impact of the known global modes on TC activity in the NWAUS basin. However, in this case, the global modes do not appear to have large explanatory power.

4.5 NWAUS TC Season Composite Maps

Composite maps, constructed from NCEP–NCAR reanalysis variables, can be used to identify changes in global atmospheric patterns between active and inactive TC seasons. The composite maps are calculated as the 10 most active seasons and the 10 least active seasons for the entire global domain for various atmospheric parameters. To highlight more effectively the changes between those seasons, anomalies from the long-term means of each field are used.

Inspection of the geopotential height fields at 700, 500, and 250-hPa yield noticeable pattern differences between the active and inactive seasons (Fig. 4.16 and 4.17). Each level contains approximately the same pattern, with magnitude of the height differences increasing slightly with decreasing pressure for both active and inactive seasons. There are a number of different areas around the globe that experience a change in sign of the geopotential height anomaly between active and inactive TC seasons. In the Northern Hemispheric polar region there are higher geopotential heights during active NWAUS TC seasons (Fig. 4.16) and lower geopotential heights during inactive seasons (Fig. 4.17). Additionally, an area of lower geopotential heights during active NWAUS TC season occurs off the coast of Japan with corresponding higher

geopotential heights during inactive seasons. With such differences in the geopotential height field, there may be atmospheric parameters prior to the TC season that have similar variations to the TC metric time series.

4.6 Correlation with Vorticity and Shear

There are a number of parameters that are important in determining whether a TC is likely to develop. Two primary limiting factors to TC development is often the existence of low-level vorticity and minimal vertical wind shear. Over the NWAUS region, the $850 - 200$-hPa zonal shear has a significant negative correlation, where during active (inactive) TC seasons a region of lower (higher) shear (Fig. 4.18) exists. This strong correlation across the equatorial Indian Ocean is embedded within a tripole mode of correlations over the Eastern Indian Ocean, crossing the equator from 45°N to 45°S. There is a mirrored tripole of opposite sign over the central Pacific Ocean; however, the correlations are smaller than the one in the Eastern Indian Ocean.

The spatial correlation map for low-level vorticity indicates a few areas of moderate negative correlation (> -0.4) over the NWAUS region, indicating higher (lower) cyclonic vorticity (which has a negative sign in the Southern Hemisphere) when there is an active (inactive) TC season (Fig. 4.19). The area of higher cyclonic vorticity is located in the SEIND Ocean, over Indonesia and along of the Northwest Australian coast. However, in general, the correlation maps present a noisy pattern from which little can be ascertained.

In general, both $850 - 200$ hPa shear and low-level vorticity are factors in modulating TC frequency in the NWAUS region. However, the vertical zonal shear has higher correlations and appears to be the dominating factor in determining active and inactive TC seasons. The global reanalysis variables are investigated for their

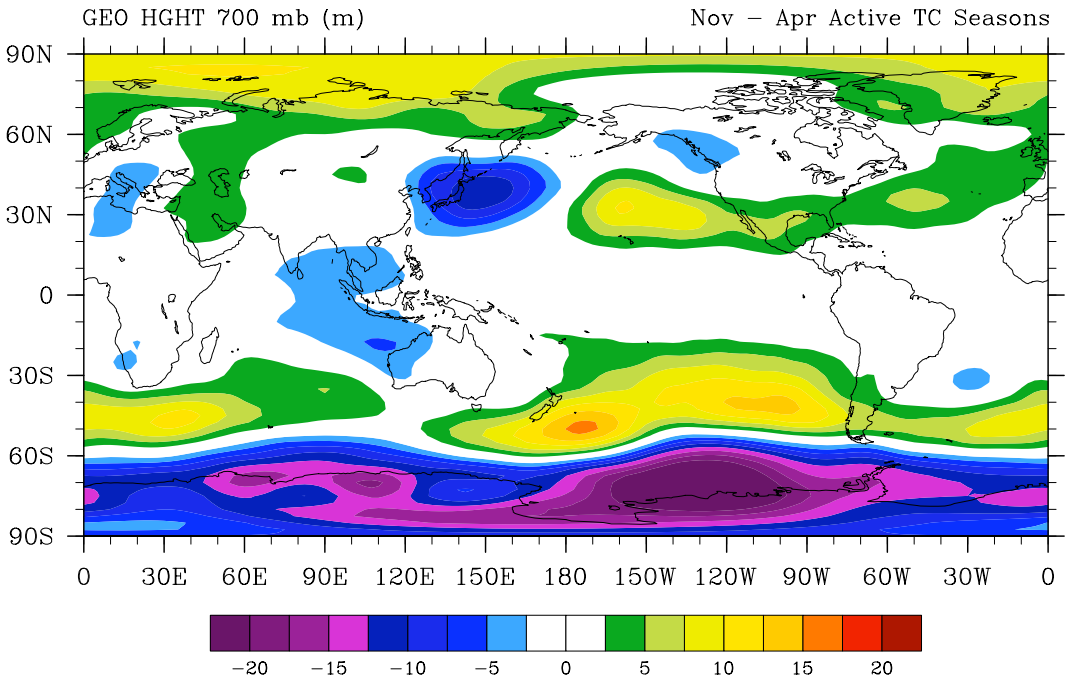

(a)

Figure 4.16 A map of the difference between the most active and least active TC seasons for the Nov–Apr geopotential heights (m) at (a) 700-hPa, (b) 500-hPa, and (c) 250-hPa.

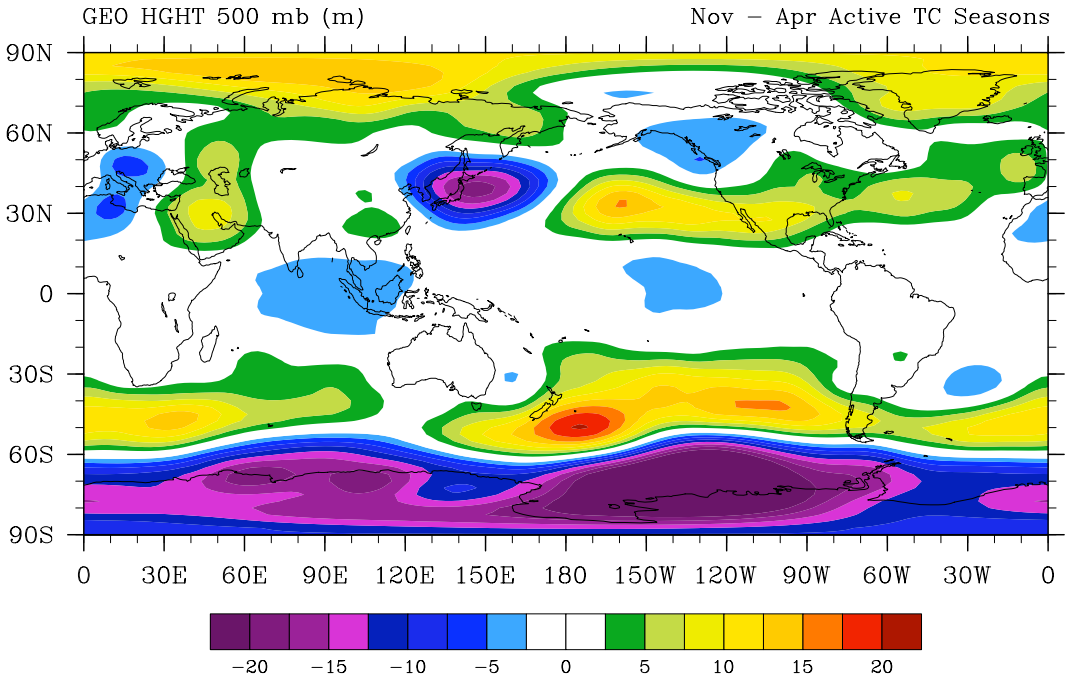

(b)

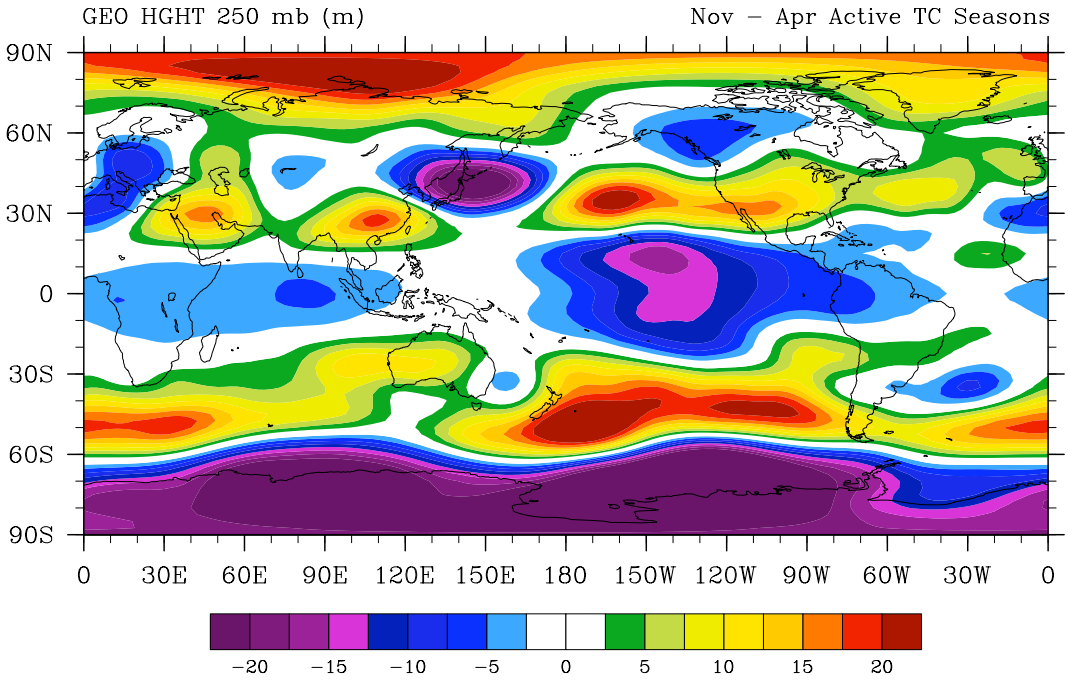

(c)

Figure 4.16 cont.

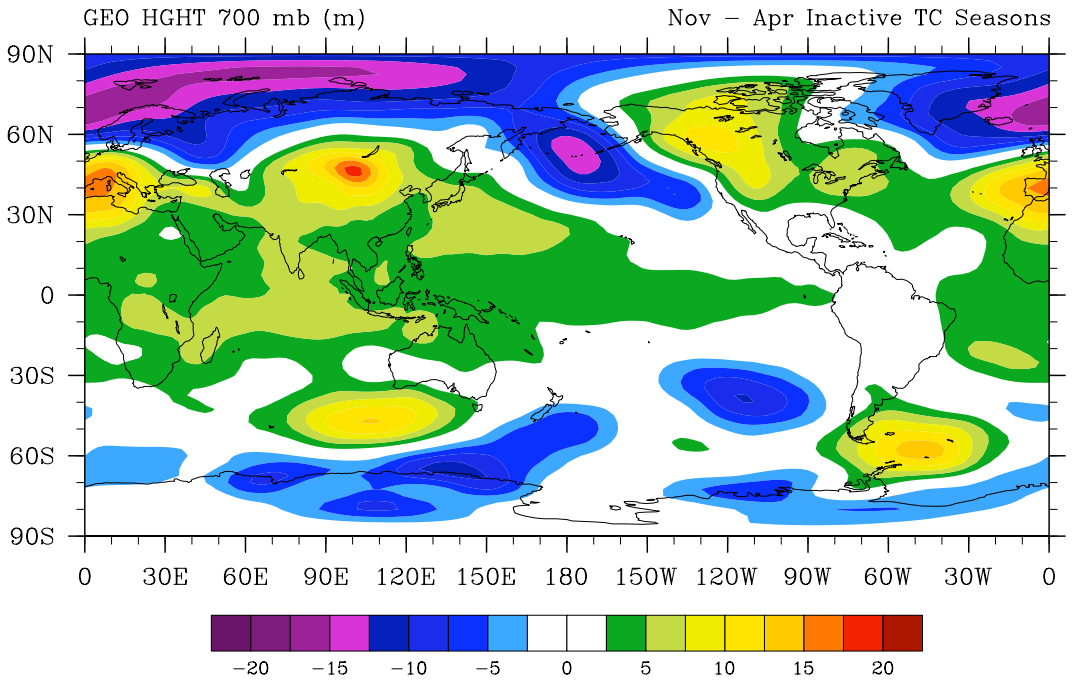

(a)

Figure 4.17 A map of the difference between the most active and least active TC seasons for the Nov–Apr geopotential heights (m) at (a) 700-hPa, (b) 500-hPa, and (c) 250-hPa.

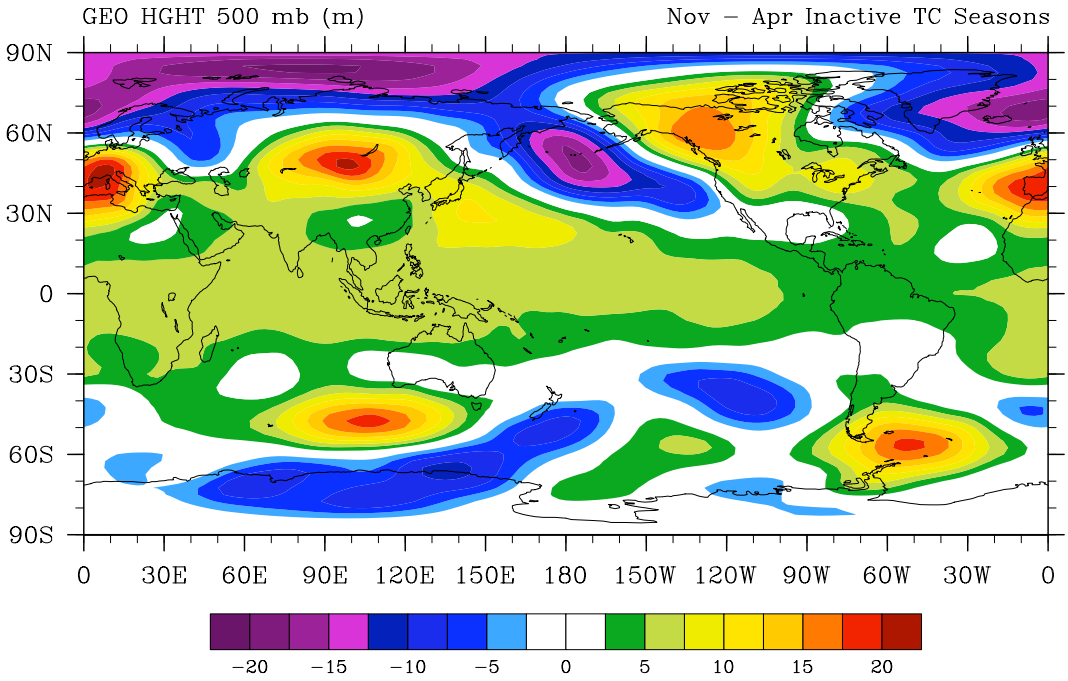

(b)

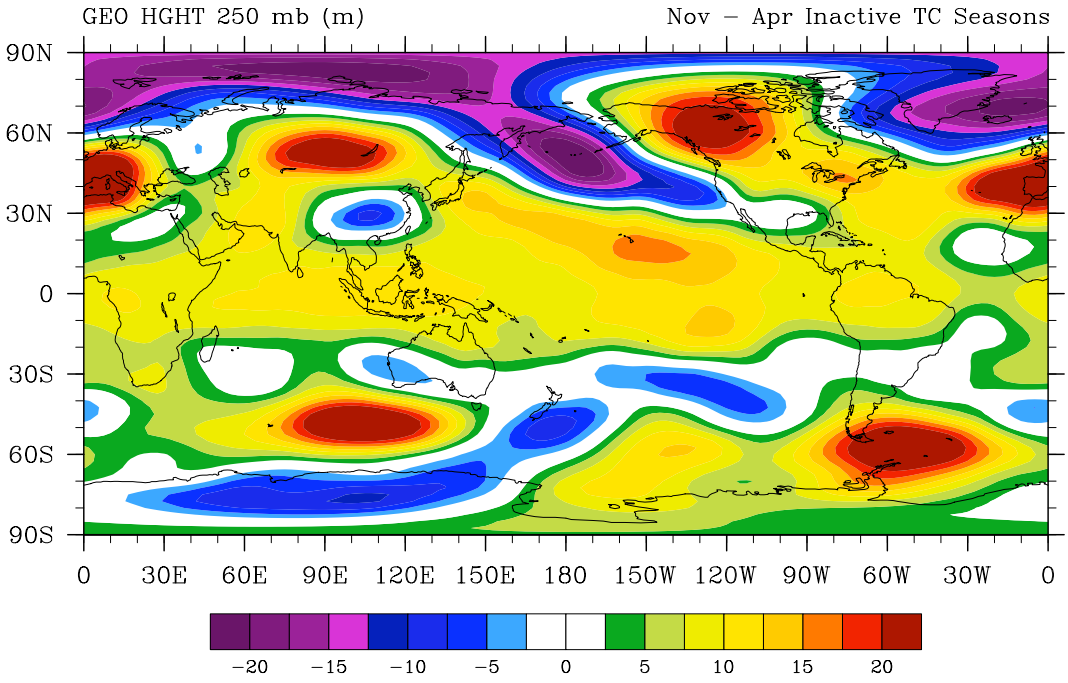

(c)

Figure 4.17 cont.

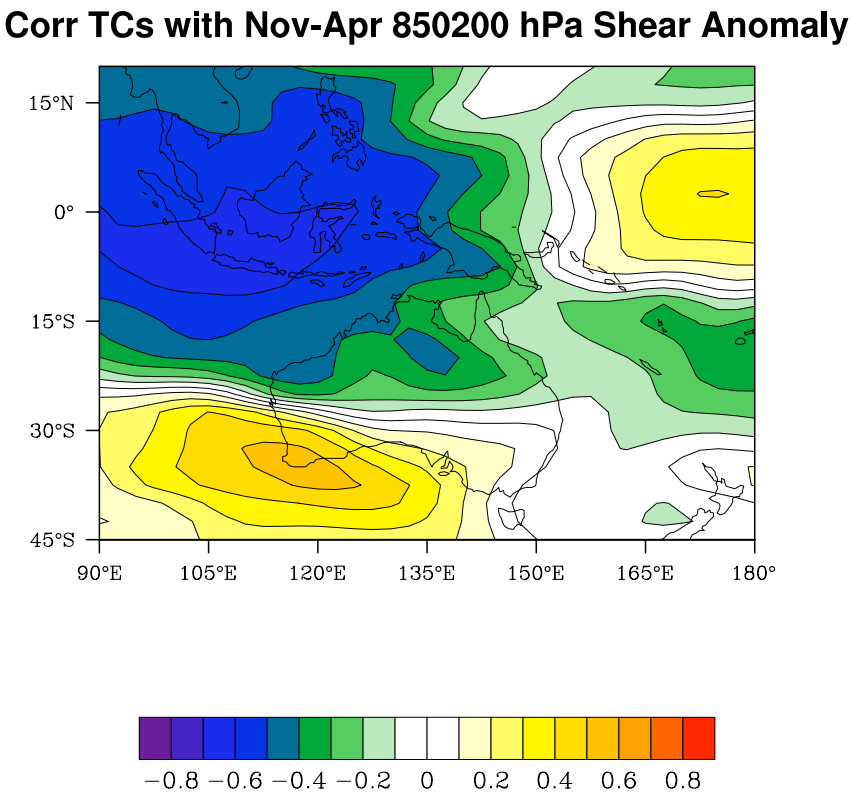

Figure 4.18 Correlation of annual TC frequency (1970/71 – 2005/06) with 850 – 200 hPa vertical shear computed from the NCEP–NCAR Reanalysis data

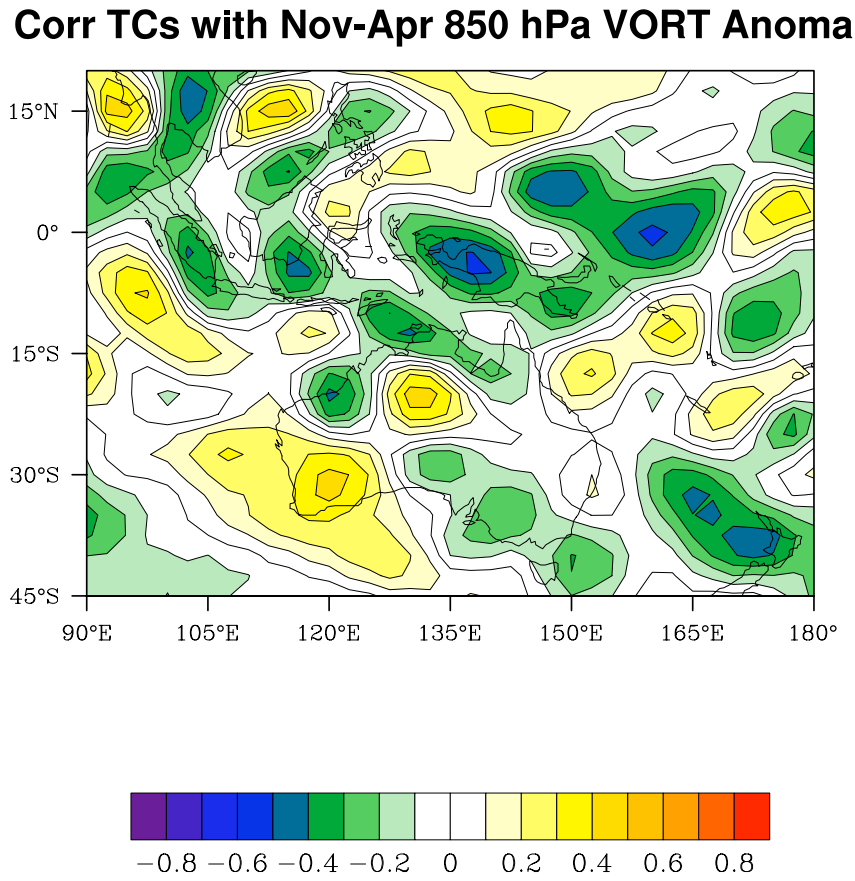

Figure 4.19 Correlation of annual TC frequency (1970 – 2005) with 850-hPa vorticity computed from the NCEP–NCAR Reanalysis data

correlation with the yearly TC frequency and with the $850 - 200$ hPa shear in the NWAUS region.

4.7 Global teleconnections for TC Frequency

While correlation maps of vorticity and $850 - 200$ hPa vertical shear are important in understanding the variability of TC frequency in the NWAUS TC basin, high correlations during the TC season do not provide any information toward predicting any TC metric prior to the beginning of the season. To further investigate potential global teleconnections it is necessary to go beyond the pre-identified global modes discussed in the previous section. Using the NCEP–NCAR reanalysis data (Kalnay et al. 1996), spatial correlations between class A variables and the NWAUS TC frequency are investigated to identify parameters that exhibit strong correlation patterns with yearly TC frequency. Many different variables were investigated including air temperature, geopotential height, sea level pressure, u- and v-wind, and $850 - 250$ hPa zonal shear. Additionally, global SSTAs from the NOAA Extended Re-constructed SST dataset are correlated with TC frequency to identify possible predictors. The correlation analyses identified a number of different parameters that are highly correlated with the TC frequency of the NWAUS basin, prior to the beginning of the TC season. The three-month bins and variables discussed are those that will be used in the development of a seasonal prediction scheme for TC counts in chapter 5.

4.7.1 NCEP–NCAR Reanalysis

Correlation maps were generated for all levels of the NCEP–NCAR global reanalysis dataset for three-month bins beginning with the Jan–Mar period prior to beginning of the TC season, through Sep–Nov at the very beginning of the TC season. Described below are the correlation maps that yielded areas of strong correlation with TC

frequency. A common problem that occurs in identifying potential seasonal predictors is in determining if a correlation of a reanalysis field is significant. To address this issue, the number of TCs time series has been split into two nearly equal subsets. Each of these subsets are then correlated to its respective time series of reanalysis data. If the correlation appears in a similar location in both subsets, then the correlation for the entire period can be considered to exist (Karoly 2009, personal communication).

The correlation map of the 500-hPa geopotential heights for Mar–May over Russia (RUS500; $55-67.5°$N, $70-85°$E) is moderately correlated (< -0.40) to the NWAUS TC frequency (Fig. 4.20). After splitting the time series into two, the correlation does appear in both subsets, suggesting that the correlation is not random and therefore would render this area a possible seasonal predictor for the number of TCs (Fig. 4.21). A cross-correlation between the RUS500 geopotential heights and $850-200$ hPa vertical shear yields a weak to moderate correlation reaching 0.3 over the NWAUS region (Fig. 4.22).

The correlation map of the 850-hPa geopotential heights for May–July is highly correlated ($> +0.5$; Fig. 4.23) with NWAUS TC frequency over South Indian Ocean (SIND850; $42.5-55°$S, $47.5-72.5°$E). Before an active (inactive) TC season there are anomalously higher (lower) heights over the South Indian Ocean. A moderate to strong correlation exists across the time series as evident from the correlation maps of half the time series (Fig. 4.24). The spatial cross-correlation map for vertical shear and SIND850 heights suggests the two parameters are not strongly correlated with vertical shear over the Northwest Australian region. In general, correlations rarely exceed a correlation of magnitude 0.3 throughout the entire Southern Indian Ocean (Fig. 4.25).

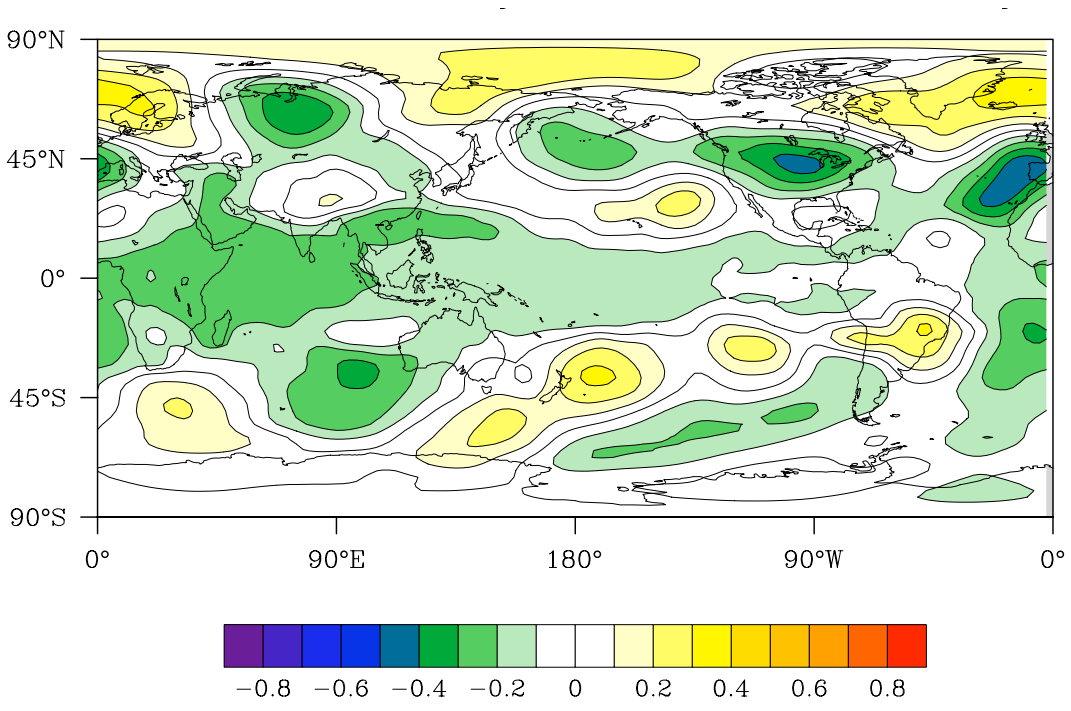

Figure 4.20 Correlation map between NWAUS TC frequency and Mar–May 500-hPa geopotential heights.

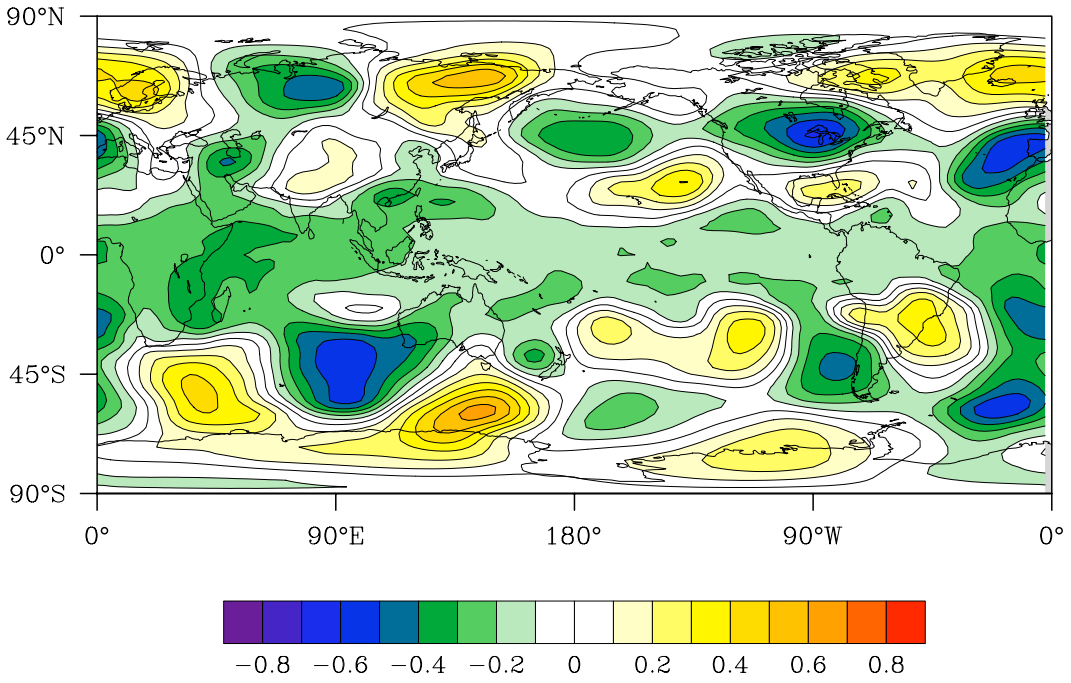

(a)

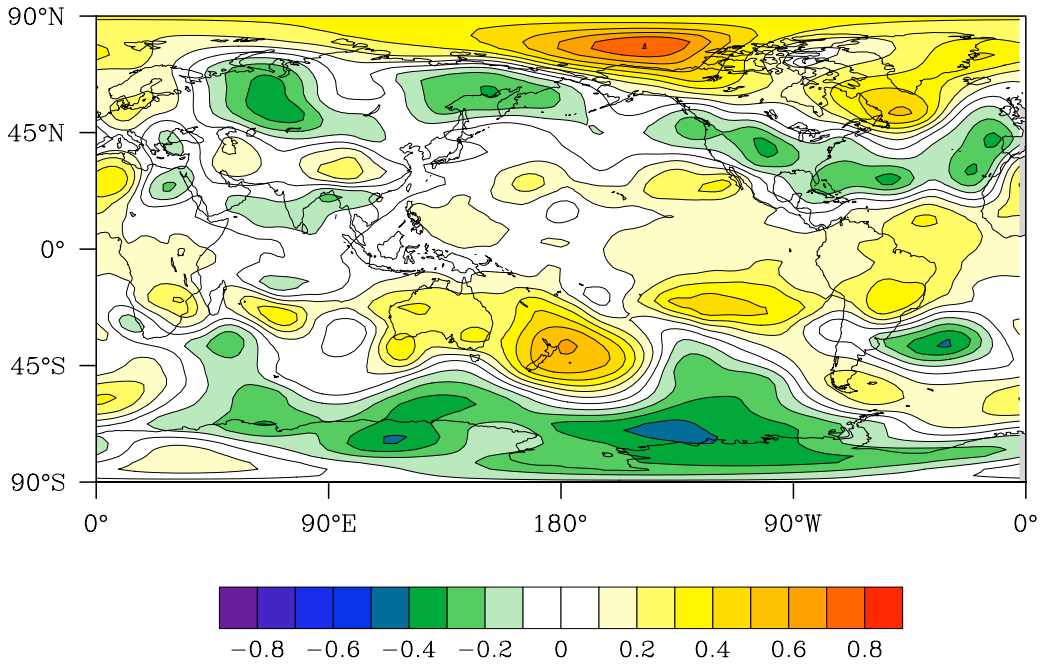

(b)

Figure 4.21 Same as in Fig. 4.20 except for (a) 1970–1989 and (b) 1990–2007.

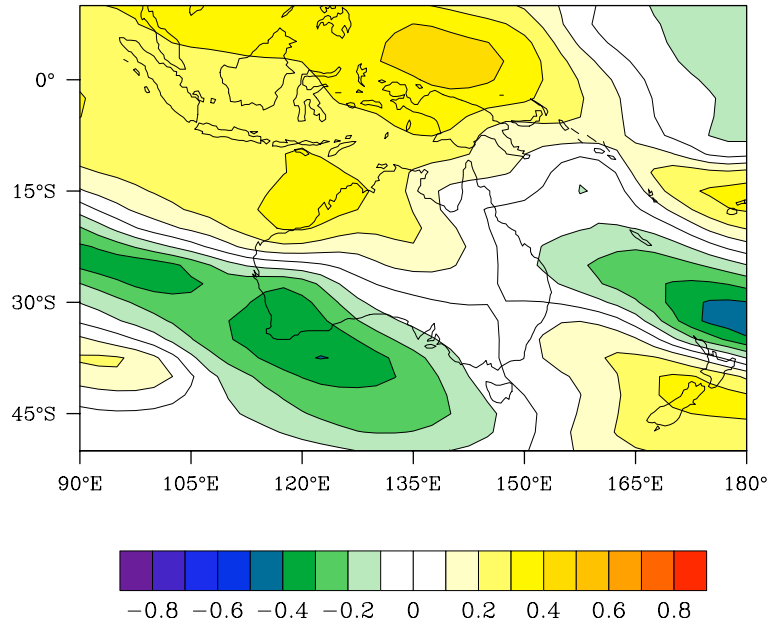

Figure 4.22 Cross-correlation between Mar–May RUS 500 hPa geopotential heights and 850–200 hPa zonal shear.

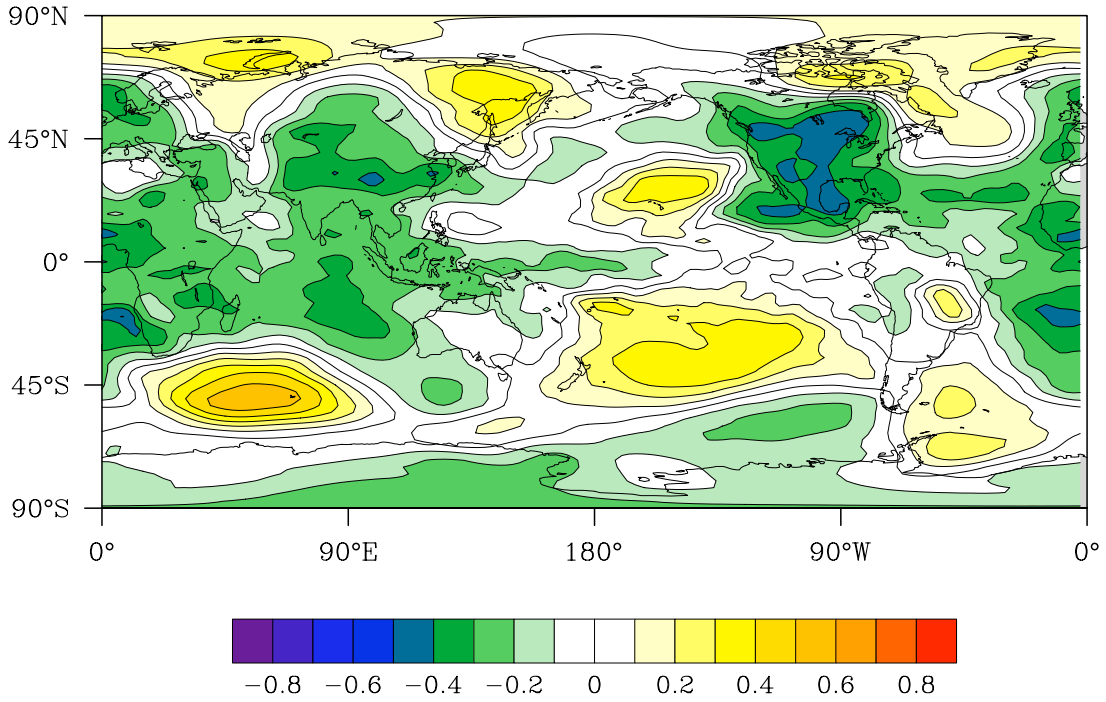

Figure 4.23 Same as in Fig. 4.20 except for May–Jul 850-hPa geopotential heights.

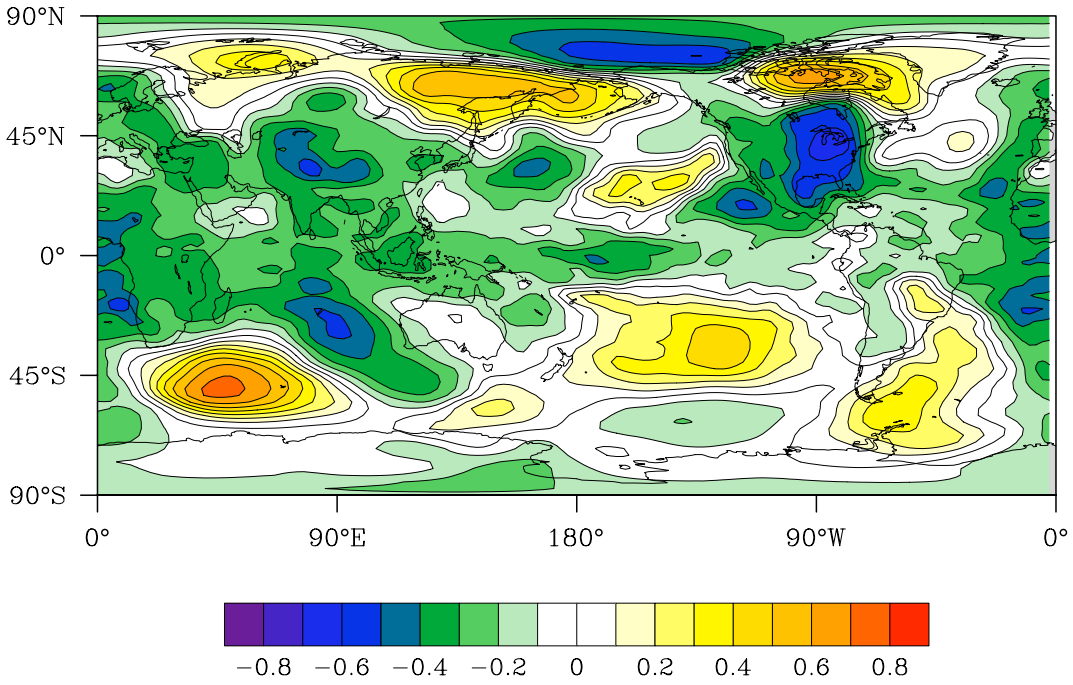

(a)

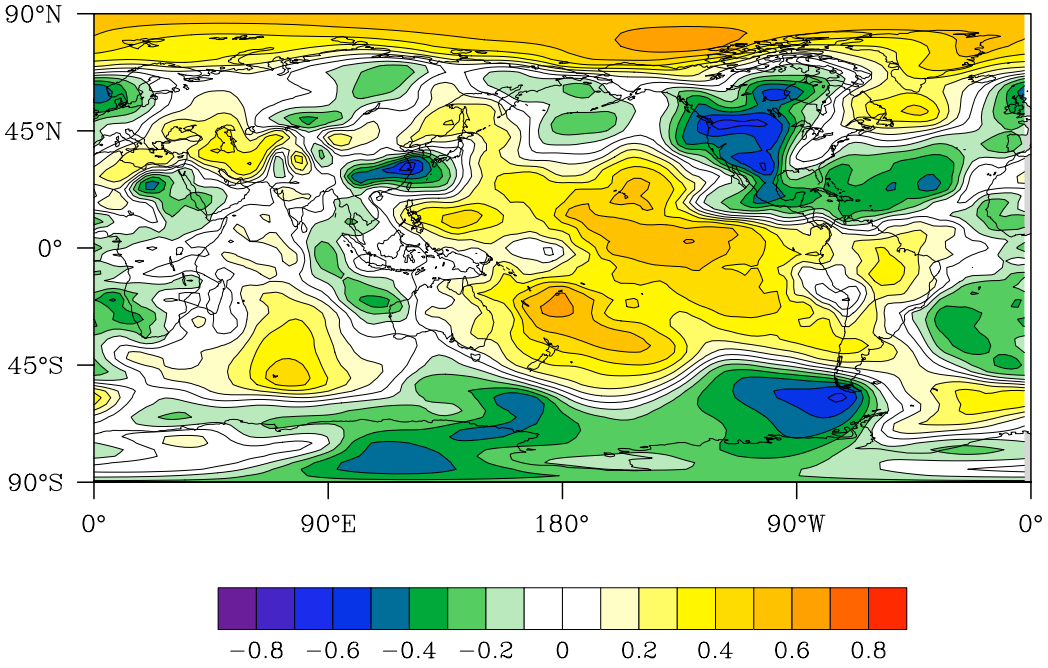

(b)

Figure 4.24 Same as in Fig. 4.21 except for SIND 850 hPa Geopotential Heights.

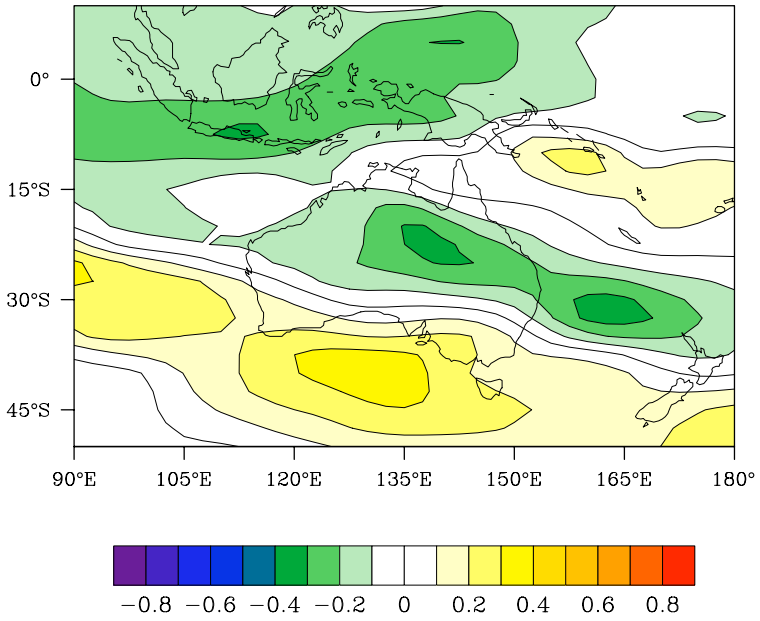

Figure 4.25 Same as Fig. 4.22 except for May–Jul SIND 850-hPa geopotential heights.

April–June 700-hPa geopotential heights are significantly correlated to TC activity in the NWAUS region (< -0.6; Fig. 4.26) over central North America (NA700; $37.5 - 47.5°$N, $102.5 - 82.5°$W). When broken into two time series, the correlation remains over the same region (Fig. 4.27). The spatial pattern of correlations between the NA700 heights and global vertical shear is moderately positive correlated over the region from 0° to 15°S and 90° to 140°E). Lower (higher) heights at 700 hPa over North America are coincident with lower (higher) vertical shear over the NWAUS region (Fig. 4.28).

The correlation map of 850-hPa air temperature over the central North Pacific (HI850; $10 - 20°$N, $155 - 132.5°$W) for May–July is significantly correlated with TC activity in the NWAUS region (-0.63; Fig. 4.29). Correlating the two halves of the TC time series, the area of strong correlation is maintained (Fig. 4.30). The spatial correlation map for HI850 air temperature and vertical shear indicates a significant correlation over the NWAUS region ($> +0.7$). When there are cooler (warmer) temperatures to the Southeast of HI there is less (more) shear over the NWAUS region (Fig. 4.31). An east-west dipole in the Indian Ocean and a north-south tripole in the Central Pacific Ocean are present in the correlation map.

The spatial correlation of the 925-hPa geopotential heights for June–August is significantly correlated (< -0.70; Fig. 4.32) with NWAUS TC frequency over the South Atlantic Ocean (SATL925; $17.5 - 32.5°$S, $12.5 - 0°$W). There is a second area of high correlation in the Eastern Pacific Ocean (EPAC925; $15-27.5°$N, $130-115°$W), off the coast of California. This secondary area does not appear as a prominent feature in the composite difference map and its variability is likely related to the variability of ENSO. There are additional areas of weak to moderate correlations across the central Pacific and eastern Indian Ocean regions, but the correlations are not statistically significant. Both areas of high correlation hold up through splitting the dataset into two subsets (Fig. 4.33).

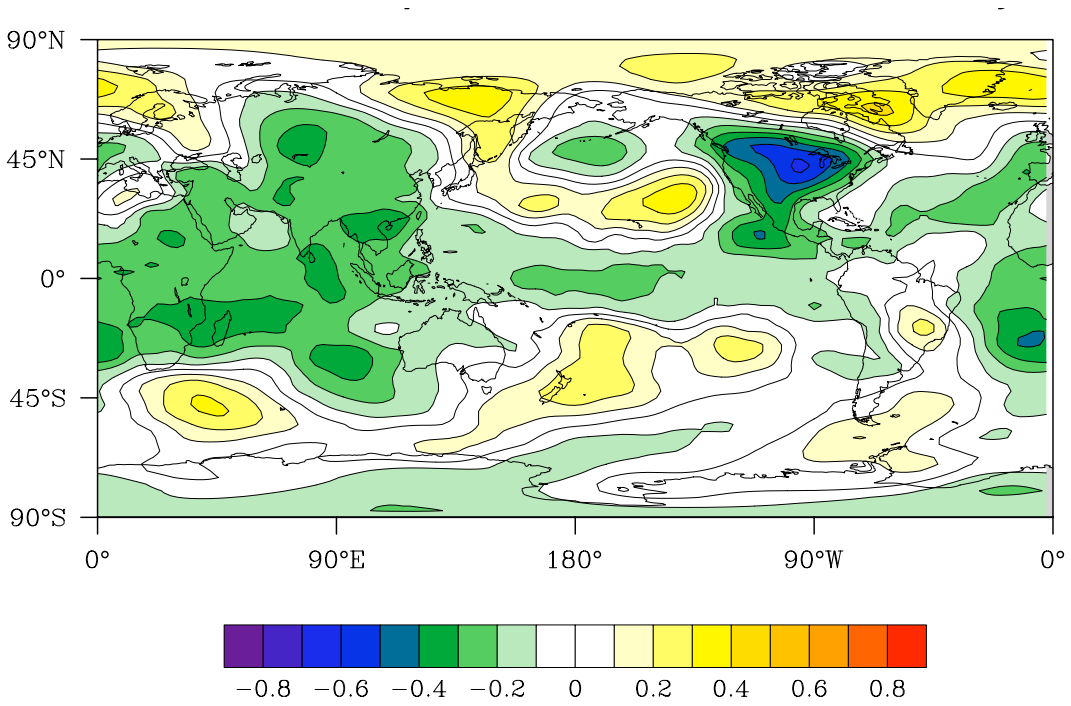

Figure 4.26 Same as in Fig. 4.20 except for Apr–Jun 700-hPa geopotential heights.

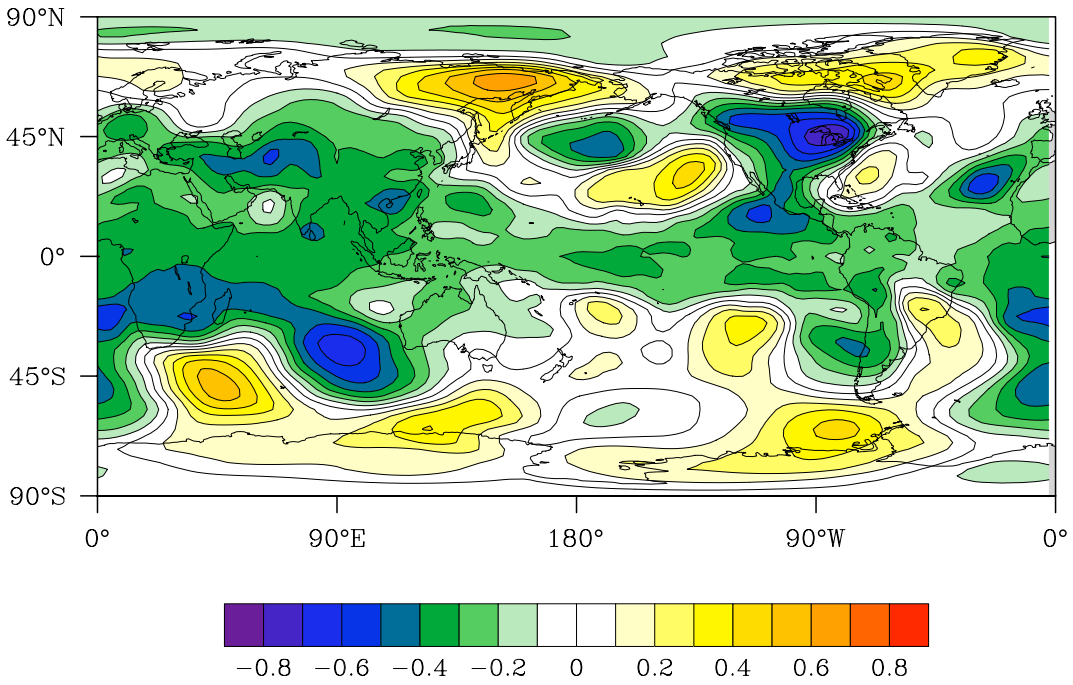

(a)

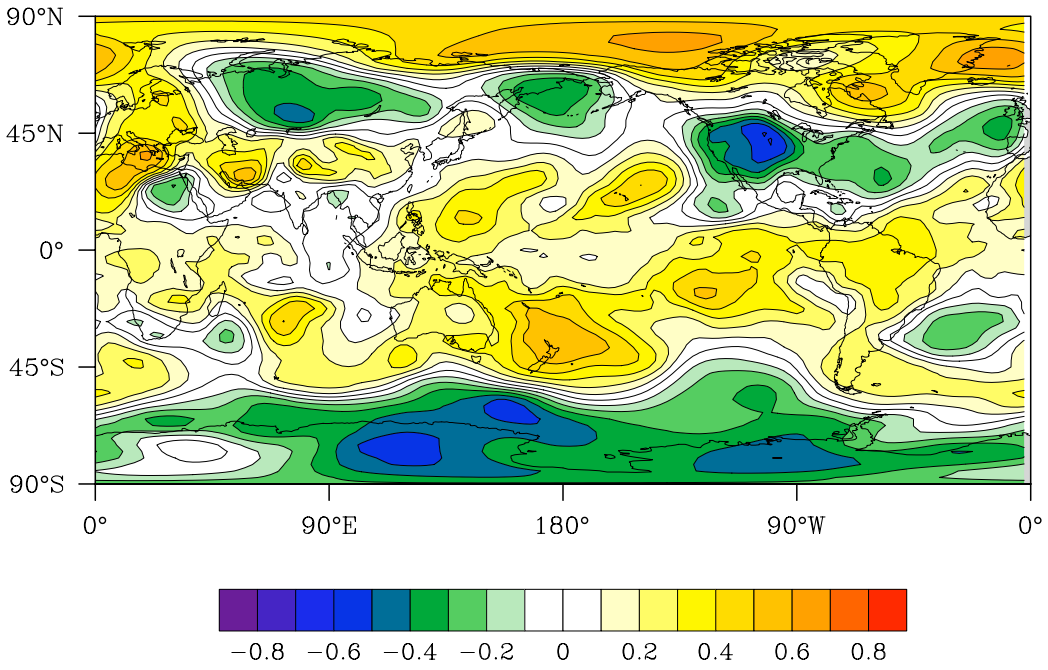

(b)

Figure 4.27 Same as in Fig. 4.21 except for NA 700 hPa Geopotential Heights.

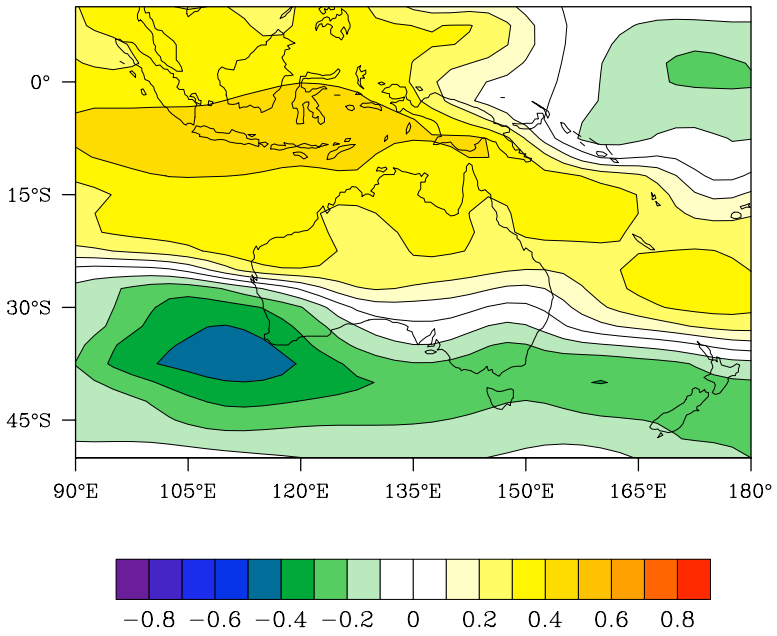

Figure 4.28 Same as in Fig. 4.22 except for Apr–Jun 700-hPa geopotential heights.

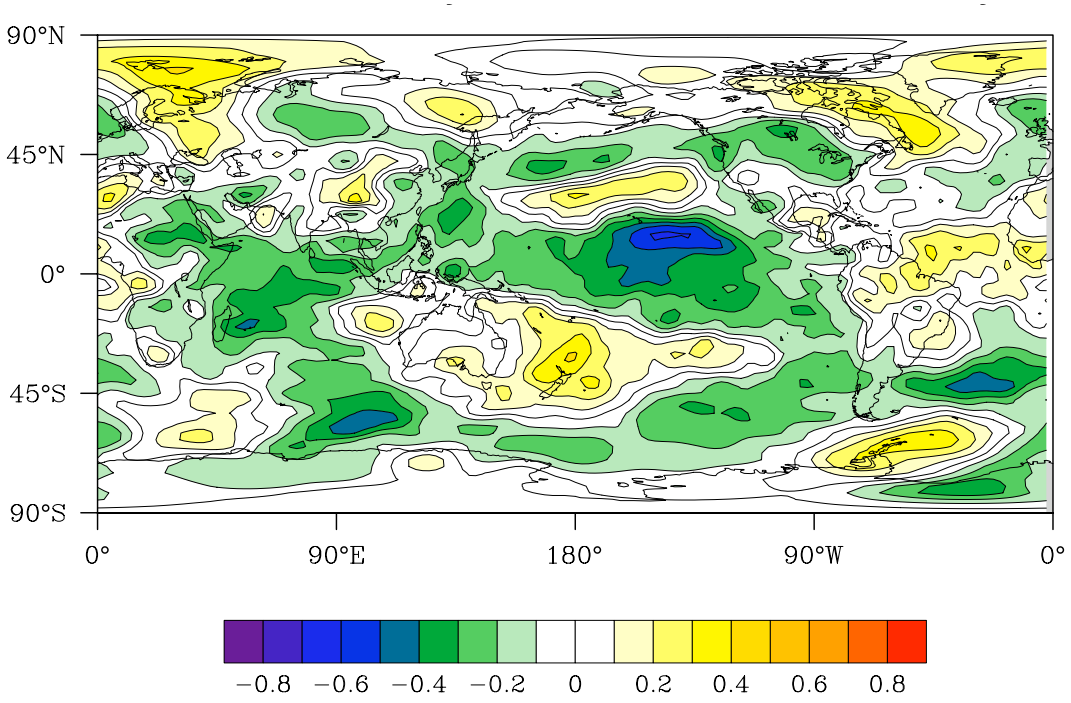

Figure 4.29 Same as in Fig. 4.20 except for May–Jul 850-hPa air temperature.

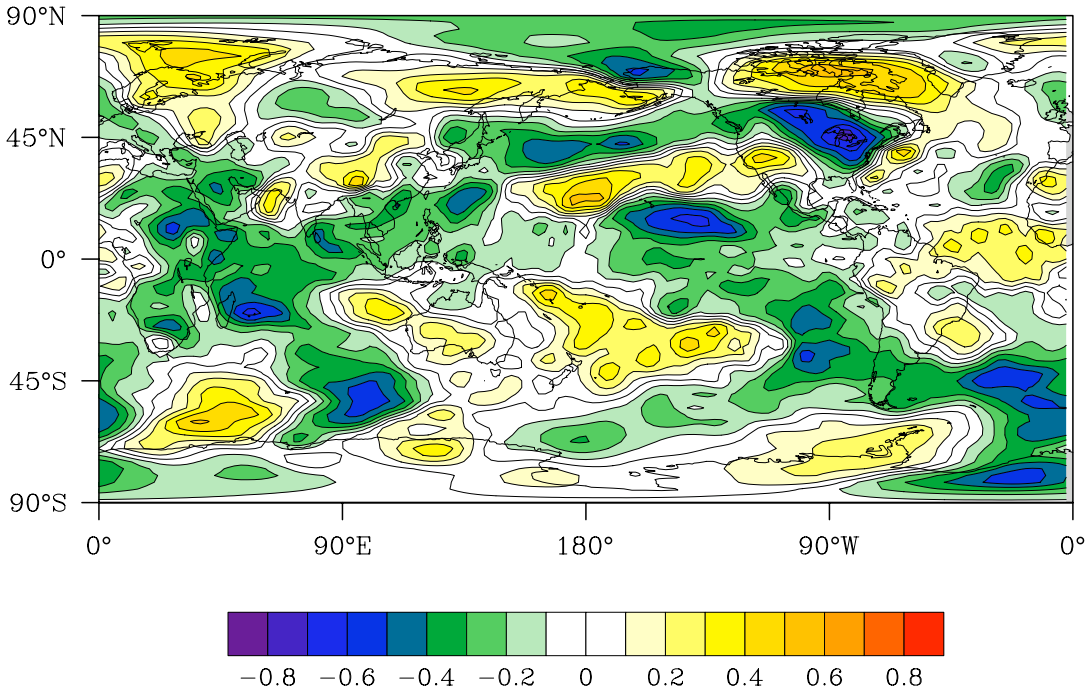

(a)

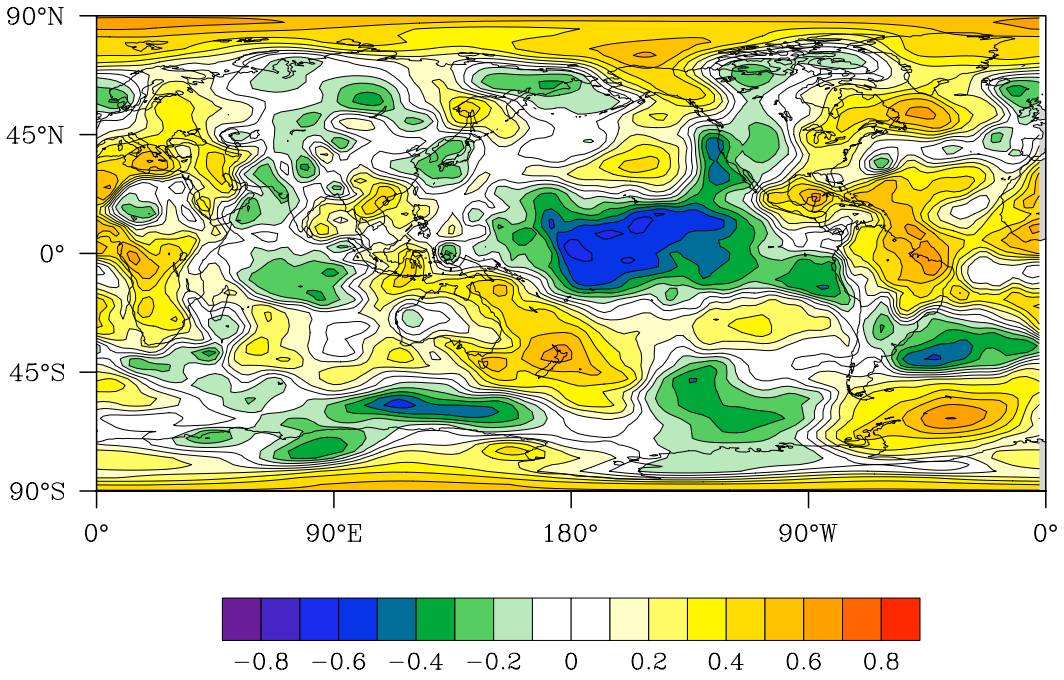

(b)

Figure 4.30 Same as in Fig. 4.21 except for HI 850 hPa Air Temperature.

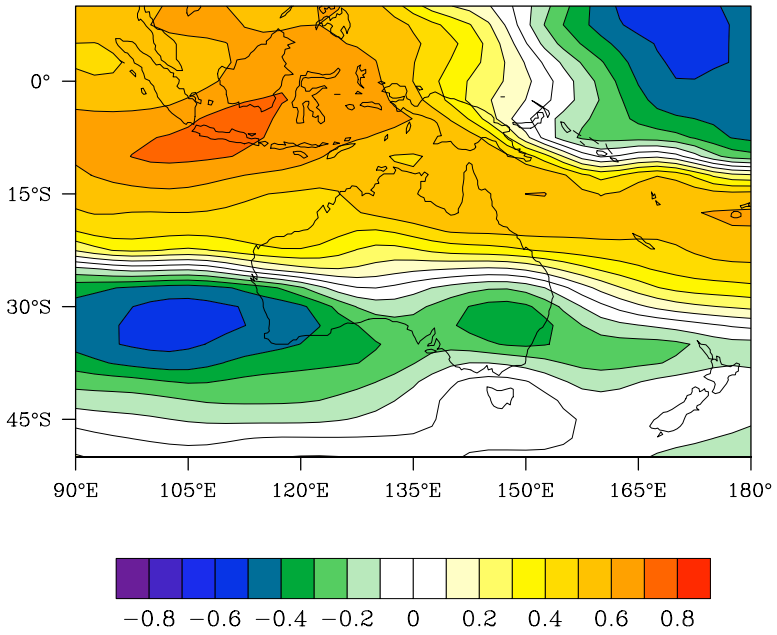

Figure 4.31 Same as in Fig. 4.22 except for May–Jul 850-hPa air temperature.

The spatial correlation between $850 - 200$ hPa shear and the EPAC925 region are moderately positive ($> +0.5$) in a region between 0° and 10°S and from 105° to 140°E (Fig. 4.34a). Additionally, there is a larger area of correlation exceeding +0.4 throughout the northern half of the SEIND Ocean. This positive correlation suggests that when the EPAC925 heights are anomalously low (high) it leads to anomalously low (high) shear in the NWAUS region, which leads to active (inactive) TC seasons in that region. Also, a similar tripole structure is present over the eastern Indian Ocean between 50°N and 45°S. Additionally, the SATL925 region is moderately negative correlated with vertical wind shear along the Northwest Australian coast ($> +0.3$), and further to the northwest, correlations are stronger ($> +0.4$) extending out to at least 90°E (Fig 4.34b).

All of these parameters represent atmospheric teleconnections that are highly correlated with the variability of TC frequency in the NWAUS region. These teleconnections are intra-hemispheric, inter-hemispheric, and cross-hemispheric and explain more of the year to year variations in TC frequency and TC days than one obtains from the classic global modes.

4.7.2 Global Sea Surface Temperatures

Previous work has investigated ENSO related sea surface temperatures. However, it is beneficial to investigate global Sea Surface Temperature Anomalies (SSTAs) for any other areas that may influence the global circulation and explain a portion of the NWAUS TC frequency time series. Composite maps of the 10 most active and 10 least active NWAUS TC season yields an ENSO-like signal for Nov–Apr (Fig. 4.35). A correlation of global SSTAs with the TC frequency yields a similar patterns to the composite maps for Mar–May SSTAs (Fig. 4.36). Of particular interest is the area

in the south Atlantic Ocean (SATL; $28-42°$S, $36-14°$W) where the correlation with the NWAUS TC frequency is -0.53. Prior to the onset of the NWAUS TC season there is not a strong correlation between Niño region SSTs. The SATL SSTAs correlate strongly with the $850-200$ hPa vertical shear over the NWAUS region (Fig. 4.37). With the high correlations the SATL SSTs it is potentially a good predictor of NWAUS TC activity.

4.8 Global teleconnections for TC Days

Global teleconnections for the number of TC days were investigated in a similar manner to those for TC frequency. Overall, there were a number of different areas that indicated substantial correlation with the number of TC days occurring within a season. However, many of the regions identified were strongly correlated with other variables. The following three regions discussed were correlated less than magnitude 0.31 with each of the potential predictors.

The first area of interest is from the Jan–Mar 100 hPa v-component of the wind over the southern Pacific Ocean (SPAC100; $40-65°$S, $170-140°$W). This region is moderately correlated with the TC days time series ($+0.52$; Fig. 4.38) and similar regions appear in the first and second half correlations of the time series (Fig. 4.39). This area of common variability between the TC days time series and 100 hPa v-component of the wind is a very early predictor of the following TC season.

A second area of interest is in a similar region to one of the ares for TC frequency over North America (NA850; $30-50°$N, $105-80°$W). The correlation map for Apr–Jun 850 hPa geopotential heights indicates a region of strong correlation over the western Great Lakes region (-0.58; Fig. 4.40). The NA850 region is likely partially related to the NAO and AO, which are known to affect Northern Hemispheric climate

patterns. Consistent through time, an area of strong correlation exists when the time series is broken into two nearly equal segments (Fig. 4.41).

Finally, a region over the south Atlantic Ocean (SATL1000; $5-45°$S, 35°W-10°E), similar to the SATL925 region identified for the TC frequency variability, exhibits a strong correlation with TC days (Fig. 4.42). The SATL1000 region is correlated with TC days at -0.7, significant at the 99% significance interval. Splitting the time series into two, yields a correlation in the same region (Fig. 4.43).

4.9 Discussion

Trends in the TC frequency for the NWAUS region are similar to those for the entire Australian region as found by Nicholls et al. (1998) for all TCs. For intense TCs, Nicholls et al. found that there was a slight increase in the number of intense storms between 1969 and 1994, this study finds no overall increase or decrease in the number of intense TCs for the NWAUS region (Fig. 4.1). The difference could be due to differences in the basins studied, but another factor could be a multi-decadal trend that was only partially observed in the Nicholls et al. dataset. Ramsay et al. (2008) found a similar trend as Nicholls et al. (1998), however, the trend in the NWAUS region is substantially smaller compared to the trend for the entire Australian region and the trend is not statistically significant. Similar results are obtained for other TC metrics, for which no significant trends in any of the TC metrics were found.

Additionally, Kuleshov et al. (2008) observed no linear trend in the occurrence of all TCs, but did observe an identifiable upward trend in TCs with minimum pressures less than 945 hPa. The upward trend observed in Kuleshov et al. (2008) is only for the period 1981 to 2005. Eleven years of reliable Southern Hemispheric data ($1970-1980$) are not used and likely a multidecadal trend is being only partially observed and therefore may be an artifact of a small TC dataset. Depending on where you split a

TC frequency time series, the general downward trend could be reversed, similar to the point made by Ramsay et al. (2008, see their Fig. 11a). With such a relatively short, reliable dataset it is not possible to determine trends longer than the decadal time scale, or to ascertain any affects that a warming climate would be having on the number or strength of TCs in the NWAUS region.

The results indicate that there are a number of teleconnections modulating the frequency of TCs and TC days in the NWAUS region. However, previously identified global teleconnections such as Niño 3.4, Niño 4, SOI, NOI, PDO, NAO, etc. generally were found not to be significantly correlated to the variability of TC frequency in the NWAUS region. Specifically, previously identified teleconnections of Niño 3.4 and Niño 4 SST regions were found to be barely, significantly correlated to TC frequency and TC days. These correlations do not provide a high confidence in understanding the variability of TC frequency or TC days.

Previous work by Ramsay et al. (2008) found significant correlations between TC frequency in the entire Australian region and Central Pacific SSTs. In the SWPAC Ocean, Basher and Zheng (1995) found a strong relationship between the ENSO related variables and TC frequency for a number of subbasins. In this study of the NWAUS region, the correlations for ENSO variables are substantially lower before, during, and after the TC season.

Other studies have used SOI and ENSO related variables to predict the number of TCs and TC days for the Australian region. Nicholls (1979) introduced a method for forecasting TC numbers before the season began using only SOI for the entire Australian region. In this study it is found that SOI does not explain a substantial amount of variation in TC frequency or TC days of the NWAUS region. The results for the NWAUS region are similar to Broadbridge and Hanstrum (1998) for SOI over the entire season. However, due to the serial correlation of the TC time-series, confidence that the correlation is meaningful, is low.

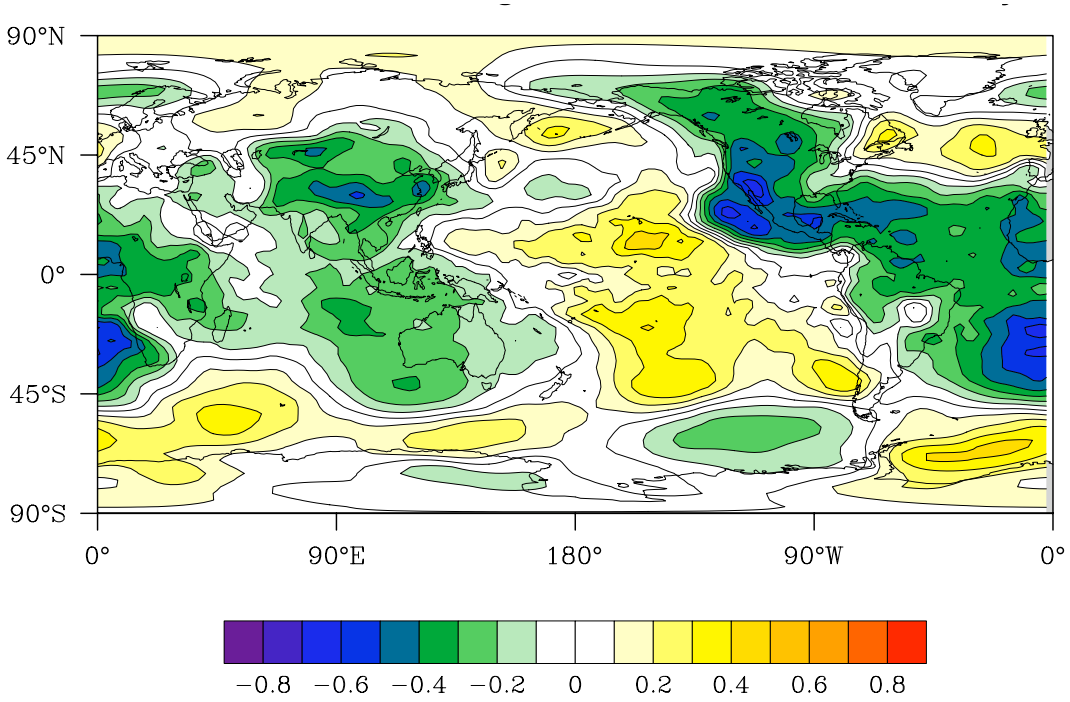

Figure 4.32 Same as in Fig. 4.20 except for Jun–Aug 925-hPa geopotential heights.

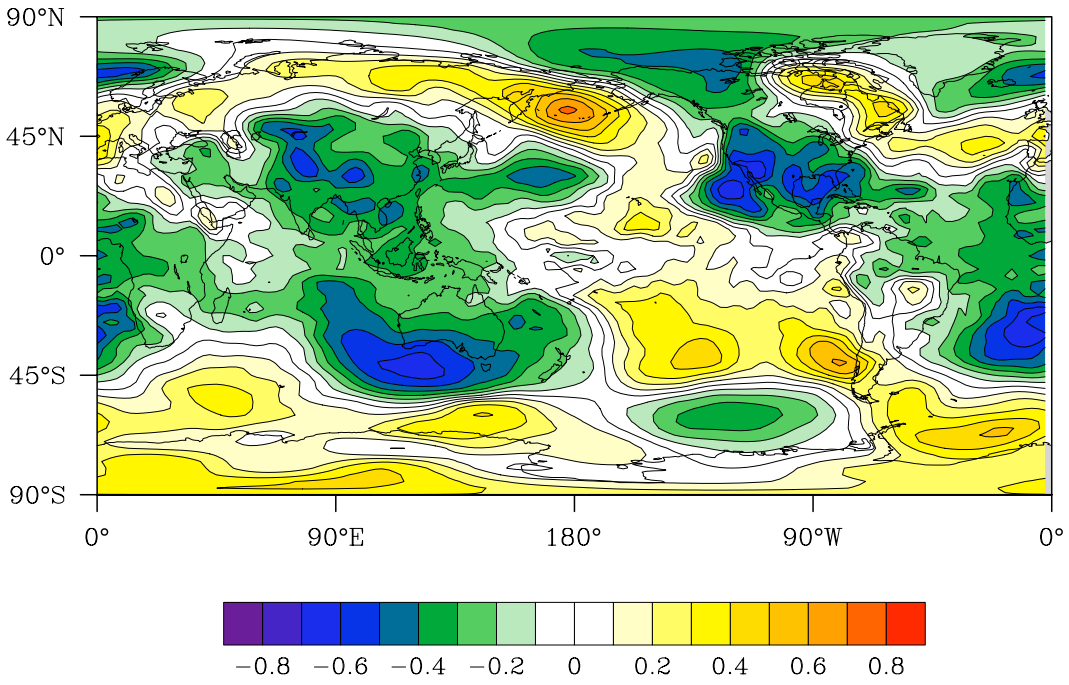

(a)

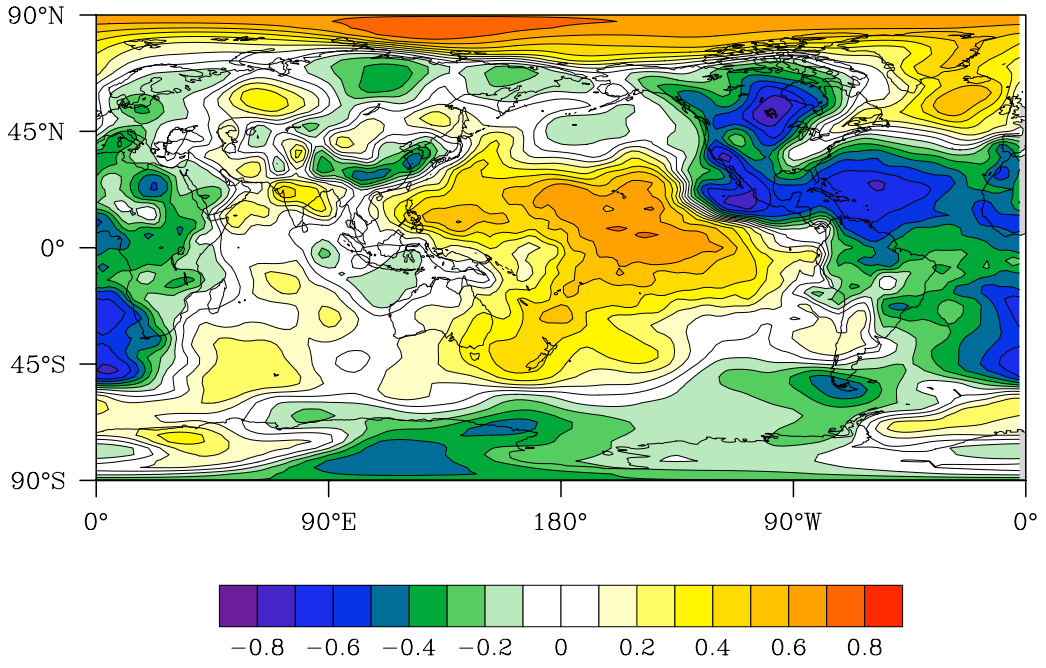

(b)

Figure 4.33 Same as in Fig. 4.21 except for 925 hPa geopotential heights.

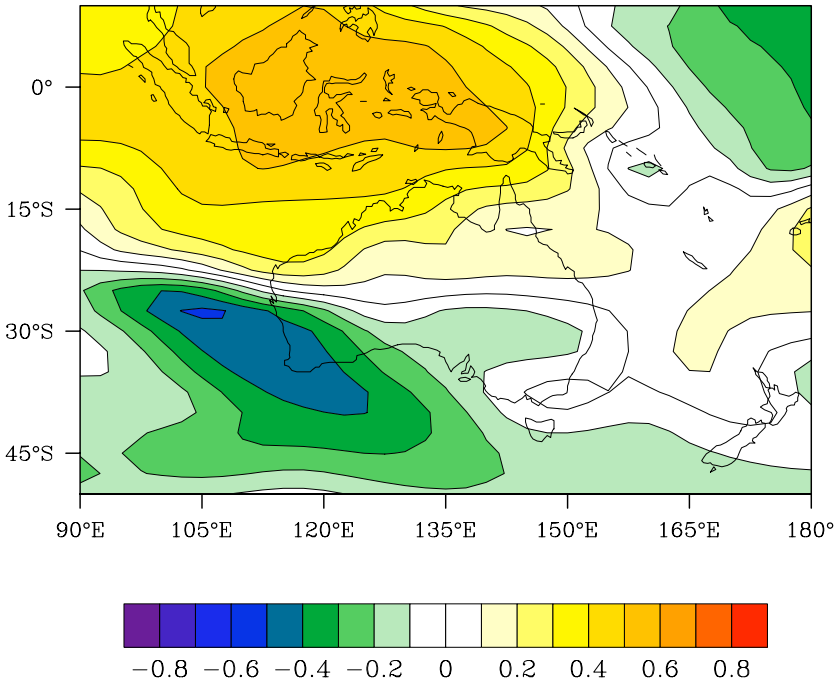

(a)

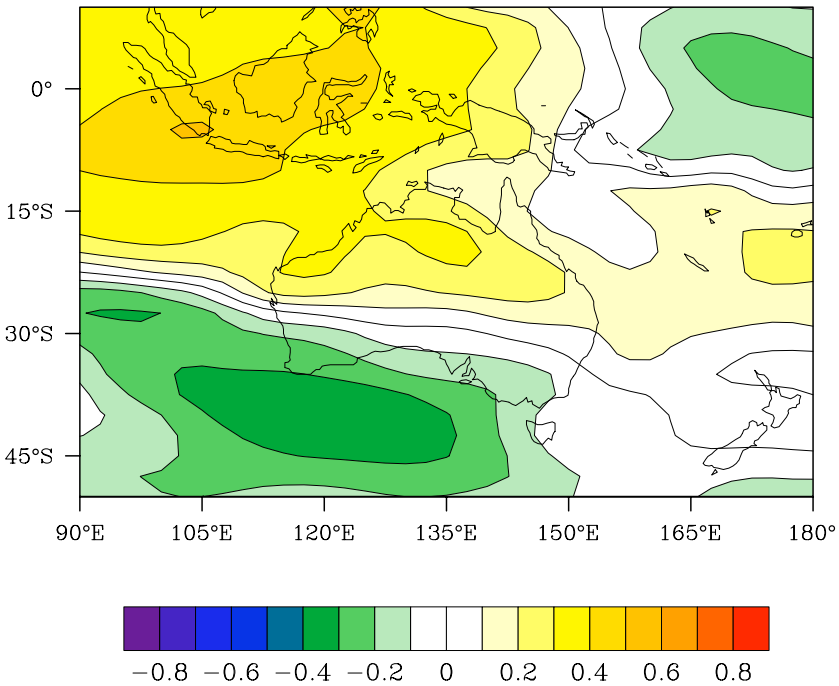

(b)

Figure 4.34 Same as in Fig. 4.22 except for Jun–Aug 925-hPa geopotential heights.

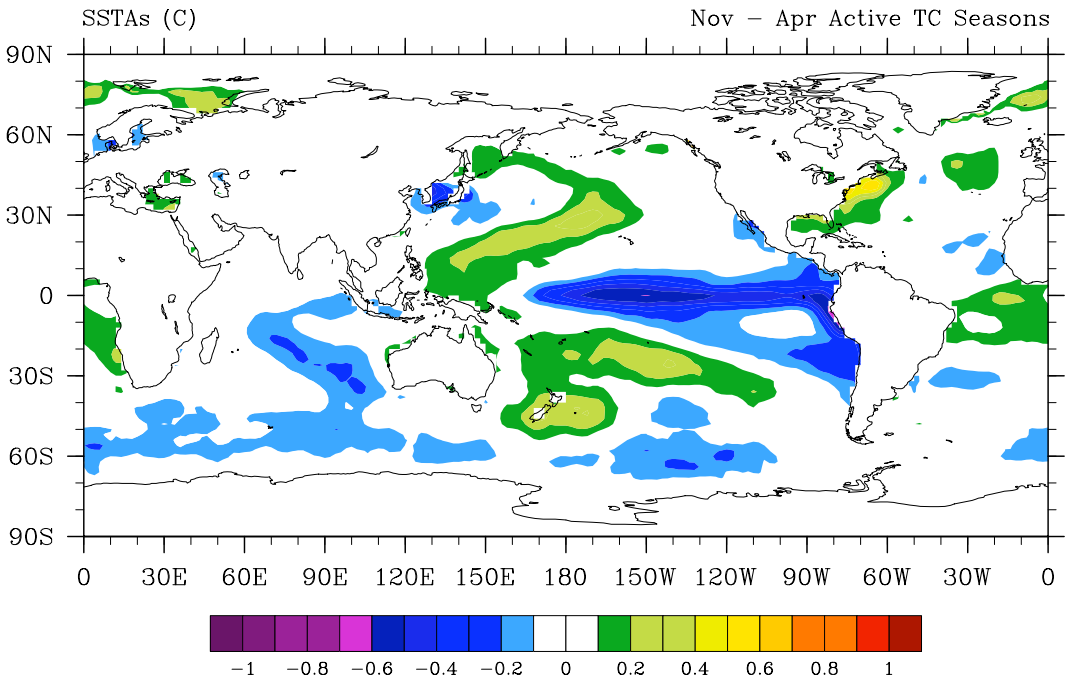

(a)

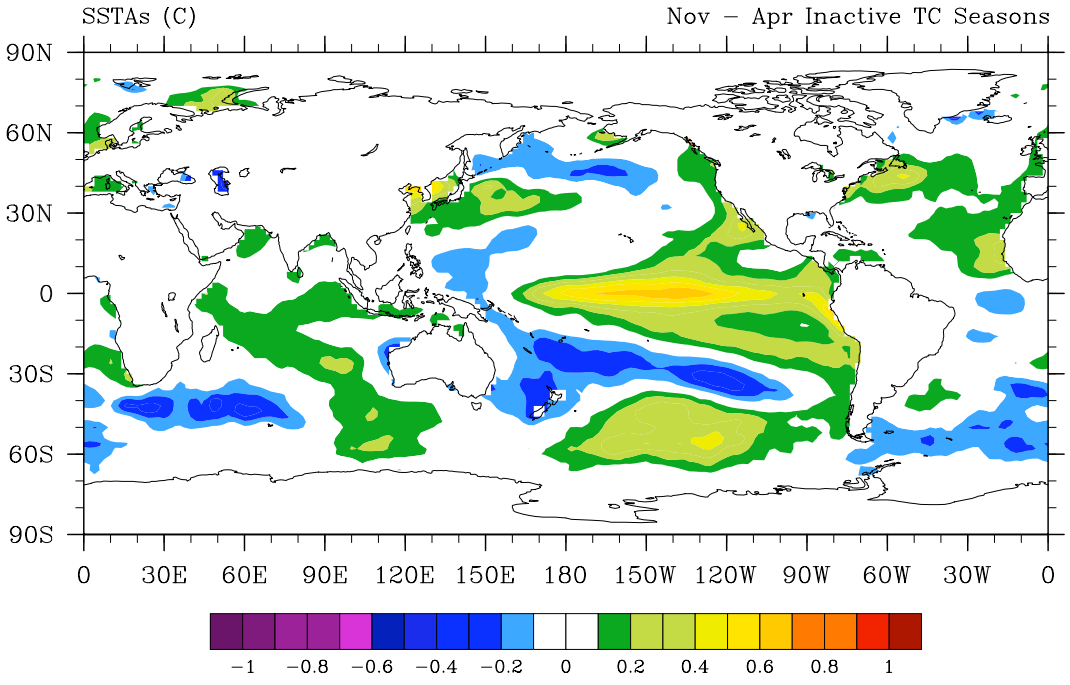

(b)

Figure 4.35 Composite maps for Nov–Apr SSTAs (a) ten most active seasons and (b) ten least active seasons.

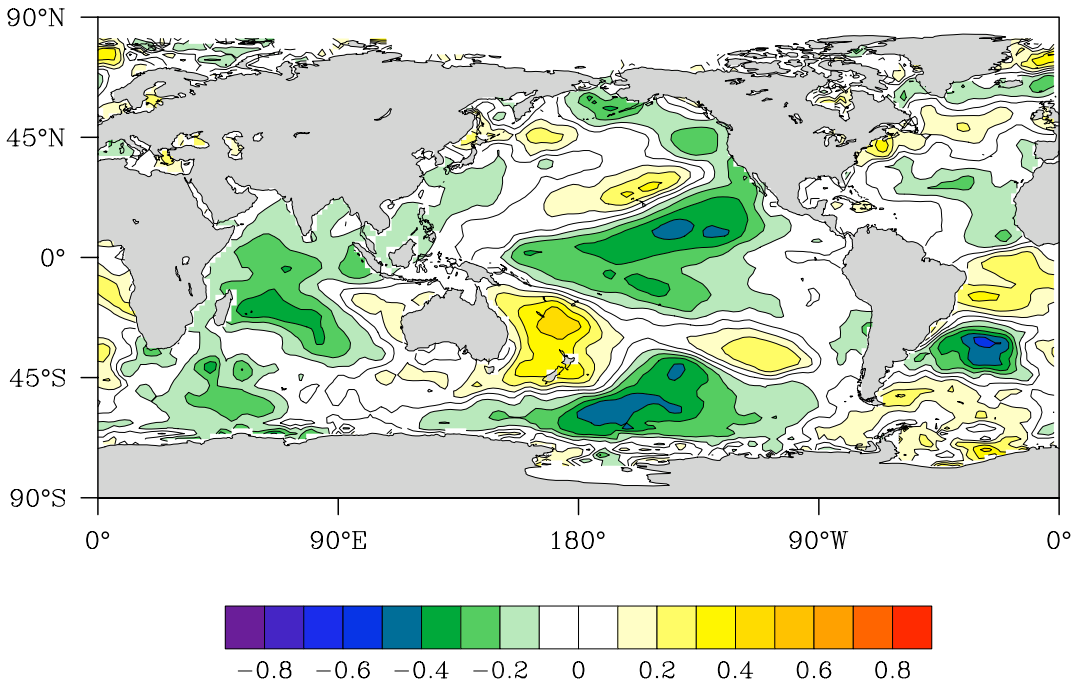

Figure 4.36 Same as in Fig. 4.20 except for Mar–May SSTAs.

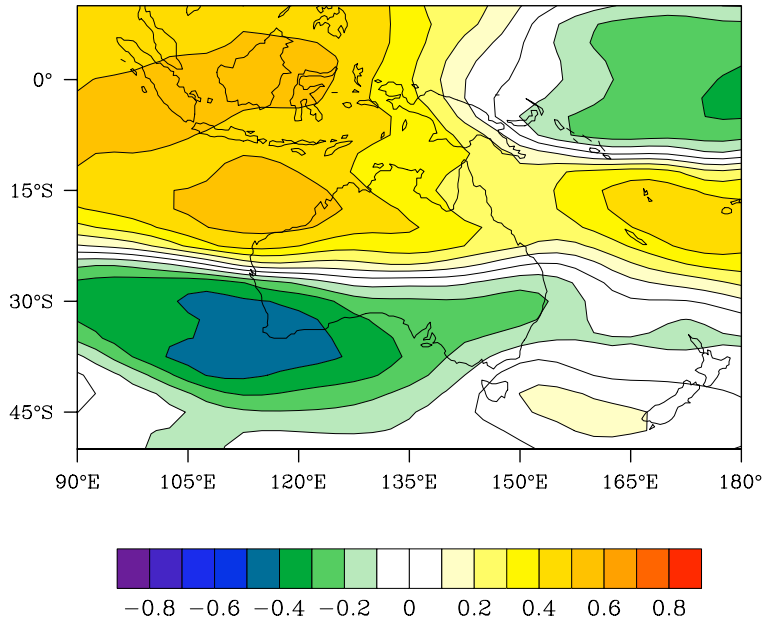

Figure 4.37 Same as in Fig. 4.22 except for Mar–May SSTAs.

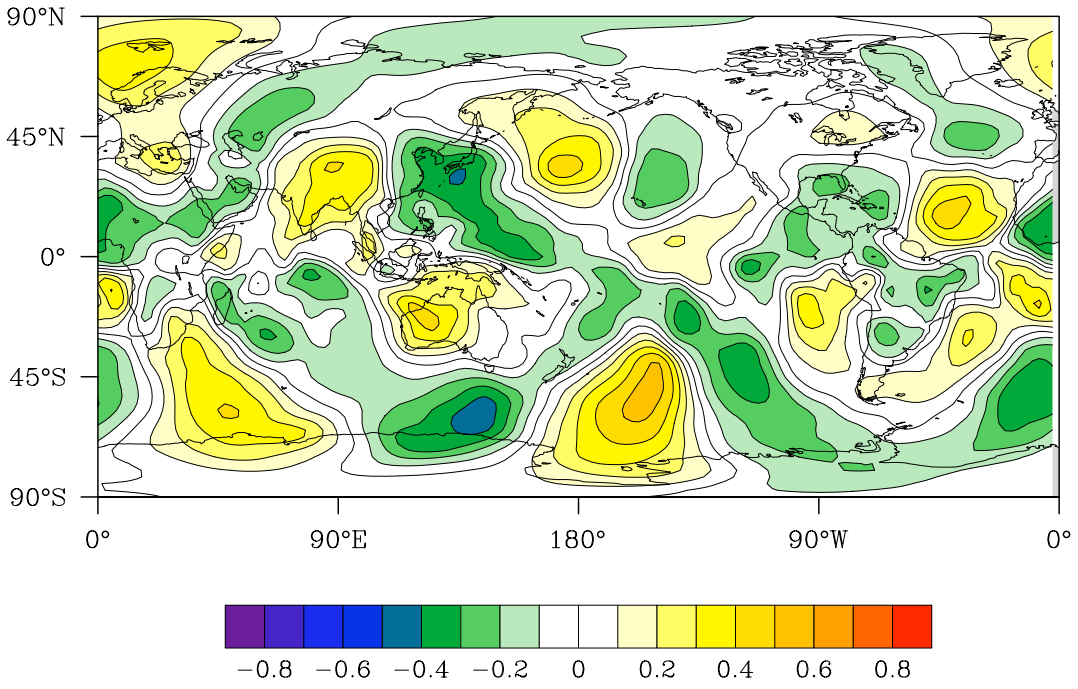

Figure 4.38 Correlation between Jan–Mar 100 hPa v-component of the wind and the number of TC days.

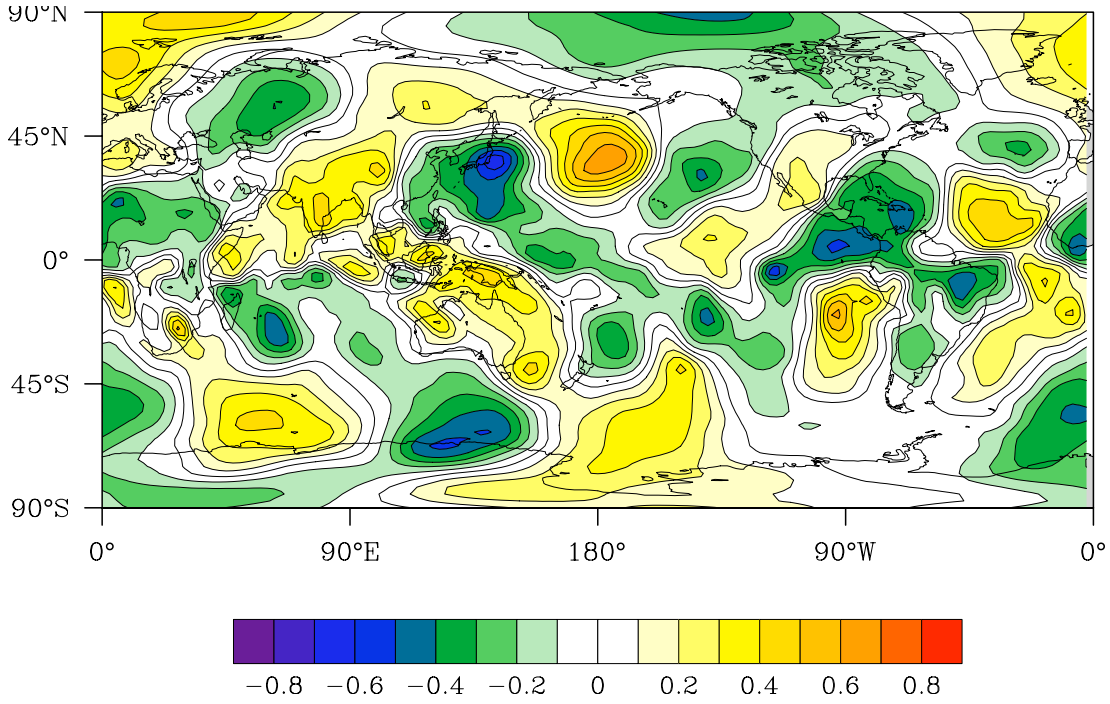

(a)

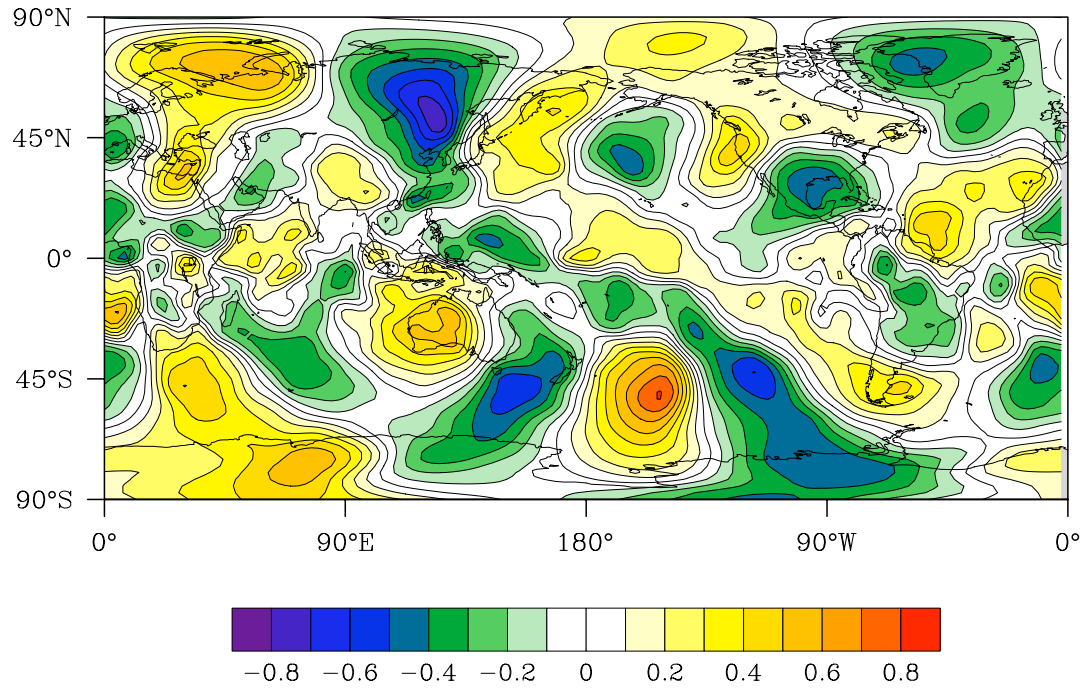

(b)

Figure 4.39 Same as in Fig. 4.42 except for (a) 1970–1989, and (b) 1990-2007.

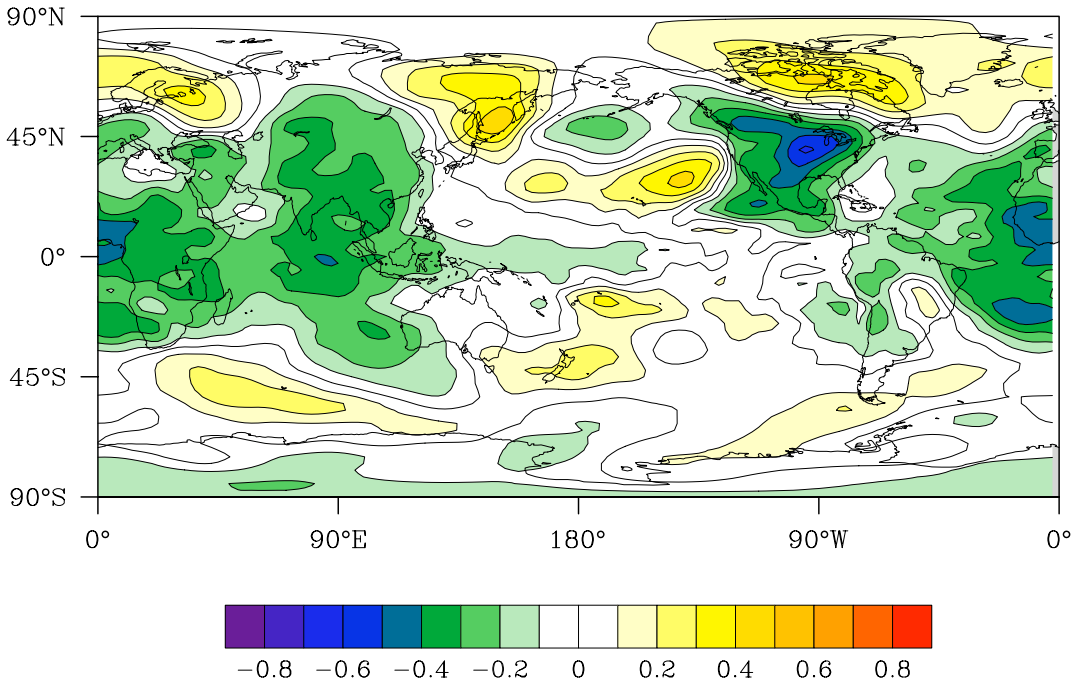

Figure 4.40 Correlation between Apr–Jun 850 hPa geopotential heights and the number of TC days.

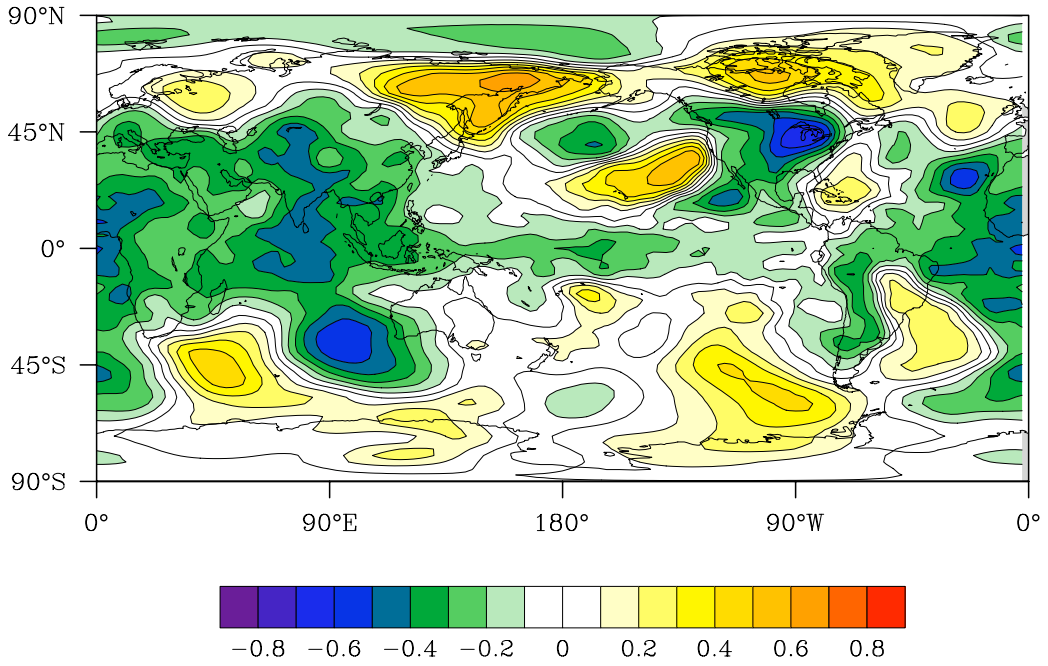

(a)

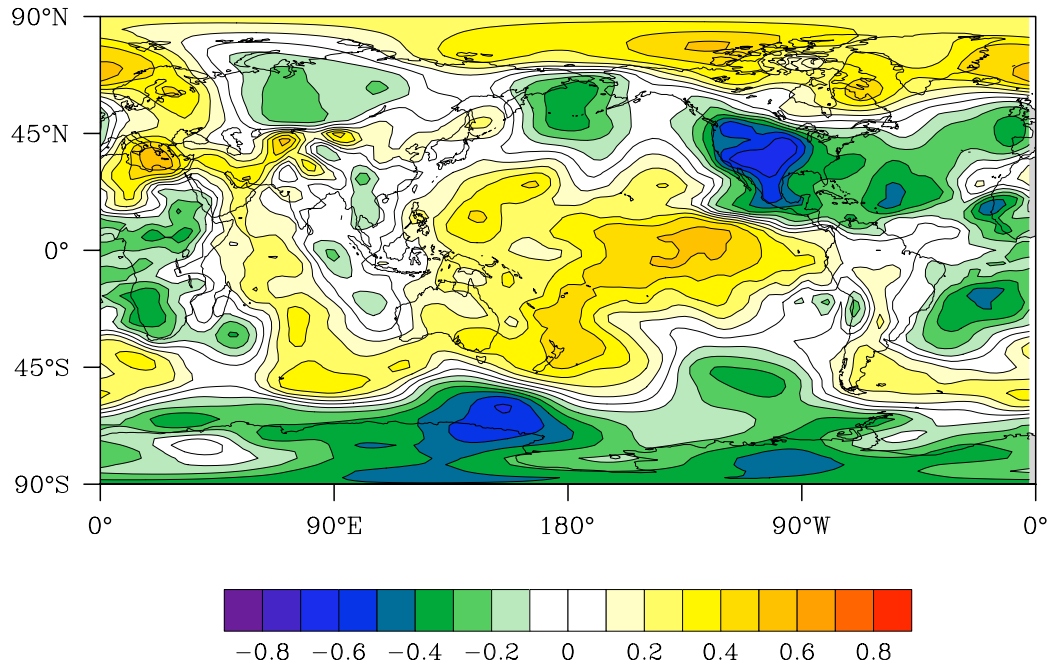

(b)

Figure 4.41 Same as in Fig. 4.40 except for (a) 1970–1989, and (b) 1990-2007.

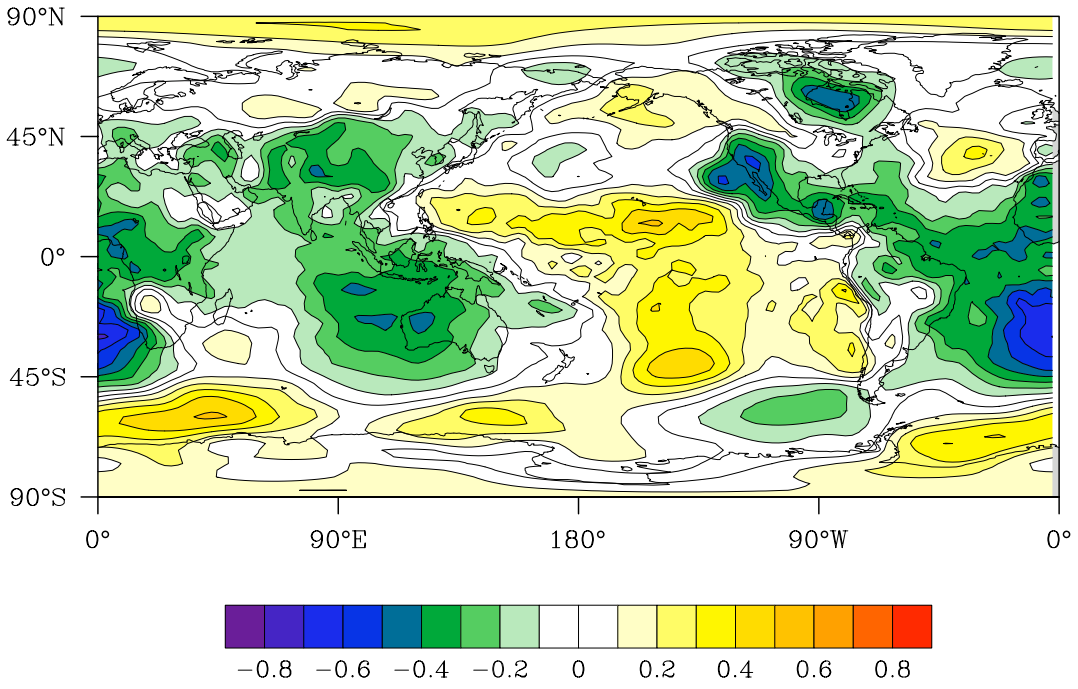

Figure 4.42 Correlation between Jul–Sep 1000 hPa geopotential heights and the number of TC days.

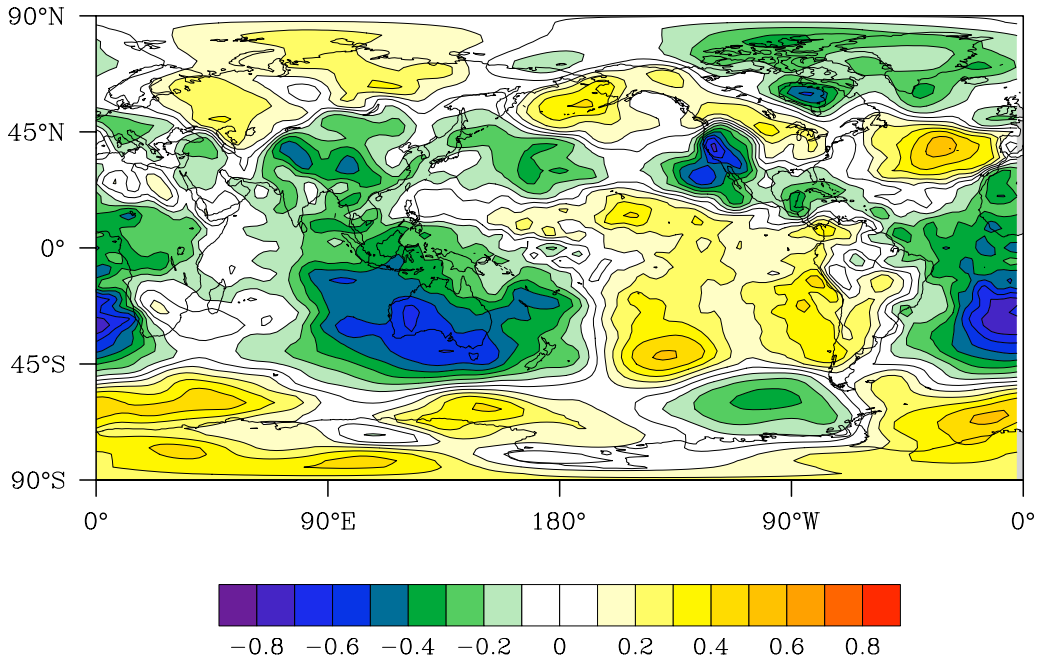

(a)

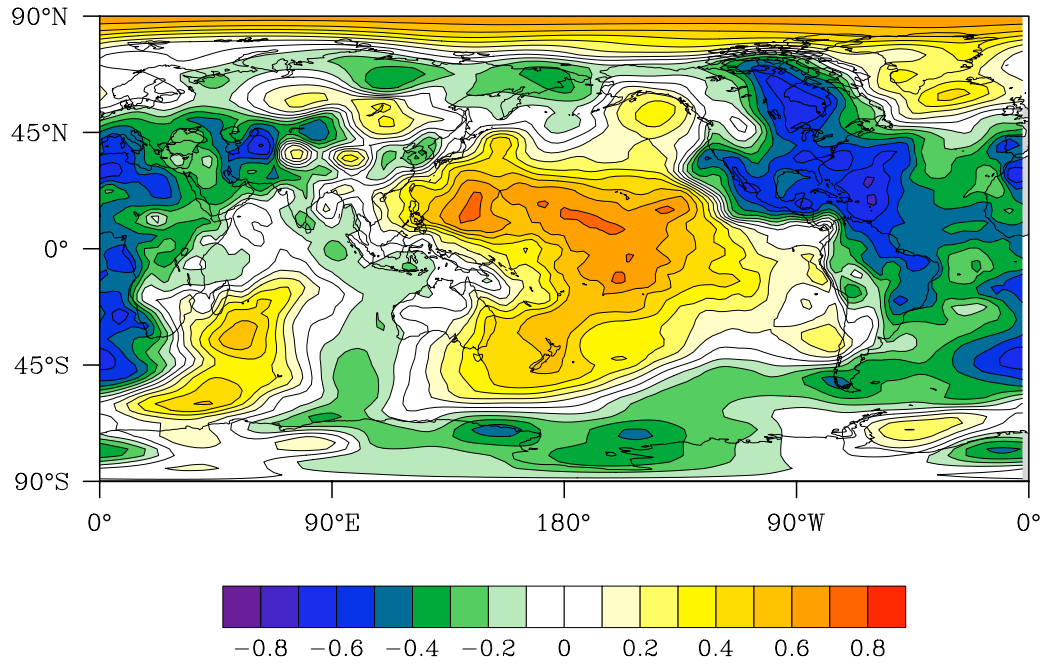

(b)

Figure 4.43 Same as in Fig. 4.42 except for (a) 1970–1989, and (b) 1990-2007.

There have been other global teleconnections identified, that are not directly linked to ENSO that are investigated in this study for both TC frequency and TC days. More research has been done on Northern Hemispheric teleconnections, therefore most research has been primarily focused on how the teleconnections affect precipitation patterns and storm tracks in that hemisphere. During most periods these teleconnection patterns were not significantly correlated to TC activity. One teleconnection pattern that has been used to explain the variations of hurricanes in the Atlantic region is the QBO (Gray 1984a; Gray et al. 1992), however, this study finds no link between the variability of the QBO and the variability of TC frequency in the NWAUS region.

Other already identified global teleconnections are generally not significantly correlated to the TC frequency or TC days in the NWAUS region. Some of the modes (e.g., NAO and AO) that were investigated were developed for other specific regions and thus do not adequately capture the atmospheric variability that influences the NWAUS region. A more encompassing approach may result from looking for new areas of variability in global reanalysis data.

Studies of the North Atlantic region have identified teleconnections from global reanalysis data in both the Northern and Southern Hemisphere to use as predictors for seasonal prediction schemes (e.g., Klotzbach and Gray 2003). A study of tropical cyclogenesis in the Australian region by McDonnell and Holbrook (2004a) used the six classic parameters discussed by Gray (1968), but their prediction was for individual cyclones and not a seasonal, basin-wide forecast. To search for parameters that better explain the variance of TC frequency and TC days in the NWAUS region, global parameters from the NCEP–NCAR reanalysis data were used. The areas where base state variables are strongly correlated with TC frequency and TC days also are related to the large-scale vertical wind shear, which is described by Dare and Davidson (2004) to be important to TC formation in the Australian region. The links between the extratropics and the tropics through global teleconnections are not well known.

The set of highly correlated base state variables from the NCEP–NCAR reanalysis, discussed previously, would be candidates for a seasonal prediction scheme of TC frequency and TC days in the NWAUS region. Previous studies of the NWAUS and entire Australian regions (Nicholls 1979, 1985, 1992; Solow and Nicholls 1990; Nicholls et al. 1998; Broadbridge and Hanstrum 1998) have only used ENSO related variables, where a multivariate approach may produce a more robust seasonal prediction scheme using the teleconnections identified in this study. In Chapter 5 a seasonal prediction scheme is developed and assessed using the moderate to highly correlated NCEP–NCAR reanalysis variables identified in this chapter.

Chapter 5

Seasonal TC Prediction for the NWAUS Region

Previous TC seasonal prediction schemes for the Australian region have focused primarily on the Southern Oscillation Index as a single linear predictor (e.g., Nicholls 1979, 1985, 1992; Nicholls et al. 1998). Recently, the SOI has been used in conjunction with the "Gray" parameters for use in a gridded prediction scheme using a Poisson statistical model. In this study, predictors other than the SOI have been investigated for use in a multiple linear regression prediction scheme. Using composite analyses and correlation maps a number of global reanalysis variables have been identified as possible predictors for a seasonal prediction scheme for the Northwest Australian region. In this chapter, a multiple-linear regression scheme is developed using the previously identified predictor variables from global reanalysis data for predicting: (i) the number of TCs reaching at least 17 m s^{-1} surface wind speed; and (ii) the number of TC days, for the NWAUS basin.

5.1 Multiple-Linear Regression

A common statistical technique is regression analysis and usually this is a least squares analysis with one dependent and independent variable. The goal is to fit a single line of regression to minimize the residual error in a least squares sense. The technique can be expanded to have more than one independent variable and then it is commonly referred to as multiple linear regression (MLR). The following is the development of

the MLR equations using typical matrix notation. We assume that there is a linear model that can be written as,

$$\boldsymbol{Y} = \boldsymbol{X}\beta + \epsilon \tag{5.1}$$

where $\mathbf{Y}$ is an $(n \times 1)$ vector of dependent observations, $\mathbf{X}$ is an $(n \times p)$ matrix of independent predictor variables, β is a $(p \times 1)$ vector of parameters, ϵ is an $(n \times 1)$ vector of errors, and the elements of ϵ are uncorrelated because the vector of errors is expected to sum to zero with variance, $V(\epsilon) = \mathrm{I}\sigma^2$. The unknown parameter β is estimated by minimizing the error sum of squares. The error sum of squares can be written as,

$$\varepsilon'\varepsilon = (\boldsymbol{Y} - \boldsymbol{X}\beta)'(\boldsymbol{Y} - \boldsymbol{X}\beta) \tag{5.2}$$

$$= \boldsymbol{Y}'\boldsymbol{Y} - 2\beta'\boldsymbol{X}'\boldsymbol{Y} + \beta'\boldsymbol{X}'\boldsymbol{X}\beta \tag{5.3}$$

The final estimate of β is denoted by $\mathbf{b}$ and is calculated by differentiating (5.2) with respect to β and setting the resultant matrix equation equal to zero and simultaneously replacing β with $\mathbf{b}$. This will give the value of $\mathbf{b}$ for which the error sum of squares is minimized. The differentiation yields the equation,

$$(\boldsymbol{X}'\boldsymbol{X})\boldsymbol{b} = \boldsymbol{X}'\boldsymbol{Y} \tag{5.4}$$

The only solution to (5.4) is if the matrix $\mathbf{X}'\mathbf{X}$ is not singular. If $\mathbf{X}'\mathbf{X}$ is singular, then the model must contain fewer parameters or have larger assumed restrictions. For the matrix not to be singular the equations cannot depend on each other and $\mathbf{X}$ must be a square matrix. Then, $\mathbf{b}$ can be estimated as,

$$\boldsymbol{b} = (\boldsymbol{X}'\boldsymbol{X})^{-1}\boldsymbol{X}'\boldsymbol{Y} \tag{5.5}$$

where the estimate of β minimizes the error sum of squares $\epsilon'\epsilon$ with no assumptions on the distribution of errors, the elements of $\mathbf{b}$ are linear functions of the dependent observations, $\mathbf{Y}$; and if the errors are independent and $\epsilon \sim N(0, \sigma^2)$; then $\mathbf{b}$ is the maximum likelihood estimate of β (Draper and Smith 1982).

5.2 Model Development

A common problem that arises during regression analysis is overfitting a model to the development data. There are many ways to guard against overfitting: selecting only physically relevant predictors, demanding minimal cross-correlation between predictors, using stepwise or best subset formations to select only the most important predictors, test the regression equation developed from a set of data on an independent data set, and have a reasonably large development data set. This study has attempted to account for overfitting by using various techniques to ensure that overfitting the forecast equation is controlled as much as possible.

Initially, all possible predictor variables for TC frequency from the global reanalysis data are subjectively analyzed to identify the areas with highest correlation to the TC time series. Next, all possible predictors, including known global climate modes, were cross-correlated to remove any predictors that were strongly correlated with another variable (Table 5.1). For example, the Niño 3.4 and Niño 4 SSTAs were found to be highly correlated with the HI 850-hPa air temperature (HI850), thus the HI850 predictor was retained with a higher correlation to the TC time series when compared with the SSTAs. In general, cross-correlations exceeding magnitude 0.4 would lead to the exclusion of one of the two predictor variables. From the final set of predictors used in the development of the prediction equation for TC numbers, only one cross-correlation exceeded magnitude 0.4. It is important to note that no Niño SSTAs are used explicitly in the prediction equations derived here.

After the final set of seven potential predictors was selected for TC frequency (Fig. 5.1), stepwise regression was used to further reduce the set of predictors to only include the fewest number of predictors needed to create a forecast model that minimized the forecast error. The stepwise scheme steps both forward and backward to select the final prediction model using the Akaike Information Criteria (AIC) to

determine which predictor variable to discard, before doing another iteration. If the residual sum of squares can be written as,

$$RSS = \sum_{i=1}^{n} \hat{\varepsilon}_i^2 \tag{5.6}$$

Then the formulation for the AIC in the case of least squares can be written as,

$$AIC = n[\ln(RSS)/n] + 2k \tag{5.7}$$

where k is the number of parameters in the statistical model and n is the number of observations. The first term represents the maximum-log likelihood estimate for the model and the second term is a penalty for too many predictor parameters in the model. The penalty term can also be thought of as helping to prevent overfitting. In this study, the model used was the one that attained the lowest value of AIC. This produced the best compromise between a good fit model and the least number of parameters to describe the variance of the data being modeled.

Similarly, for the prediction of TC days, the three reanalysis predictors (Fig. 5.2) to develop a multiple linear regression equation. The cross-correlation between the TC days predictors are all less than | 0.3 | (Table 5.2). The prediction equation developed uses the same stepwise regression technique with the lowest AIC value indicating the most robust prediction equation.

To provide an assessment of skill for a prediction scheme, it is useful to compare the prediction scheme against forecasts obtained from climatology and from persistence. A persistence forecast uses the previous year TC metric as the TC metric that will occur during the following season, whereas climatological forecasts predict the average of the TC metric to occur every year. To assess the skill of a particular prediction scheme, it is essential to have a way to identify the amount of error that results from its prediction. A commonly used measure of error is the Mean Square Error (MSE),

$$MSE = \frac{1}{n} \sum_{i=1}^{n} (y_i - o_i)^2 \tag{5.8}$$

Table 5.1 Cross-correlation of selected predictors to be used in the multiple linear regression scheme.

Mar-May RUS 500 hPa Geo Hght	Mar-May SATL SSTA	Apr-Jun NA 700 hPa Geo Hght	May-Jul Hi 850 hPa Air Temp	May-Jul SIND 850 hPa Geo Hght	Jun-Aug EPAC 925 hPa Geo Hght	Jun-Aug SEATL 925 hPa Geo Hght
1.000	0.319	0.132	0.309	-0.331	0.398	-0.194
	1.000	0.325	0.312	-0.116	0.243	0.222
		1.000	0.378	-0.416	0.287	0.232
			1.000	-0.331	0.303	0.100
				1.000	-0.339	-0.012
					1.000	0.132
						1.000

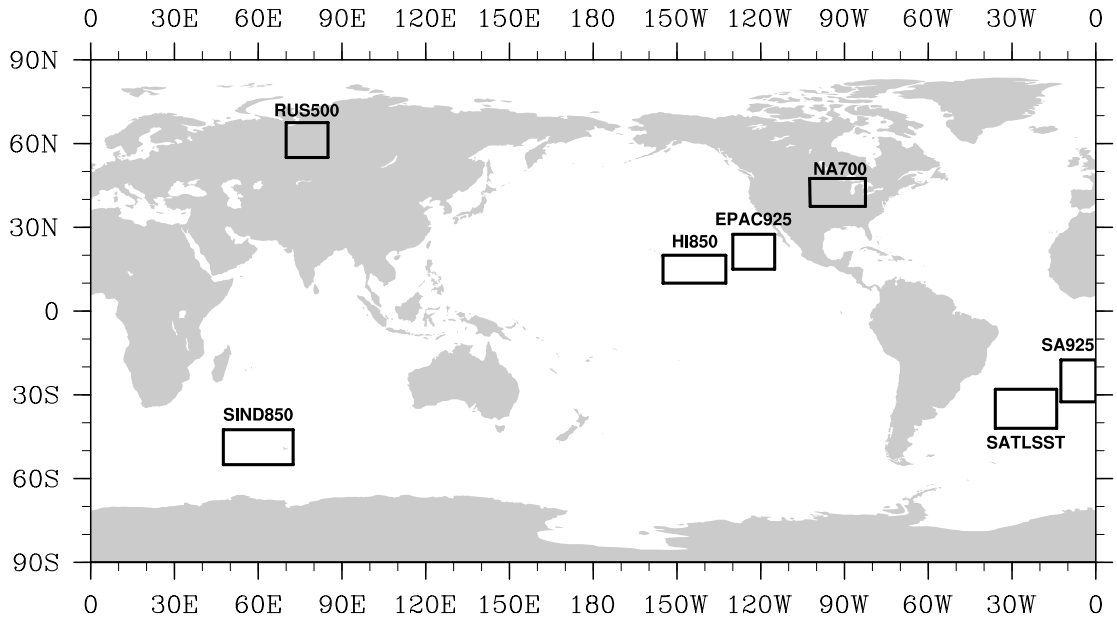

Figure 5.1 A location map of the seven predictors used in a seasonal forecast prediction scheme for TC frequency in the NWAUS region.

Table 5.2 Cross-correlation of selected predictors to be used in the multiple linear regression scheme.

Jan-Mar SPAC 100 hPa V-wind	Apr-Jun NA 850 hPa Geo Hght	Jul-Sep SATL 1000 hPa Geo Hght
1.000	0.286	-0.185
	1.000	-0.245
		1.000

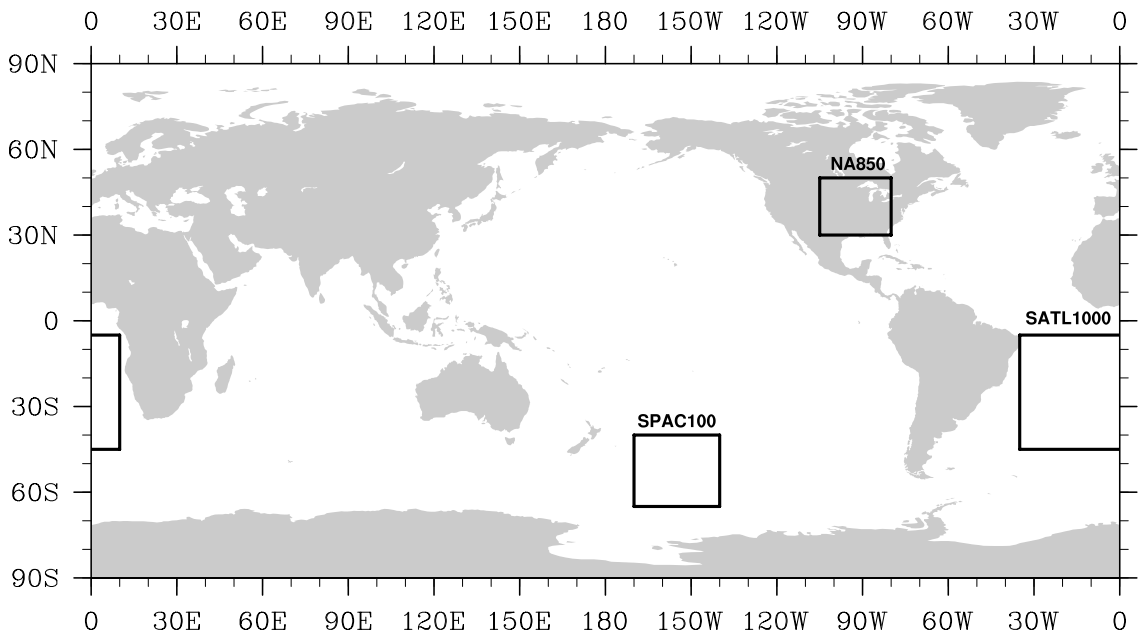

Figure 5.2 A location map of the three predictors used in a seasonal forecast prediction scheme for TC days in the NWAUS region.

where y_i is the predicted TC count for a given year, i, and o_i is the observed TC count for that same given year. The MSE is the average squared difference between the prediction and observation pairs. A MSE of zero would indicate a perfect prediction scheme. Many times the MSE is reported as a root mean square error (RMSE), where RSME = $\sqrt{MSE}$, which puts the error in the same dimensions as the observations. Another measure of error commonly used to is the Mean Absolute Error (MAE),

$$MAE = \frac{1}{n}\sum_{i=1}^{n}|y_i - o_i| \tag{5.9}$$

where y_i is the predicted TC count for a given year, i, and o_i is the observed TC count for that same given year. Similar to the MSE, except that the MAE uses the absolute difference between the prediction and observation pairs. The MAE is in the same dimensions as both the MSE and MAE provide a measure of the accuracy of a given prediction scheme.

The prediction equation developed for TC frequency and TC days have been assessed using all 39 years of available data. The leave-one-out cross validation technique to estimate the forecast ability of the seasonal prediction schemes. The leave-one-out cross validation method develops a seasonal prediction equation, using the method described above, while leaving one year out to independently predict that single year up to the number of years used for the development dataset. After that point the prediction equations 5.10 and 5.11 are used to hindcast the respective TC metrics. Using the leave-one-out method will provide a more accurate assessment of the skill of the forecast scheme because the year being predicted was not a part of the development data set.

Using the leave-one-out method and the RMSE discussed earlier, the number of years used in the development dataset was varied between 5 and 35 years, in an effort to determine the minimum number of years needed to provide a stable prediction (Fig. 5.3). Too few years in the development data set and insufficient variance is known

to inhibit the ability to accurately determine the coefficients in the MLR prediction scheme. A sharp decrease in RMSE is observed as the development length increases to 10 years for TC frequency (Fig. 5.3a). The RMSE continues to decrease when adding additional years to the development dataset, leveling off when the development data set contained 28 or more years. Therefore, in this study the development data set for TC frequency contains the 28 years from 1970 to 1997.

For TC days, there is a similarly large decline in the RMSE as the number of years increases in the development dataset. However, the RMSE does not level off until approximately 32 years of data in the development data set is used (Fig. 5.3b). Therefore, the development dataset for the TC days prediction scheme covers the 34 years from $1970 - 2003$.

The seasonal prediction schemes then were derived using each respective development data set and yielded the following prediction equation for TC frequency

$$y = 5.5714 + -0.8835X_3 + -0.5758X_4 + 0.5856X_5 + -0.4619X_6 + -0.8047X_7, \quad (5.10)$$

where y is the predicted number of TCs, X_3 is NA 700 hPa geopotential heights, X_4 is HI 850 hPa air temperature, X_5 is SIND 850 hPa geopotential heights, X_6 is EPAC 925 hPa geopotential heights, and X_7 is SATL 925 hPa geopotential heights. The Analysis of Variance (ANOVA) table for the TC frequency prediction scheme indicates that all predictors are significant at least at the 95% confidence interval (Table 5.3). Inspecting the residuals from the TC frequency prediction equation yields residual errors that appear to be constant and normal (Fig. 5.4).

The seasonal prediction equation for TC days

$$y = 43.641 + -11.072X_1 + -7.854X_2 + 7.002X_3 \quad (5.11)$$

where y is the predicted number of TC days, X_1 is SATL 1000 hPa geopotential heights, X_2 is NA 850 hPa geopotential heights, and X_3 is SPAC 100 hPa v-component

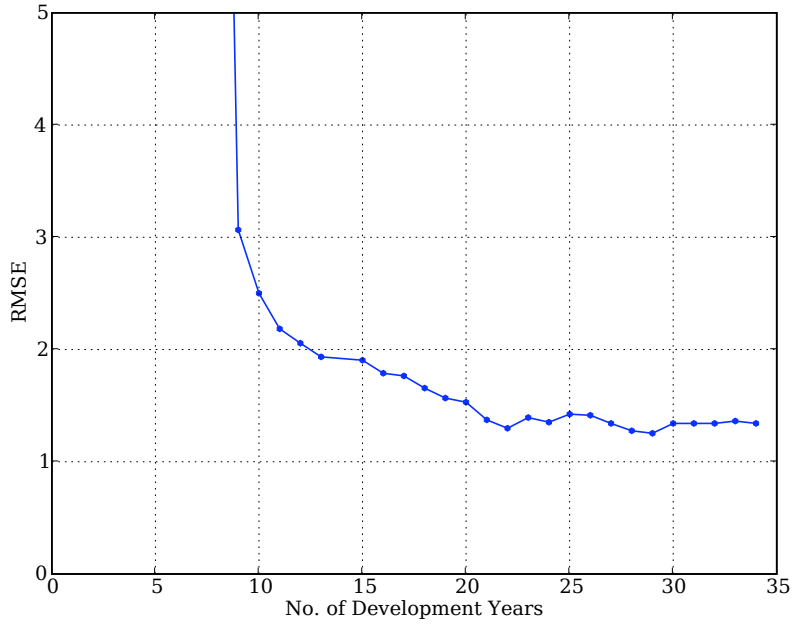

(a)

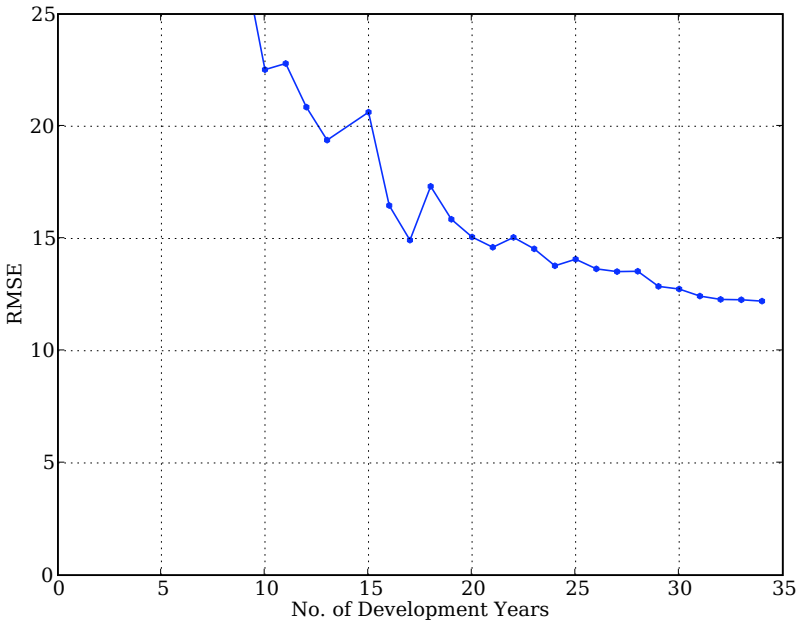

(b)

Figure 5.3 A plot of the number of years used in the development prediction scheme and its reported RMSE for (a) TC frequency and (b) TC days.

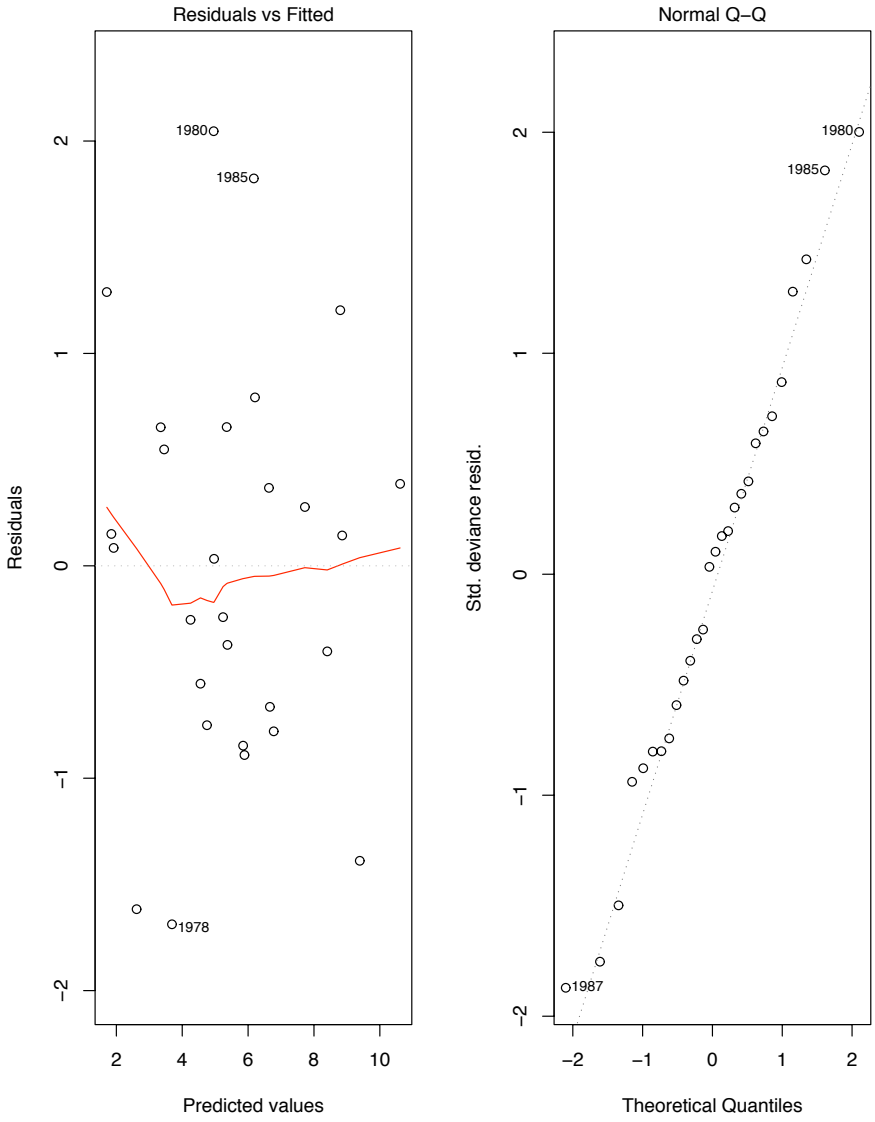

Figure 5.4 A plot of residuals versus fitted values and a Q-Q plot to inspect the error variance of the TC frequency prediction equation.

of the wind. For the TC days prediction equation, all of the predictors are significant at least at the 99% confidence interval (Table 5.4). Residual analysis appears to indicate that there is constant variance, which is normally distributed, although less so than for the prediction of TC frequency (Fig. 5.5).

Due to the serial correlation of the TC frequency time series, the leave-one-out method likely over-estimates the true skill of the prediction scheme. To mitigate the impact of the serial correlation, the process was repeated, leaving out five consecutive years and predicting the middle three years from the developed equation for the remaining data using 28 years in total for the development dataset. Similar results are found using this technique as to the leave-one-out method. A direct comparison of the number of TCs predicted using the leave-one-out method to the number of observed TCs show a qualitatively good agreement (Fig. 5.6a). A Pearson product-moment correlation yields a cross-correlation of 0.840. The leave-five-out predict three hindcast predicted TC frequency time series corresponds nearly as well with the observed numbers of TCs (Fig. 5.6b) and the correlation coefficient is 0.801. Due to the more conservative results, the second method will be preferred in order to not over-estimate the true skill of the prediction scheme.

Development of the prediction equation for TC days follows similarly to TC frequency. Using the leave-one-out method the observed and hindcast predicted time series of TC days indicate good agreement (Fig. 5.7a) with a correlation coefficient of 0.810. Again, owing to the non-negligible seriel correlation of the TC days time series, the TC Days scheme was re-evaluted leaving five consecutive years out and predicting the middle three years. Doing so still yields good agreement between observed and hindcast predicted TC days, with a nearly the same correlation coefficient of 0.797.

To further assess the skill of the forecast equations, the RMSE, and MAE can be analyzed. The MSE and MAE for persistence and climatological forecasts of the number of TCs and TC Days for the NWAUS region are given in Tables 5.5 and 5.6,

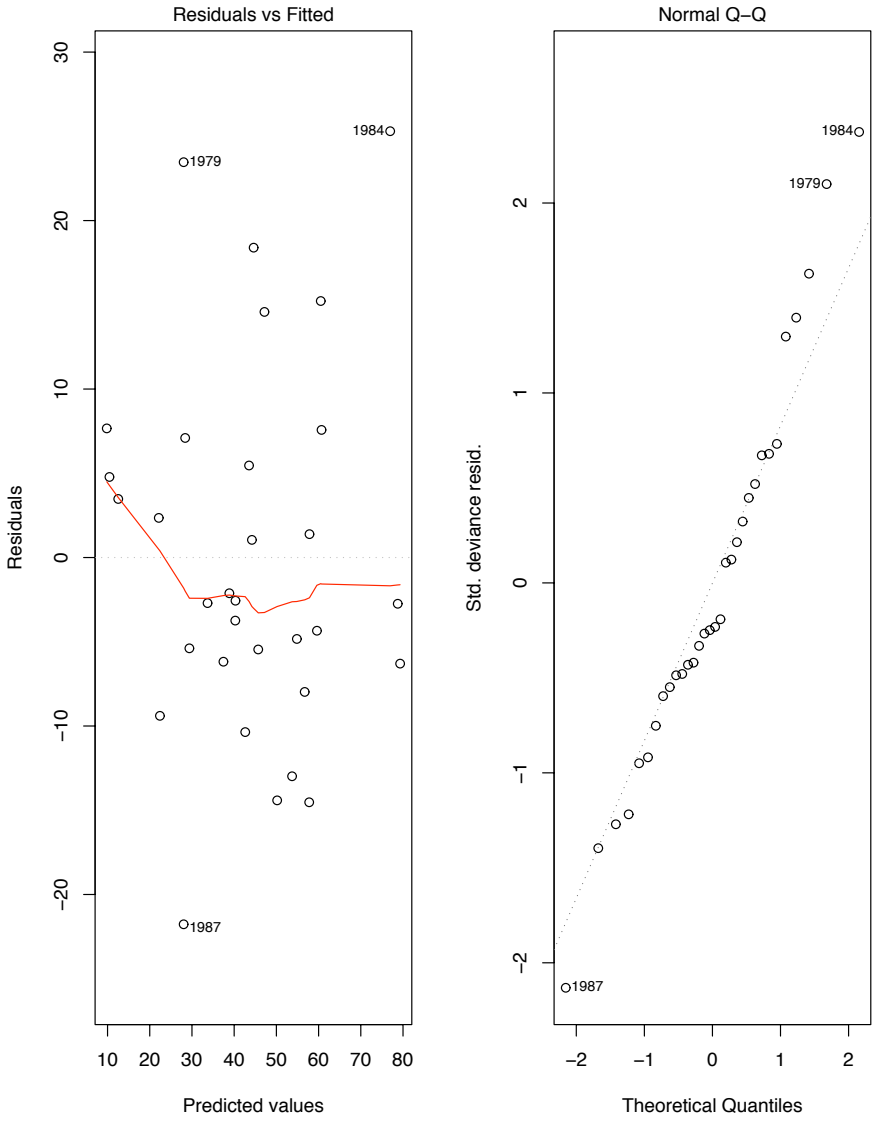

Figure 5.5 A plot of residuals versus fitted values and a Q-Q plot to inspect the error variance of the TC Days prediction equation.

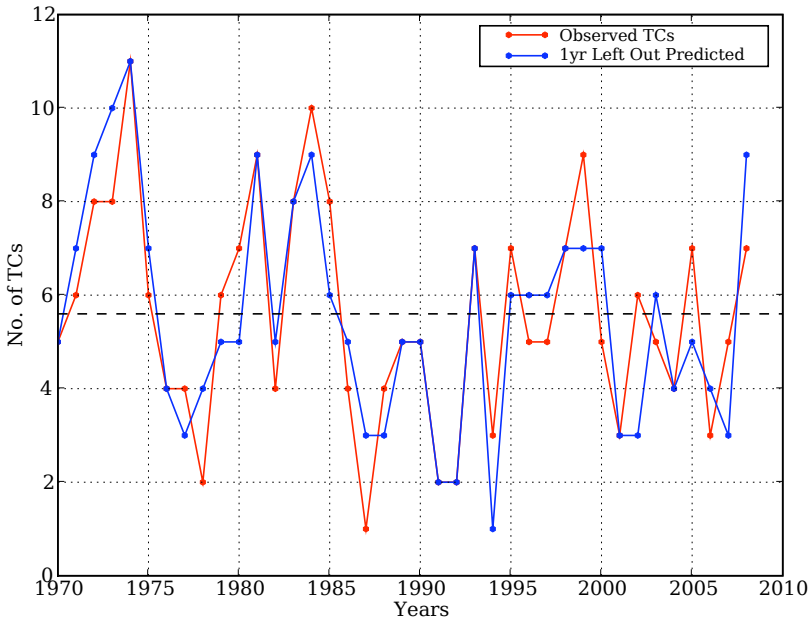

(a)

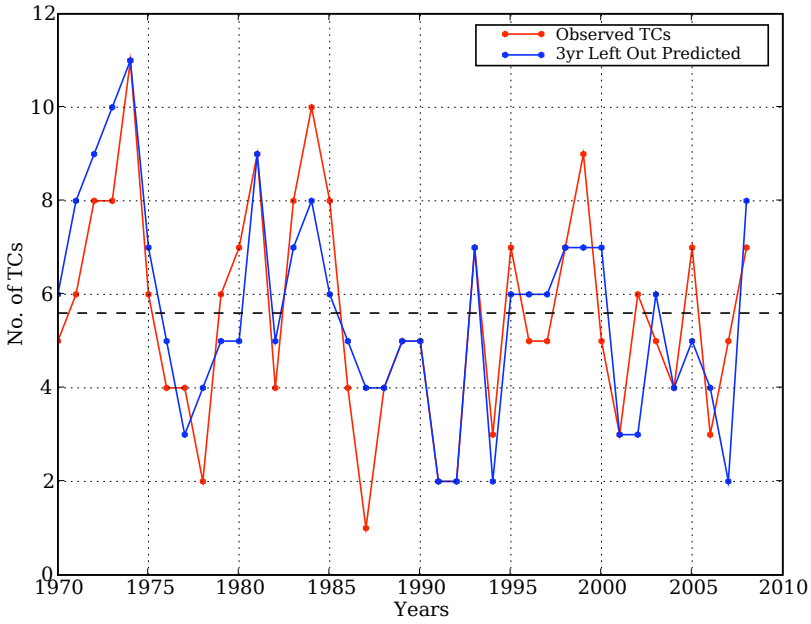

(b)

Figure 5.6 Number of TCs occurring in a given year (red) and the jack-knifed hindcast from the TC frequency prediction scheme (blue) for (a) leave-one-out method and (b) leave-out-five predict three method.

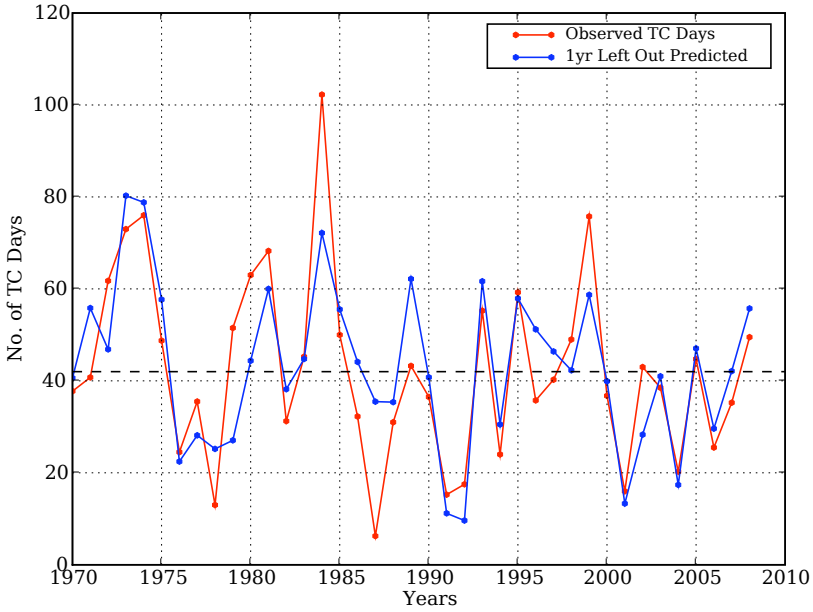

(a)

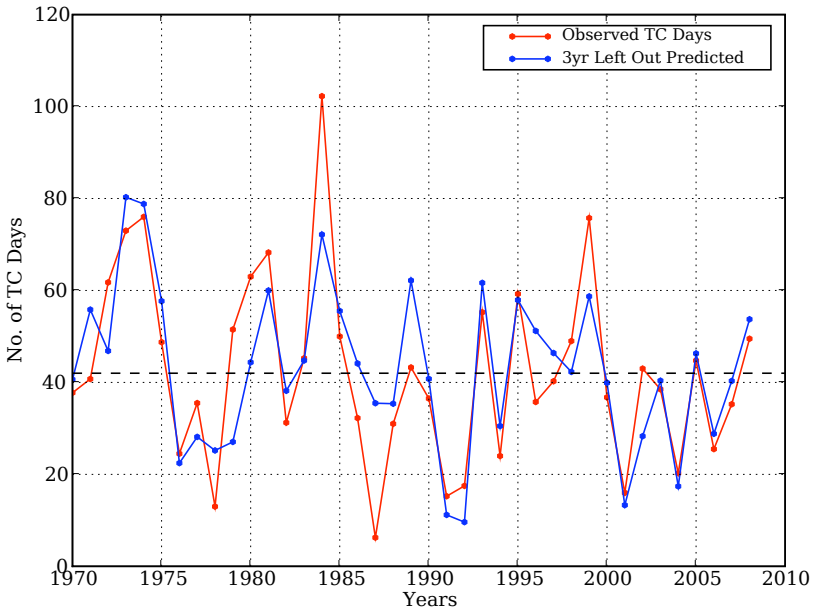

(b)

Figure 5.7 Number of TC Days occurring in a given year (red) and the jack-knifed hindcast from the TC frequency prediction scheme (blue) for (a) leave-one-out method and (b) leave-out-five predict three method.

respectively. It is evident from the table that the climatological forecasts are superior to the persistence forecasts. However, we can quantify how much better a one forecast is when compared with another using a skill score. A common skill score (SS) can be written as,

$$SS = \frac{MSE - MSE_{\text{Ref}}}{0 - MSE_{\text{Ref}}} = 1 - \frac{MSE}{MSE_{\text{Ref}}} \tag{5.12}$$

where MSE_{Ref} is the MSE of a reference forecast and where MSE can be replaced by MAE or another estimate of the error of a prediction scheme (Wilks 2005). A perfect SS of 1 is achieved when the $\text{MSE}_{Ref} >>$ MSE and the prediction scheme being tested would be considered to be 100% better than the reference forecast.

For this study, both the forecast of TC frequency and TC days have lower RMSE and AME as compared to a forecast using persistence; therefore, the climatology forecast will be used as the reference forecast to asses the skill of each prediction equation. The RMSE for TC frequency prediction is 1.41 TCs (Table 5.5) and utilizing a tilted bootstrap (Efron and Tibshirani 1994), with 1000 replications, to assess a 95% confidence interval the RMSE likely ranges between 0.92 and 1.85 TCs (Fig. 5.8). Similarly, the AME of TC frequency prediction is 1.08 TCs with a 95% confidence interval between 0.71 and 1.44 TCs. Conducting a tilted bootstrap using climatology of 5.6 storms per year as the prediction yields a RMSE of 2.32 storms with a 95% confidence interval between 1.61 and 3.06 storms (Fig. 5.8). The confidence intervals for the RMSE of TC frequency prediction by 5.10 and climatology only slightly overlap. With moderate certainty it can be concluded that 5.10 is significantly better than climatology at forecasting the number of TCs for the oncoming season using Tukey's rule of thumb (Fig. 5.8; Tukey 1991). Overall predictions improved over 60% from a climatological forecast for the median values of the bootstrapped RMSE. Similar results for AME can be obtained.

For the prediction of TC days, the RMSE is 12.03 days with the 95% confidence interval falling between 7.47 and 16.3 days (Fig. 5.8). The AME is 9.51 days with

Table 5.3 ANOVA table for the TC frequency prediction scheme.

	Df	Sum Sq	Mean Sq	F value	Pr(>F)	
X3	1	79.656	79.656	72.8329	1.986E-08	***
X4	1	30.887	30.887	28.2409	2.47E-05	***
X5	1	15.314	15.314	14.0020	0.001129	**
X6	1	7.887	7.887	7.2117	0.013512	*
X7	1	13.053	13.083	11.9347	0.002256	**
Residuals	22	24.061	1.094			
Signif. Codes: *** 0.001, ** 0.01, * 0.05, . 0.1						

Table 5.4 ANOVA table for the TC Days prediction equation.

	Df	Sum Sq	Mean Sq	F value	Pr(>F)	
X1	1	6824.0	6824.0	50.911	9.169E-08	***
X2	1	2298.5	2298.5	17.148	0.0002876	***
X3	1	1413.3	1413.3	10.544	0.0030216	**
Residuals	28	3753.1	134.0			
Signif. Codes: *** 0.001, ** 0.01, * 0.05, . 0.1						

Table 5.5 Observed RMSE error for persistence and climatological forecasts for the TC frequency prediction using persistence and climatology NWAUS region for the period 1970 to 2005.

	RMSE	AME
Persistence	2.77	2.33
Climatology	2.32	1.92
MLR Prediction	1.41	1.08

Table 5.6 Observed RMSE error for persistence and climatological forecasts for the TC Days prediction using persistence and climatology NWAUS region for the period 1970 to 2005.

	RMSE	AME
Persistence	24.22	19.96
Climatology	19.72	15.12
MLR Prediction	12.03	9.51

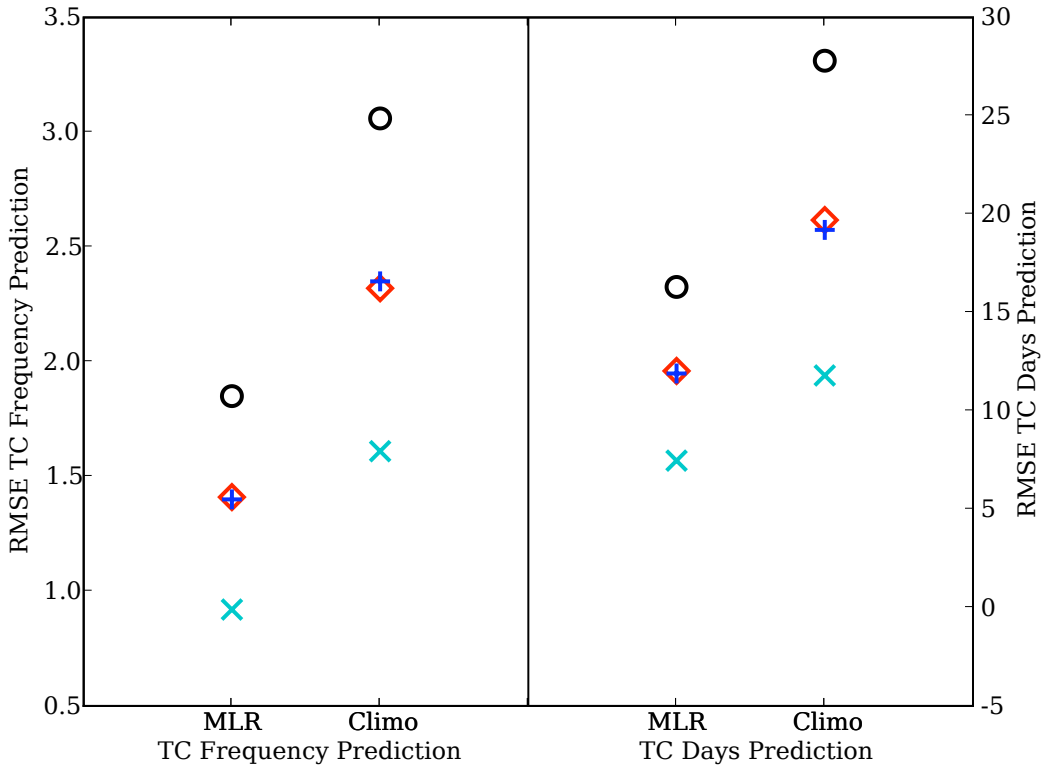

Figure 5.8 A plot of the confidence intervals (97.5% black circle, 50% red diamond, 2.5% cyan cross, observed value blue plus) of the RMSE of TC frequency and Days prediction from the multiple linear regression technique developed in this study versus a prediction RMSE using climatology.

a 95% confidence interval between 5.89 and 13.6 days. Using climatology as a predictor yields a RMSE of 19.72 days, and after a tilted bootstrap a 95% confidence interval between 11.8 and 27.8 days (Fig. 5.8). In this case, the confidence intervals slightly overlap and a direct determination cannot be made of whether the hindcast predictions made with 5.11 is significantly better that a prediction using climatology. A Mann-Whitney-Wilcoxon test (Mann and Whitney 1947) to assess if the two populations of bootstrapped RMSE are likely from the same population. The test returns a value of $W = 84044$ and a p-value $< 2.2\text{E}^{-16}$, indicating that the RMSE are significantly different. Thus, the TC days prediction equation developed in this study performs better than climatology.

Overall, both the TC frequency and TC days prediction equations are an improvement over a climatological forecast of each. Previous studies, including McDonnell and Holbrook (2004a,b), were not able to produce successful seasonal predictions of TC activity in the NWAUS region. For the entire Australian region, Nicholls (1985) had similar MAE for both persistence and climatological forecasts (19.5 and 12.7 days, respectively), to the values obtained for the NWAUS region in this study (Table 5.6). Nicholls (1985) reported MAE for his prediction scheme for the entire Australian region was 9.4 days using a leave-one-out method, as compared to 9.51 days for this study.

Comparing the prediction equations to similarly developed equations for other TC basins, indicates that the equations for the NWAUS are as skillfull. Using the verification statistics ($1984 - 2008$) for the forecasts for the North Atlantic Ocean conducted by the Gray research group yields a skill score over climatology of 31% for named tropical storms and 18% for names tropical storm days for their June forecasts of the oncoming TC season. The Gray research group has also issued forecasts during April from $1995 - 2008$, these forecasts have not performed better than climatology

as the calculated skill scores are less than zero for both the predicted named storms and predicted named storm days.

5.3 Contingency Tables

Another verification tool to assess the ability of the TC metric forecast equations developed in this study are the use contingency tables. There are different ways to assess the skill of the forecast schemes developed in this study using contingency tables, one involving three categories and another involving just two categories. Contingency tables are classically used on binary (yes,no) categorizations of events, in this study we separate the individual forecasts into three categories (below average, average, and above average) and two categories (below average, average and above) to ascertain the skill of the prediction equations.

5.3.1 Three Categories

Initially, the forecasts produced by the TC frequency and TC days prediction schemes are separated into three categories (Below Average, Average, and Above Average). The inner-quartile was used to define the average number of TCs per season, which is 4 to 7 storms. While an above average season is defined as any year in which there are more than 7 storms and below average year to be on in which there are fewer than 4 storms. The observed contingency table is give in Table 5.7. The forecast equation for TC frequency was never off by more than one category.

For the prediction of TC days, the inner-quartile was again used to define the average number of TC days per season, which was 31.75 to 57.25 TC days per year. An above-average season is one which has more than 57.25 TC days per year and a below-average season has less than 31.75 storms per year. The observed contingency table for TC days is given in Table 5.9. Similar to the prediction of TC frequency,

the forecast scheme never predicted the number of TC days to be off by more than one category.

A limited number of attributes can be calculated for the three by three contingency table. The following are the attributes calculated for each prediction scheme: proportion correct (PC), probability of detection (POD), Bias, Peirce Skill Score (PSS), and Heidke Skill Score (HSS). The PC is a measure of accuracy and is calculated for the three by three contingency table as

$$PC = \frac{r + v + z}{n}, \tag{5.13}$$

where n is the total number of forecast-observation pairs, and r, v, and z follow the convention of Wilks (2005), which are correct categorizations of below average, average, and above average, respectively. The POD is a measure of discrimination for the "event" of interested. The calculation of the POD for a three by three contingency table is reported as three separate PODs for each "event" or category as

$$\begin{aligned} POD_1 &= \frac{r}{r + u + x} \\ POD_2 &= \frac{v}{s + v + y} \\ POD_3 &= \frac{z}{t + w + z} \end{aligned} \tag{5.14}$$

where the subscript (1,2,3) indicate the categories (below average, average, above average) for which the POD is valid, and the denominators are the sum of the observations within a given category, which also follow the conventions of Wilks (2005). The bias of a forecast is a comparison of the average forecast to the average observation, where unbiased forecasts yield a bias score of 1. The bias ratio for the three by three contingency table is reported similarly to the POD as

$$\begin{aligned} Bias_1 &= \frac{r + s + t}{r + u + x} \\ Bias_2 &= \frac{u + v + w}{s + v + y} \\ Bias_3 &= \frac{x + y + z}{t + w + z} \end{aligned} \tag{5.15}$$

Table 5.7 Three by three contingency table of forecasted and observed TC frequency using the multiple linear regression model developed in this study.

	Obs Below Avg.	Obs Avg.	Obs Above Avg.
Fcst Below Avg.	4	3	0
Fcst Avg.	3	19	3
Fcst Above Avg.	0	1	6

Table 5.8 Three by three contingency table of forecasted and observed TC frequency using climatology as the predictor.

	Obs Below Avg.	Obs Avg.	Obs Above Avg.
Fcst Below Avg.	0	0	0
Fcst Avg.	7	23	9
Fcst Above Avg.	0	0	0

Table 5.9 Three by three contingency table of forecasted and observed TC days.

	Obs Below Avg.	Obs Avg.	Obs Above Avg.
Fcst Below Avg.	8	3	0
Fcst Avg.	3	14	2
Fcst Above Avg.	0	3	6

Table 5.10 Three by three contingency table of forecasted and observed TC days.

	Obs Below Avg.	Obs Avg.	Obs Above Avg.
Fcst Below Avg.	0	0	0
Fcst Avg.	11	20	8
Fcst Above Avg.	0	0	0

where the numerators are the sum of the forecasted categories and the denominators are the sum of the observed categories. Finally, the skill scores computed represent two estimates of the possible improvement of correct forecasts over random forecasts. The HSS is defined as

$$HSS = \frac{(\frac{r+v+z}{n}) - [(\frac{r+s+t}{n}) * (\frac{r+u+x}{n}) + (\frac{u+v+w}{n}) * (\frac{s+v+y}{n}) + (\frac{x+y+z}{n}) * (\frac{t+w+z}{n})]}{1 - [(\frac{r+s+t}{n}) * (\frac{r+u+x}{n}) + (\frac{u+v+w}{n}) * (\frac{s+v+y}{n}) + (\frac{x+y+z}{n}) * (\frac{t+w+z}{n})]}, \tag{5.16}$$

and the PSS is defined as

$$PSS = \frac{(\frac{r+v+z}{n}) - [(\frac{r+s+t}{n}) * (\frac{r+u+x}{n}) + (\frac{u+v+w}{n}) * (\frac{s+v+y}{n}) + (\frac{x+y+z}{n}) * (\frac{t+w+z}{n})]}{1 - [(\frac{r+u+x}{n})^2 + (\frac{s+v+y}{n})^2 + (\frac{t+w+z}{n})^2]} \tag{5.17}$$

following the conventions of Wilks (2005).

A tilted bootstrap is used to estimate the previous attributes of the three by three contingency table for both the TC frequency and TC days prediction equations (Tables 5.11 and 5.12). Both prediction equations yield approximately the same median PC, with the TC days prediction having a larger confidence interval. There are larger differences between the different POD categories for TC frequency prediction, likely due to the few seasons in which a non-average season occurred. The POD categories for TC days have similar median values for each, however, the confidence interval is smallest for the average category, which is the most commonly observed category by design. All bias estimates for both TC frequency and TC days have a relatively narrow range around 1.0 in the 95% confidence interval, with the lowest spread across the average forecast category for both prediction schemes. Both schemes indicate that they are skillful over a random reference forecast, as both the PSS and HSS are greater than 0. Each scheme gives approximately the same median values around 0.5; however, the 95% confidence interval for the TC days prediction scheme is quite large, so it is more likely than not that each equation performs better than a climatological forecast.

The three by three contingency table using climatology as the prediction scheme (Table 5.8) indicates that the proportion correct drops to 0.5 and the skill scores drop to zero. Similarly, for TC days the proportion correct is near 0.5 and the skill scores again are zero (Table 5.10). In neither case do the climatological forecasts show any skill over a random forecast.

5.3.2 Two Categories

Another option is to categorize the hindcasts only using two categories. The two categories used are (i) average and above and (ii) below average. These are chosen because average or above seasons have a potentially large impact on resources in the region.

Observed contingency tables for the two category hindcasts for TC frequency and TC days indicate similar results (Tables 5.13 and 5.14). For the hindcasts of TC frequency and TC days, there were three years for which the prediction scheme hindcasted a below average number of TCs to occur during the season and there were an average or above number of storms. Additionally, there were three years that both schemes predicted average or above, but actually it was a below average season.

Just as with the three by three contingency table, there are a number of different attributes that can be calculated to assess the effectiveness of the forecast scheme. Just as with the three by three scheme the Proportion Correct (PC) can be calculated as

$$PC = \frac{a+d}{n}, \tag{5.18}$$

where n is the sum of all forecasts (a, b, c, d), and a and d are hits and correct nulls. The PC is a measure of the accuracy of the forecast scheme, where a PC = 1 would

Table 5.11 Bootstrap results of the three by three contingency table attributes for TC frequency with a 95% confidence interval and median values

	2.5%	50%	97.5%
PC	0.66	0.743	0.825
POD_1	0.333	0.571	0.802
POD_2	0.731	0.825	0.911
POD_3	0.478	0.672	0.866
$Bias_1$	0.625	1.01	1.59
$Bias_2$	0.93	1.09	1.28
$Bias_3$	0.559	0.781	1.05
PSS	0.365	0.518	0.666
HSS	0.377	0.532	0.671

Table 5.12 Bootstrap results of the three by three contingency table attributes for TC days with a 95% confidence interval and median values

	2.5%	50%	97.5%
PC	0.462	0.718	0.923
POD_1	0.333	0.727	1.00
POD_2	0.409	0.7	0.941
POD_3	0.333	0.778	1.00
$Bias_1$	0.583	1.00	1.67
$Bias_2$	0.654	0.952	1.36
$Bias_3$	0.625	1.143	2.143
PSS	0.141	0.567	0.869
HSS	0.139	0.554	0.867

Table 5.13 Two by two contingency table of forecasted and observed TC frequency.

	Obs Avg. and Above	Obs Below Avg.
Fcst Avg. and Abov	29	3
Fcst Below Avg.	3	4

Table 5.14 Two by two contingency table of forecasted and observed TC days.

	Obs Avg. and Above	Obs Below Avg.
Fcst Avg. and Abov	25	3
Fcst Below Avg.	3	8

be that all forecasts are correct. The bias is a comparison of the average forecast to the average observation, represented by a ratio

$$Bias = \frac{a+b}{a+c}, \tag{5.19}$$

where an unbiased forecast with have Bias = 1, meaning that the event is forecast as often as it is observed. To represent the reliability and resolution of the forecast scheme, the false alarm ratio (FAR) can be computed as

$$FAR = \frac{b}{a+b}, \tag{5.20}$$

where the FAR is the proportion of forecast events that turn out to be wrong. Unlike the previous attributes, where the highest value is preferred, a low value is desired for the FAR. Finally, there are two measures of discrimination, the probability of detection (POD) and the false alarm rate, also known as the probability of false detection (POFD). The POD is defined similarly to that of the three by three contingency table

$$POD = \frac{a}{a+c}, \tag{5.21}$$

where the POD is a ratio of the correct forecasts to the number of times the event was observed. The POFD is the ratio of false alarms to the total number of non-occurrences of the event being forecasted,

$$POFD = \frac{b}{b+d}. \tag{5.22}$$

Additionally, skill scores for the forecast scheme compared to random forecasts can also be computed. A total of three skill scores are computed for the two by two contingency tables in this study. Each skill score uses a slightly different formulation for the reference accuracy measure. The Heidke skill score (HSS), which is based on the proportion correct

$$HSS = \frac{2(ad-bc)}{(a+c)(c+d)+(a+b)(b+d)}, \tag{5.23}$$

where a perfect forecast scheme would yield HSS = 1, forecasts equivalent to a reference forecast would be zero, and forecasts worse than the reference forecast would have negative scores. The reference forecast for the HSS are random forecasts that are statistically independent of the observations (Wilks 2005). The reference forecast is constructed from two marginal probabilities of a 'yes' forecast and a 'yes' observation (Wilks 2005). Similar to the HSS in construct, the Peirce skill score (PSS) is another measure of forecast skill, but with the reference forecast being constrained to be unbiased. The PSS is computed as

$$PSS = \frac{ad - bc}{(a + c)(b + d)}, \tag{5.24}$$

for the two by two contingency table, where the reference forecast is the marginal distribution that is qual to climatology (Wilks 2005). The PSS can also be understood to be the difference between the POD and the POFD (Wilks 2005). Finally, the Clayton skill score (CSS) indicates positive skill when the event occurs more frequently when forecast than when not forecast (Wilks 2005). The CSS is computed as

$$CSS = \frac{ad - bc}{(a + b)(c + d)}, \tag{5.25}$$

where a CSS = 1 indicates a perfect forecast and CSS = 0 indicates random forecasts.

A limiting factor in the success of the two by two contingency table as defined in this section is the relative frequency of non-occurrence events. This will be evident in the results from the bootstrap of the 39 observed years. For both TC frequency and TC days prediction the proportion correct and probability of detection are 0.846 and 0.9, respectively. Both confidence intervals are relatively narrow. However, for the probability of false detection, the confidence interval ranges across the entire range of possibilities, especially for the prediction of TC frequency. This result impacts the confidence intervals for the Heidke, Peirce, and Clayton skill scores as they range from near zero to 1.0. Despite that fact, there is a low false alarm ratio and a bias near 1

for both TC frequency and TC days prediction. Ultimately, we can not say with certainty that the TC forecasts of average and above and below average are significantly different from a random forecast (as all of the skill scores 95% confidence intervals include 0), but the TC days prediction scheme indicates at least some measurable skill over random forecasts with the range of skill scores not including zero. However, what we are more interested in is the correct prediction of the average and above category. As such, the proportion correct and probability of detection both yield high values. The PC has a 95% confidence interval between 0.641 and 1.0 with a median value of 0.846 for TC frequency and TC days. The 95% confidence interval for the POD is between 0.733 and 1.0 with a median value of 0.909 for TC frequency prediction and between 0.714 and 1.0 with a median value of 0.9 for TC days prediction. As expected from Tables 5.15 and 5.15, both prediction schemes are effective in identify seasons when there will be average and above numbers of TCs and TC days.

5.3.3 Discussion

In the preceding sections of this chapter a seasonal prediction scheme has been developed to predict both TC frequency and TC days for an upcoming TC season using the global teleconnections defined in 4. With the relatively limited variation from season to season in the number of TCs that occur in the NWAUS basin, climatology can be a difficult forecast to out perform. The results of the contingency tables, along with the evaluation of RMSE and AME, indicate that both schemes are skillfull relative to random and climatological forecasts of each metric. By providing forecasts for the entire season before the season begins, adequate resources therefore can be allocated for use in mitigating the effects of a TCs impact on the NWAUS region.

The final four seasons, which did not play any role in choosing the predictors or in the development of the prediction scheme, can be used for independent verification (Tables 5.17 and 5.18). Initially, the five prediction variables TC frequency and three

Table 5.15 Bootstrap results of the two by two contingency table attributes for TC frequency with a 95% confidence interval and median values

	2.5%	50%	97.5%
PC	0.641	0.846	1.0
POD	0.733	0.909	1.0
POFD	0.0	0.429	0.857
FAR	0.0	0.091	0.265
Bias	0.853	1.0	1.185
PSS	-0.025	0.478	1.0
HSS	-0.026	0.478	1.0
CSS	-0.025	0.478	1.0

Table 5.16 Bootstrap results of the two by two contingency table attributes for TC days with a 95% confidence interval and median values

	2.5%	50%	97.5%
PC	0.641	0.846	1.0
POD	0.714	0.90	1.0
POFD	0.0	0.265	0.636
FAR	0.0	0.102	0.290
Bias	0.833	1.0	1.208
PSS	0.149	0.623	1.0
HSS	0.148	0.621	1.0
CSS	0.149	0.623	1.0

predictor variables for TC days were gathered and scaled according to the mean and standard deviation of the development data set. The prediction variables were then input into (5.10) and (5.11), which yielded the prediction for that season (Tables 5.17 and 5.18). Predictions for TC frequency were never off by more than 3 storms, and the final season (2008) was a correct prediction of 8 TCs. For TC days, the number of TC days, as well as the predicted percentile for that season, are reported. For this small sample of predictions, all forecasts were within 9 days and the predicted percentile was within 11%. The predictions for TC days range from low seasonal percentiles to high seasonal percentiles, for an overall successful prediction.

Since the season was already passed these seasons, they are still considered a hindcasted. Future predictions for a given season should be able to be completed on 1 September preceding the beginning of the NWAUS TC season for TC frequency and 1 October for TC days.

Table 5.17 Summary of seasonal predictions on independent data not included in development dataset for TC frequency.

Years	Independent Prediction TC Count	Observed TC Count	Difference
2005	5	7	-2
2006	4	3	+1
2007	2	5	-3
2008	8	8	0

Table 5.18 Summary of seasonal predictions on independent data not included in development dataset for TC days. Numbers in parentheses indicate the percentile at which the predicted and observed values occur relative to the observed values.

Years	Independent Prediction TC Count	Observed TC Count	Difference
2005/06	47 (64%)	44.75 (62%)	+2.25 (+2%)
2006/07	29.5 (23%)	22.75 (15%)	+6.75 (+8%)
2007/08	42 (54%)	33 (33%)	+9 (+11%)
2008/09	55.75 (79%)	51.75 (77%)	+4 (+2%)

Chapter 6

Conclusions and Future Work

New global teleconnections have been identified for the NWAUS TC basin; the teleconnections are intra-basin, inter-basin, and cross-hemispheric. Through correlation analysis, previously identified ENSO parameters were found not to be primary factors in describing the variability of TCs in the NWAUS region; however, other NCEP–NCAR reanalysis variables that explain some of the variability in TCs in the NWAUS region are in, part related, to ENSO variability and other known global modes. Previous studies for the NWAUS basin have primarily investigated ENSO as a means for describing the year to year variations in TC frequency and TC days, among other TC metrics. This study goes beyond ENSO to investigate global climate variability to describe year to year variations of thirteen TC metrics, which has never been done before for this basin.

In this study a small subset of the nearly many possible teleconnection patterns have been investigated. This study is not meant to be an all inclusive search for every possible teleconnection, but rather an initial investigation of previously identified global teleconnections and basic state variables. There are other possible predictors for seasonal prediction of TCs, which could provide more explanatory power to the variability of TCs in the NWAUS region.

A successful seasonal prediction was made of the number of TCs and TC days for the NWAUS region using multiple linear regression with global atmospheric variables available from the NCEP–NCAR reanalysis dataset as predictors. This is the first seasonal prediction for the NWAUS region that uses global atmospheric variables and

has skillful forecasts relative to using persistence, climatology, or random forecasts. Previous work in the NWAUS region has relied solely on ENSO or local predictors of atmospheric variables. A successful seasonal prediction scheme will allow people and industries to prepare adequately for an oncoming TC season, especially in a region that has a large amount of natural resources that are exported each year, like the northwest coast of Australia.

In the future, seasonal prediction equations can be developed for predicting any TC metric defined for the NWAUS region. Each metric adds a piece of the seasonal TC puzzle and would provide more informative forecasts. The prediction schemes can be developed in a similar manner to those described in this study. It also would be useful to try other statistical techniques to accomplish the prediction of TC metrics. One such technique is the Support Vector Machine, which been increasingly used in meteorology (Mercer et al. 2008; Lee et al. 2004).

Bibliography

Ambaum, M. H., B. J. Hoskins, and D. B. Stephenson, 2001: Artic Oscillation or North Atlantic Oscillation? *J. Climate*, **14**, 3495–3507.

AMS, 2000: *Glossary of Meteorology*. Amer. Meteor. Soc., 2nd edition, 855 pp.

Andreas, E. L. and K. A. Emanuel, 2001: Effects of sea spray on tropical cyclone intensity. *J. Atmos. Sci.*, **58**, 3741–3751.

Anthes, R. A., 1982: *Tropical cyclones: Their evolution, structure, and effects*, Amer. Meteor. Soc., volume 19 of *Meteor. Monographs*, 208.

Baldwin, M. P., L. Gray, T. J. Dunkerton, K. Hamilton, P. H. Haynes, W. J. Randel, J. R. Holton, M. J. Alexander, I. Hirota, T. Horinouchi, D. B. A. Jones, and J. S. Kinnersley, 2001: The Quasi-biennial Oscillation. *Rev. Geophys.*, **39**, 179–229.

Ballenzweig, E. M., 1957: Fluctuations in frequency of tropical storms. *Weatherwise*, **99**, 121–125.

—, 1959: Relation of long-period circulation anomalies to tropical storm formation and motion. *J. Meteorology*, **16**, 121–139.

Barnston, A. G. and R. E. Livezey, 1987: Classification, seasonality and persistence of low-frequency atmospheric circulation patterns. *Mon. Wea. Rev.*, **115**, 1083–1126.

Basher, R. E. and X. Zheng, 1995: Tropical cyclones in the Southwest Pacific: Spatial patterns and relationships to southern oscillation and sea surface temperature. *J. Climate*, **8**, 1249–1260.

Bell, G. D., M. S. Halpert, C. F. Ropelewski, V. E. Kousky, A. V. Douglas, R. S. Schnell, and M. E. Gelman, 2000: Climate assessment for 1999. *Bull. Amer. Meteor. Soc.*, **81**, S1–S50.

Bennett, J. R. and J. A. Young, 1971: The influence of latitudinal wind shear upon large-scale wave propagation into the tropics. *Mon. Wea. Rev.*, **99**, 202–214.

Bister, M. and K. Emanuel, 1998: Dissipative heating and hurricane intensity. *Meteorol. Atm. Phys.*, **65**, 233–240.

Bjerknes, J., 1969: Atmospheric teleconnections from the equatorial Pacific. *Mon. Wea. Rev.*, **97**, 163–172.

Blake, E. S. and W. M. Gray, 2004: Prediction of August Atlantic basin hurricane activity. *Wea. Forecasting*, **19**, 1044–1060.

Bretherton, C. S., M. Widmann, V. P. Dymnikov, J. M. Wallace, and I. Blade, 1999: The effective number of spatial degrees of freedom of a time-varying field. *J. Climate*, **12**, 1990–2009.

Broadbridge, L. W. and B. N. Hanstrum, 1998: The relationship between tropical cyclones near Western Australia and the Southern Oscillation Index. *Aus. Met. Mag.*, **47**, 183–189.

Buckley, B. W., L. M. Leslie, and M. S. Speer, 2003: The impact of observational technology on climate database quality: Tropical cyclones in the Tasman Sea. *J. Climate*, **16**, 2640–2645.

Camargo, S. J., A. G. Barnston, P. J. Klotzbach, and C. W. Landsea, 2007: Seasonal tropical cyclone forecasts. *WMO Bull.*, **56**, 297–309.

Chan, J. C. L., 1985: Tropical cyclone activity in the northwest Pacific in relation to the El Niño/Southern Oscillation phenomenon. *Mon. Wea. Rev.*, **113**, 599–606.

—, 2008: A simple seasonal forecast update of tropical cyclone activity. *Wea. Forecasting*, **23**, 1016–1021.

Chan, J. C. L. and K. S. Liu, 2004: Global warming and western north Pacific typhoon activity from an observational perspective. *J. Climate*, **17**, 4590–4602.

Chan, J. C. L., J. E. Shi, and C. M. Lam, 1998: Seasonal forecasting of tropical cyclone activity over the western North Pacific and the South China Sea. *Wea. Forecasting*, **13**, 997–1004.

—, 2001: Improvements in the seasonal forecasting of tropical cyclone activity over the western North Pacific. *Wea. Forecasting*, **16**, 491–498.

Charney, J., 1969: A further note on large-scale motions in the tropics. *J. Atmos. Sci.*, **26**, 182–185.

Dare, R. A. and N. E. Davidson, 2004: Characteristics of tropical cyclones in the Australian region. *Mon. Wea. Rev.*, **132**, 3049–3065.

Depperman, R. C. E., 1947: Notes on the origin and structures of Philippine typhoons. *Bull. Amer. Meteor. Soc.*, **28**, 399–404.

Dong, K., 1988: El Niño and tropical cyclone frequency in the Australian region and the northwest Pacific. *Aust. Met. Mag.*, **36**, 219–225.

Draper, N. R. and H. Smith, 1982: *Applied Regression Analysis*. John Wiley and Sons, 2 edition, 709 pp.

Dvorak, V. F., 1975: Tropical cyclone intensity analysis and forecasting from satellite imagery. *Mon. Wea. Rev.*, **103**, 420–430.

—, 1984: Tropical cyclone intensity analysis using satellite data. NOAA Tech. Report NESDIS 11, [Available from NOAA/NESDIS, 5200 Auth Rd., Washington DC, 20233.].

Efron, B. and R. J. Tibshirani, 1994: *An Introduction to the Bootstrap*. Chapman and Hall/CRC, 436 pp.

Elsner, J. B. and T. H. Jagger, 2004: A hierarchical Bayesian approach to seasonal hurricane modeling. *J. Climate*, **17**, 2813–2827.

—, 2006: Prediction models for annual U.S. hurricane counts. *J. Climate*, **19**, 2935–2952.

Elsner, J. B. and B. Kocher, 2000: Global tropical cyclone activity: A look to the North Atlantic Oscillation. *Geo. Phys. Rea.*, **27**, 129–132.

Elsner, J. B. and C. P. Schmertmann, 1993: Improving extended-range seasonal predictions of intense Atlantic hurricane activity. *Wea. Forecasting*, **8**, 345–351.

Emanuel, K., 1986: An air-sea interaction theory for tropical cyclones. Part I: Steady state maintenance. *J. Atmos. Sci.*, **43**, 585–604.

—, 1995: Sensitivity of tropical cyclones to surface exchange coefficients and a revised steady-state model incorporating eye dynamics. *J. Atmos. Sci.*, **52**, 3969–3976.

—, 2003a: A similarity hypothesis for air-sea exchange at extreme wind speeds. *J. Atmos. Sci.*, **60**, 1420–1428.

—, 2003b: Tropical cyclones. *Annu. Rev. Earth Planet. Sci.*, **31**, 75–104.

—, 2005: *The Divine Wind*. Oxford University Press, 285 pp.

Evans, J. L. and R. J. Allan, 1992: El Niño/Southern Oscillation modification to the structure of the monsoon and tropical cyclone activity in the Australiasian region. *Int. J. Climatol.*, **12**, 611–623.

Foster, I. J. and T. J. Lyons, 1988: The development of tropical cyclones in the north-west of Australia. *Quart. J. Roy. Meteor. Soc.*, **114**, 1187–1199.

Frank, W. M. and G. S. Young, 2007: The interannual variability of tropical cyclones. *Mon. Wea. Rev.*, **135**, 3587–3598.

Gershunov, A. and T. P. Barnett, 1998: Interdecadal modulation of ENSO teleconnections. *Bull. Amer. Meteor. Soc.*, **79**, 2715–2725.

Goodrich, G. B., 2007: Influence of the Pacific decadal oscillation on winter precipitation and drought during years of neutral ENSO in the western United States. *Wea. Forecasting*, **22**, 116–124.

Gray, W. M., 1968: Global view of the origin of tropical disturbances and storms. *Mon. Wea. Rev.*, **96**, 669–700.

—, 1984a: Atlantic season hurricane frequency. Part I: El Niño and 30 mb quasi-biennial oscillation influences. *Mon. Wea. Rev.*, **112**, 1649–1668.

—, 1984b: Atlantic season hurricane frequency. Part II: Forecasting its variability. *Mon. Wea. Rev.*, **112**, 1669–1683.

—, 1990: Strong association between West African rainfall and U.S. landfall of intense hurricanes. *Science*, **249**, 1253–1256.

Gray, W. M., C. W. Landsea, P. W. M. Jr., and K. J. Berry, 1992: Predicting Atlantic seasonal hurricane activity 6–11 months in advance. *Wea. Forecasting*, **7**, 440–455.

—, 1993: Predicting Atlantic basin seasonal tropical cyclone activity by 1 August. *Wea. Forecasting*, **8**, 73–86.

—, 1994: Predicting Atlantic basin seasonal tropical cyclone activity by 1 June. *Wea. Forecasting*, **9**, 103–115.

Gray, W. M. and D. J. Shea, 1973: The hurricanes inner core region: Part II: Thermal stability and diurnal characteristics. *J. Atmos. Sci.*, **30**, 1565–1576.

Hall, J. D., A. J. Matthews, and D. J. Karoly, 2001: The modulation of tropical cyclone activity in the Australian region by the Madden-Julian Oscillation. *Mon. Wea. Rev.*, **129**, 2970–2982.

Harper, B. A., S. A. Stroud, M. McCormack, and S. West, 2008: A review of historical tropical cyclone intensity in North-Western Australia and implications for climate change trend analysis. *Aus. Meteor. Mag.*, **57**, 121–141.

Hastings, P. A., 1990: Southern Oscillation influences on tropical cyclone activity in the Australian/Southwest Pacific region. *Int. J. Climatol.*, **10**, 291–298.

Hendon, H. and B. Liebmann, 1994: .

Higgins, R. W., A. Leetmaa, Y. Xue, and A. Barnston, 2000: Dominant factors influencing the seasonal predictability of U.S. precipitation and surface air temperature. *J. Climate*, **13**, 3994–4017.

Holland, G. J., 1980: An analytic model of the wind and pressure profiles in hurricanes. *Mon. Wea. Rev.*, **108**, 1212–1218.

—, 1981: On the quality if the Australian tropical cyclone data base. *Aust. Meteor. Mag.*, **29**, 169–181.

Hurrell, J. W., 1995: Decadal trends in the North Atlantic Oscillation: Regional temperatures and precipitation. *Science*, **269**, 676–679.

Jagger, X. N., T. H. and J. B. Elsner, 2002: A space-time model for seasonal hurricane prediction. *J. Climatology*, **22**, 451–465.

Kalnay, E., M. Kanamitsu, R. Kistler, W. Collins, D. Deaven, L. Gandin, M. Iredell, S. Saha, G. White, J. Woollen, Y. Zhu, M. Chelliah, W. Ebisuzaki, W. Higgins, J. Janowiak, K. C. Mo, C. Ropelewski, J. Wang, A. Leetmaa, R. Reynolds, R. Jenne, and D. Jospeh, 1996: The NCEP/NCAR 40-year reanalysis project. *Bull. Amer. Meteor. Soc.*, **77**, 437–471.

Kleinschmidt, E. J., 1951: Basics of a theory of the tropical cyclone. *Arch. Meteor. Geophys. Bioklimatol*, **4a**, 53–72.

Klotzbach, P. J., 2007: Revised prediction of seasonal Atlantic basin tropical cyclone activity from 1 August. *Wea. Forecasting*, **22**, 937–949.

Klotzbach, P. J. and W. M. Gray, 2003: Forecasting September Atlantic basin tropical cyclone activity. *Wea. Forecasting*, **18**, 1109–1128.

—, 2004: Updated 6–11-month prediction of Atlantic basin seasonal hurricane activity. *Wea. Forecasting*, **19**, 917–934.

Knapp, K. and J. Kossin, 2007: New global tropical cyclone data from ISCCP B1 geostationary satellite observations. *J. Appl. Remote Sens.*, **1**, 013505.

Kossin, J., K. Knapp, D. Vimont, R. Murnane, and B. Harper, 2007: A globally consistent reanalysis of hurricane variability and trends. *Geophys. Res. Lett.*, **34**, L04815, doi:10.1029/2006GL028836.

Kuleshov, Y., L. Qi, R. Fawcett, and D. Jones, 2008: On tropical cyclone activity in the Southern Hemisphere: Trends and the ENSO connection. *Geophys. Res. Lett.*, **35**, L14S08, doi:10.1029/2007GL032983.

Lander, M. A. and C. P. Guard, 1998: A look at the global tropical cyclone activity during 1995: Contrasting high Atlantic variability with low activity in other basins. *Mon. Wea. Rev.*, **126**, 1163–1173.

Landsea, C. W. and W. M. Gray, 1992: The strong association between Western Sahelian monsoon rainfall and intense Atlantic hurricanes. *J. Climate*, **5**, 435–453.

Large, W. G. and S. Pond, 1982: Open ocean momentum flux measurements in moderate to strong winds. *J. Phys. Oceanogr.*, **11**, 324–336.

Larson, E., 2000: *Isaacs Storm: A Man, a Time, and the Deadliest Hurricane in History*. Knopf Publishing Group, 336 pp.

Lee, Y., G. Wahba, and S. A. Ackerman, 2004: Cloud classification of satellite radiance data by multicategory support vector machines. *J. Atmos. Oceanic. Technol.*, **21**, 159–169.

Lehmiller, G. S., T. B. Klimberlain, and J. B. Elsner, 1997: Seasonal prediction models for North Atlantic basin hurricane location. *Mon. Wea. Rev.*, **125**, 1780–1791.

Lighthill, J., 1998: Fluid mechanics of tropical cyclones. *Theor. Comp. Fluid Dynamics*, **10**, 3–21.

Lo, F. and H. Hendon, 2000: Empirical estended-range prediction of the Madden-Julian oscillation. *Mon. Wea. Rev.*, **128**, 2528–2543.

Love, G., 1985: Cross-equatorial interactions during tropical cyclogenesis. *Mon. Wea. Rev.*, **113**, 1499–1509.

Madden, R. and P. Julian, 1994: Observations of the $40-50$-day tropical oscillation–A review. *Mon. Wea. Rev.*, **122**, 814–837.

Makin, V. K., 2005: A note on the drag of the sea surface at hurricane winds. *Boundary Layer Meteor.*, **115**, 169–176.

Mann, H. B. and D. R. Whitney, 1947: On a test of whether one of two random variables is stochastically larger than the other. *Annals of Mathematical Statistics*, **18**, 5060.

Mantua, N. J., S. R. Hare, Y. Zhang, J. M. Wallace, and R. C. Francis, 1997: A Pacific interdecadal climate oscillation with impacts on salmon production. *Bull. Amer. Met. Soc.*, **78**, 1069–1079.

Maynard, R. H., 1945: Radar and weather. *J. Meteor.*, **2**, 214–226.

McBride, J. L. and T. D. Keenan, 1982: Climatology of tropical cyclone genesis in the australian region. *J. Climatol.*, **2**, 13–33.

McBride, J. L. and R. Zehr, 1981: Observational analysis of tropical cyclone formation. Part II: Comparison of non-developing and developing systems. *J. Atmos. Sci.*, **38**, 1132–1151.

McDonnell, K. A. and N. J. Holbrook, 2004a: A Poisson regression model of tropical cyclogenesis for the Australian–Southwest Pacific Ocean region. *Wea. Forecasting*, **19**, 440–455.

—, 2004b: A Poisson regression model approach to predicting tropical cyclogenesis in the Australian/southwest Pacific Ocean region using the SOI and saturated equivalent potential temperature gradient as predictors. *Geophys. Res. Lett.*, **31**, L20110, doi: 10.1029/2004GL020843.

Mercer, A. E., M. B. Richman, H. B. Bluestein, and J. M. Brown, 2008: Statistical modeling of downslope windstorms in Boulder, Colorado. *wea. Forecasting*, **23**, 1176–1194.

Moller, J. D. and M. T. Montgomery, 1999: Vortex Rossby-waves and hurricane intensification in a bartropic model. *J. Atmos. Sci.*, **56**, 1678–1687.

Montgomery, M. T., 1997: A theory for vortex Rossby-waves and its application to spiral bands and inensity changes in hurricanes. *Quart. J. Roy. Meteorol. Soc.*, **123**, 435–465.

Nicholls, N., 1979: A possible method for predicting seasonal tropical cyclone activity in the Australian region. *Mon. Wea. Rev.*, **107**, 1221–1224.

—, 1984: The southern oscillation, sea-surface temperature, and interannual fluctuations in Australian tropical cyclone activity. *J. Climatol.*, **4**, 661–670.

—, 1985: Predictability of interannual variations of Australian seasonal tropical cyclone activity. *Mon. Wea. Rev.*, **113**, 1144–1149.

—, 1992: Recent performance of a method for forecasting Australian season tropical cyclone activity. *Aus. Meteor. Mag.*, **40**, 105–110.

—, 1999: SOI – based forecast of Australian region tropical cyclone activity. *Exp. Long Lead Forecast Bull.*, **Vol. 8, No. 4**, Climate Prediction Center, National Weather Service, Washington, DC, 71–72.

Nicholls, N., C. Landsea, and J. Gill, 1998: Recent trends in Australian region tropical cyclone activity. *Meteor. Atmos. Phys.*, **65**, 197–205.

Ooyama, K. V., 1982: Conceptual evolution of the theory and modeling of tropica cyclones. *J. Meteor. Soc. Japan*, **60**, 369–379.

Palmén, E. H. and C. W. Newton, 1969: *Atmospheric circulation systems: their structure and physical interpretation*. Academic Press, 603 pp.

Radok, U. and A. M. Grant, 1957: Variations in the high tropospheric mean flow over Australia and New Zealand. *J. Met.*, **14**, 141–149.

Ramsay, H. A., L. M. Leslie, P. J. Lamb, M. B. Richman, and M. Leplastrier, 2008: Interannual variability of tropical cyclones in the Australian region: Role of large-scale environment. *J. Climate*, **21**, 1083–1103.

Rasmusson, E. M. and T. H. Carpenter, 1982: Variations in tropical sea surface temperature and surface wind fields associated with the Southern Oscillation/El Niño. *Mon. Wea. Rev.*, **110**, 354–384.

Revell, C. G. and S. W. Goulter, 1986: South Pacific tropical cyclones and the Southern Oscillation. *Mon. Wea. Rev.*, **114**, 1138–1145.

Riehl, H., 1950: A model for hurricane formation. *J. Appl. Phys.*, **21**, 917–925.

Saji, N. H., B. N. Goswami, P. N. Vinayachandran, and T. Yamagata, 1999: A dipole mode in the tropical Indian Ocean. *Nature*, **401**, 360–363.

Schwing, F., T. Murphree, and P. Green, 2002: The Northern Oscillation Index (NOI): a new climate index for the northeast Pacific. *Progress in Oceanography*, **53**, 115–139.

Smith, T. M. and R. W. Reynolds, 2004: Improved extended reconstruction of sst (1854-1997). *J. Climate*, **17**, 2466–2477.

Solow, A. and N. Nicholls, 1990: The relationship between the southern oscillation and tropical cyclone frequency in the Australian region. *J. Climate*, **3**, 1097–1101.

Thompson, D. W. and J. M. Wallace, 1998: The Artic Oscillation signature in wintertime geopotential height and temperature fields. *Geophys. Res. Lett.*, **25**, 1297–1300.

Torrence, C. and G. P. Campo, 1998: A practical guide to wavelet analysis. *Bull. Amer. Met. Soc.*, **79**, 61–78.

Trenberth, K. E., 1976: Spatial and temporal variations of the Southern Oscillation. *Quart. J. Roy. Meteor. Soc.*, **102**, 639–653.

Tukey, J. W., 1991: The philosophy of multiple comparisons. *Statistical Science*, **6**, 100–106.

Walker, G. T. and E. W. Bliss, 1932: World Weather V. *Mem. Roy. Meteor. Soc.*, **4**, 53–84.

Wallace, J. M. and D. S. Gutzler, 1981: Teleconnections in the geopotential height field during the Northern Hemisphere winter. *Mon. Wea. Rev.*, **109**, 784–812.

Webster, P. J. and J. R. Holton, 1982: Cross-equatorial response to middle-latitude forcing in a zonally varying basic state. *J. Atmos. Sci.*, **39**, 722–733.

Wexler, H., 1947: Structure of hurricanes as determined by radar. *Amm. N.Y. Acad. Sci.*, **48**, 821–844.

Wheeler, M. and H. Hendon, 2004: An all-season real-time multivariate MJO index: Development of an index for monitoring and prediction. *Mon. Wea. Rev.*, **132**, 1917–1932.

Wilks, D. S., 2005: *Statistical Methods in the Atmospheric Sciences*. Academic Press, 2nd edition, 648 pp.

Willoughby, H. E., J. A. Clos, and M. G. Shoreibah, 1982: Concentric eye walls, secondary wind maxima, and the evolution of the hurricane vortex. *J. Atmos. Sci.*, **39**, 395–411.

Zhang, Y., J. Wallace, and D. Battisti, 1997: Enso-like interdecadal variability: 1900-93. *J. Climate*, **10**, 1004–1020.